Universität für Bodenkultur Wien

Masterarbeit

Production and Characterization of recombinant Hyaluronidase Inclusion Bodies from *Apis mellifera* in *E. coli* Bl21(DE3)

Ausgeführt am Institut für Verfahrenstechnik, Umwelttechnik und Technische Biowissenschaften (E-166) der Technischen Universität Wien

Sarah Ablasser

(01246826)

Angestrebter akademischer Grad:

Master of Science

Masterstudium: Biotechnologie

ErstbetreuerIn: Univ.Prof. Dipl. Ing. Dr. techn. Christoph Herwig

ZweitbetreuerIn: Dipl.-Ing. Dipl.-Ing. Dr. rer. nat. Dr. techn. Christoph Slouka

Wien, 16.09.2020

Table of Contents

Danksagung 5

Abbreviations 6

Abstract 7

Zusammenfassung 8

1. Introduction 10

1.1 Recombinant protein expression in *E. coli* 10

1.2 Bioprocess technology 11

1.3 Upstream processing in *E. coli* 13

1.4 Downstream processing after expression in *E. coli* 14

1.5 Inclusion Bodies and applications 17

1.6 The influence of upstream process parameters on IBs 18

1.7 Hyaluronidase of *Apis mellifera* 19

1.8 Aim of this study and scientific questions 20

- Has the hyaluronidase gene of *Apis mellifera* been successfully cloned into the pET28a(+) plasmid? 20
- Can the hyaluronidase of *Apis mellifera* be successfully expressed in *E. coli* BL21(DE3) as Inclusion Bodies? 20
- Can the hyaluronidase of *Apis mellifera* be used as model enzyme for active Inclusion Bodies and hence direct applications? 20

2 Materials and Methods 21

2.1 Strains 21

2.2 Bioreactor cultivations 23

2.3 Cultivation scheme 25

2.4 Cultivation Analytics 26

2.4.1 Biomass 26

2.4.2 Sugar analytics 26

2.4.3 Cell viability 27

2.4.4 IB Preparation 28

2.4.5 IB Size 29

2.4.6 IB Titer 29

2.4.7 IB activity 30

2.4.7.1 Activity assay 30

2.4.7.2 FT-IR spectroscopy 31

3 Results and Discussion 31

3.1 Hyaluronidase IB titer 34
3.2 Statistical evaluation 36
3.3 Hyaluronidase IB bead size 41
3.4 Hyaluronidase IB activity assay 45
3.5 Hyaluronidase IB activity using FT-IR spectroscopy 47
4. Conclusions and Outlook 50
4.1 Has the hyaluronidase gene of *Apis mellifera* been successfully cloned into the pET28a(+) plasmid? 52
4.2 Can the hyaluronidase of *Apis mellifera* be successfully expressed in *E. coli* BL21(DE3) as Inclusion Bodies? 52
4.3 Can the hyaluronidase of *Apis mellifera* be used as model enzyme for active inclusion bodies? 53
4.4 Outlook 55
4.5 Literature 56
4.6 Figures 62
5. Paper: Production of active recombinant Hyaluronidase Inclusion Bodies from *Apis mellifera* in *E. coli* Bl21(DE3) and characterization by FT-IR Spectroscopy 64

Erklärung zur Verfassung dieser Arbeit:

Hiermit erkläre ich, dass ich diese Arbeit selbstständig verfasst, alle verwendeten Quellen und Hilfsmittel vollständig angegeben habe und Stellen der Arbeit - einschließlich Tabellen und Abbildungen -, die andere Werken oder dem Internet im Wortlaut oder Sinn entnommen sind, auf jeden Fall unter Angabe der Quelle als Entlehnung kenntlich gemacht habe.

_____

Sarah Ablasser

Danksagung

An dieser Stelle möchte ich mich bei allen bedanken, die mich während meiner Masterarbeit unterstützt haben.

Besonderer Dank gilt Christoph Herwig, der es mir ermöglicht hat, meine Arbeit am Institut der TU Wien durchzuführen.

Weiters möchte ich mich für die Betreuung und Begutachtung meiner Arbeit bei Christoph Slouka bedanken, der mir stets mit seiner Expertise und viel Geduld zur Verfügung stand.

Außerdem danke ich Julian Kopp, der mir im Laufe der Arbeit unterstützend zur Seite stand und allen weiteren Personen, die mich bei der praktischen Arbeit im Labor unterstützt haben.

Abschließend möchte ich mich bei meiner Familie bedanken, die mir durch ihre Unterstützung das Studium ermöglicht haben.

Abbreviations

ATR	Attenuated total reflection
CPP	Critical process parameter
DCW	Dry cell weight
DoE	Design of experiment
DSP	Downstream processing
FT-IR	Fourier Transformed – Infrared (Spectroscopy)
HA	Hyaluronic acid
IB	Inclusion Body
IPTG	Isopropyl β-D-1 thiogalactopyranoside
OD	Optical density
QA	Quality attribute
q_p [g/g/h]	Specific production rate
$q_{s,C}$ [g/g/h]	Specific substrate uptake rate
SEM	Scanning electron microscopy

Abstract

Being an expression host of choice for the production of recombinant proteins, *Escherichia coli* accounts for fast growth to high cell densities on inexpensive media and high expression yields. In combination with the pET expression system and IPTG as inducing agent, high replication rates and product yields can be achieved. However, the expression of complex recombinant proteins with high molecular weight and many disulfide bonds often results in the formation of Inclusion Bodies.

The misconception of Inclusion Bodies being aggregated proteins without biological activity changed in recent years when it was discovered that such Inclusion Bodies exhibit residual activity due to a native-like protein structure. Being biologically active, Inclusion Bodies are important tools for direct applications in many biotechnological fields, especially in biomedicine.

The goal of this study was to express recombinant hyaluronidase of *Apis mellifera* in *E. coli* BL21(DE3) as Inclusion Bodies using a DoE approach and furthermore, to determine the biological activity. Indicated by a high metabolic burden to the cells, hyaluronidase is hard to express for *E. coli*, which resulted in low expression yields. The best conditions to obtain high specific titers were found at a temperature of 25 °C and a specific substrate feeding rate of 0.1 g/g/h after two – four hours of induction.

The activity of hyaluronidase IBs was verified using FT-IR spectroscopy. The progression of the enzymatic degradation of the substrate hyaluronan was measured over time. We observed that the degradation of hyaluronan at same concentrations increased at higher hyaluronidase IB concentrations. Moreover, active IBs can be directly used for the degradation of hyaluronan, thus eliminating the need for further DSP steps.

Based on the results, we believe that further IR analyses will pave the way for activity characterization of Inclusion Bodies and enzymes *in situ*.

Zusammenfassung

Escherichia coli ist ein Expressionswirt der Wahl für die Produktion rekombinanter Proteine. Die Vorzüge sind schnelles Wachstum zu hohen Zelldichten auf kostengünstigen Medien und hohe Expressionsausbeuten. In Kombination mit dem pET-Expressionssystem und IPTG als Induktionsmittel können hohe Replikationsraten und Produktausbeuten erzielt werden. Die Expression von komplexen rekombinanten Proteinen mit hohem Molekulargewicht und vielen Disulfidbindungen führt jedoch häufig zur Bildung von Einschlusskörpern (Inclusion Bodies – IB). Das Missverständnis, dass IBs aggregierte Proteine ohne biologische Aktivität sind, änderte sich in den letzten Jahren, als man entdeckte, dass solche Einschlusskörper aufgrund einer teilweise nativen Proteinstruktur eine Restaktivität aufweisen. Biologisch aktive IBs stellen wichtige Werkzeuge für direkte Anwendungen in vielen biotechnologischen Bereichen dar, insbesondere in der Biomedizin.

Das Ziel dieser Studie war es, ausgehend von einem Experimentaldesign (design of experiments – DoE) rekombinante Hyaluronidase von *Apis mellifera* in *E. coli* BL21(DE3) als IB zu exprimieren und darüber hinaus die biologische Aktivität zu bestimmen. Aufgrund der hohen metabolischen Belastung, welche die Produktion des Proteins auf die Zellen ausübt, ist die Hyaluronidase für *E. coli* schwer zu exprimieren, was zu niedrigen Expressionsausbeuten führte. Die besten Bedingungen zur Erzielung hoher spezifischer Titer wurden bei einer Temperatur von 25 °C und einer spezifischen Substratzufuhrrate von 0,1 g/g/h nach zwei - vier Stunden Induktion gefunden.

Die Aktivität der Hyaluronidase-IBs wurde mittels FT-IR-Spektroskopie verifiziert. Das Fortschreiten des enzymatischen Abbaus des Substrats Hyaluronan wurde über die Zeit gemessen. Wir beobachteten, dass der Abbau von Hyaluronan bei gleichbleibender Konzentration mit höheren

Hyaluronidase-IB-Konzentrationen zunahm. Darüber hinaus können aktive IBs direkt für den Abbau von Hyaluronan verwendet werden, wodurch sich weitere DSP-Schritte erübrigen.

Aufgrund der Ergebnisse sind wir überzeugt, dass weitere IR-Analysen den Weg für die Aktivitätscharakterisierung von IBs und Enzymen *in situ* ebnen werden.

1. Introduction

1.1 Recombinant protein expression in *E. coli*

The bacterium *Escherichia coli* is one of the most extensively used prokaryotic organisms to produce recombinant eukaryotic proteins[1]. Being an expression host of choice for a long time, the genetics of *E. coli* is well characterized, and many manipulation tools are available[2]. Although *E. coli* lacks the post translational machinery, advantages like fast growth to high cell densities on comparatively inexpensive media, high biomass yields and simple scale-up make the bacterium favourable for the production of pharmaceutical products[3]. Today, various eukaryotic expression systems are used to produce recombinant proteins, but *E. coli* accounts for the production of nearly 40 % of all approved biopharmaceuticals[4]. Monoclonal antibodies and antibody fragments are currently the most important biopharmaceutical products. This further expands the use of *E. coli* as production host, as antibody fragments can be successfully expressed[5], [6].

The *E. coli* strain BL21(DE3), created by Studier and Moffatt back in 1986 [7] is often used for industrial production as it allows for high replication rates and shows low acetate formation[8]. In combination with the pET expression system, high transcriptional rates can be achieved[9]. The pET expression system uses the T7 RNA polymerase of the prophage DE3 inserted into the *E. coli* BL21 chromosome under control of the lacUV5 promotor and the pET plasmid contains the target gene under control of the T7 promotor. Upon induction with lactose or an analogue of lactose, the inducer binds the lac repressor which is thus released from the lacUV5 promotor, the T7 RNA polymerase is set free and activates the T7 promotor on the plasmid leading to the transcription of the target gene[10], [11]. The principle of the pET expression system is illustrated in figure 1.

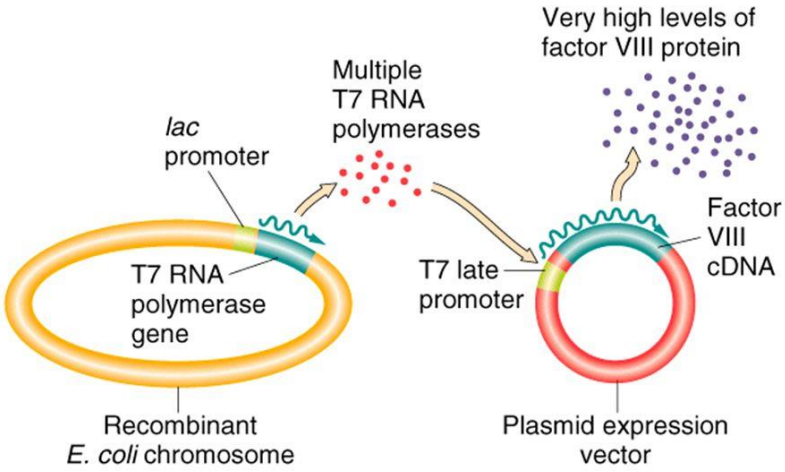

Figure 1. Principle of pET expression system: Expression of T7 RNA polymerase upon induction with lactose or an analogue of it which displaces the lac repressor from the lac promotor. The T7 RNA polymerase in turn activates the T7 promotor on the plasmid leading to the transcription of the target gene.

Using such strong expression systems combined with harsh inducers like IPTG leads to high product yields but also causes a high metabolic burden to the cells, often resulting in intracellular protein aggregates called Inclusion Bodies (IBs)[12].

1.2 Bioprocess technology

Basically, a microbial bioprocess is the conversion of raw material such as sugar into a valuable product by means of microorganisms[13]. With a rapidly growing bioeconomy, the understanding of biological processes to produce biotechnological products applicable in many fields is fundamental. Major sectors include biopharmaceuticals, industrial products and crops[14], [15].

Generally, there are three different modes of operation for a bioprocess, batch, fed batch and continuous mode. In a batch process, the nutrients required are added prior to the cultivation start and the final product is harvested at the end of the process. In a continuous process, the cells are

continuously supplied with nutrients and biomass is removed from the bioreactor at the same flow rate in order to maintain a constant volume[13].

Comprising the advantages of both, batch and continuous mode, fed batch processing is commonly applied for the production of recombinant proteins in *E. coli*[16]. Being increasingly important in bioprocesses, fed batch cultivations lead to increased microbial cell densities, high yields and improved productivities[17] while substrate inhibition, inhibitory by-product formation, end-product inhibition and dissolved oxygen limitations in aerobic cultivations can be reduced[18], [19]. The fed batch process starts with a batch cultivation until all substrate is consumed and feeding is subsequently applied throughout the cultivation process. Unlike continuous cultivation, the cell culture broth remains in the reactor until the cultivation process is finished[13]. Figure 2 shows a simplified scheme of our fed batch cultivation.

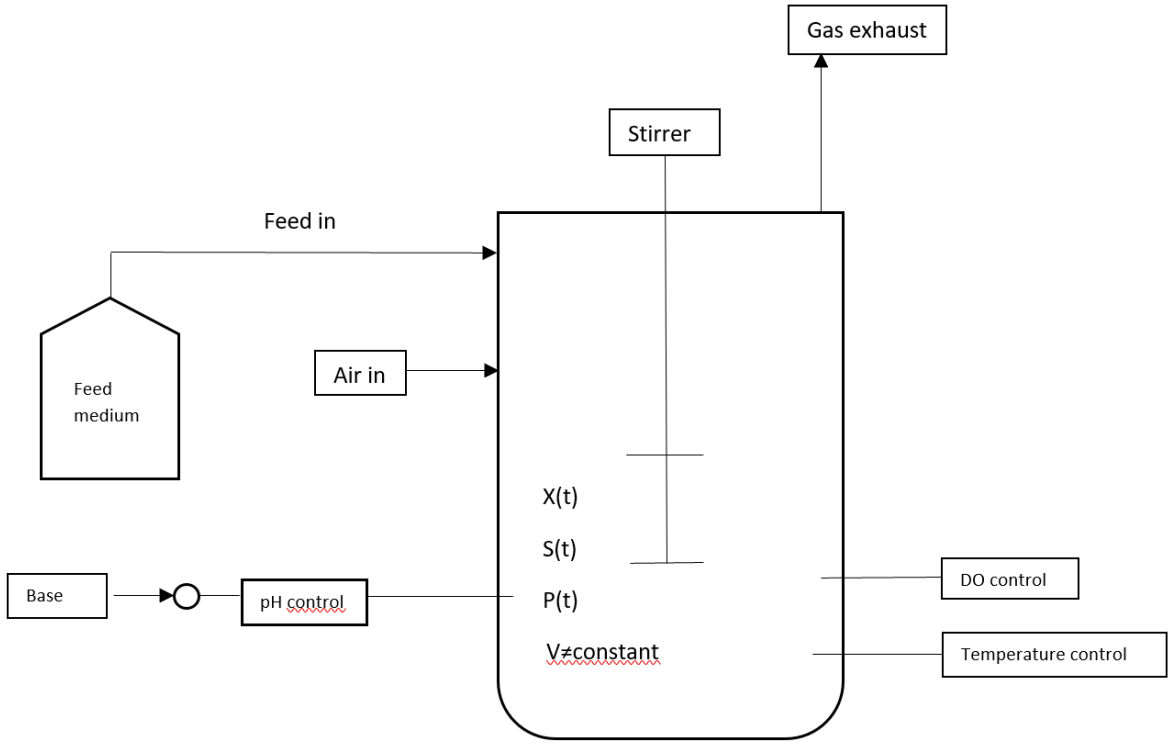

Figure 2. Simplified fed batch cultivation scheme for our cultivation; with X being the biomass concentration [g/L], S the substrate concentration [g/L] and P the product concentration [g/L].

The microbial cultivation process consists of two different phases, the biomass production phase, in which the bacteria grow to a desired cell density, also called non-induced fed batch, and the induction phase where product formation takes place[20].

Different fed batch techniques are available, depending on the feeding strategy. To control the concentration of nutrients in the bioreactor, a feeding strategy needs to be developed since the right concentration of nutrients is vital for the cells[21]. Feeding strategies include feedback methods such as DO-stat or pH-stat as well as pre-determined feeding profiles, exponential feeding[16], [18], [22]. Using an exponential feeding strategy, a constant substrate concentration can be maintained and cells can grow at a constant specific growth rate, but since there is no feedback control, upon overfeeding, substrate accumulation in the culture broth cannot be prevented[18]. However, the formation of acetate, an inhibitory by-product, can be reduced[16].

A bioprocess is generally divided into upstream and downstream processing. Upstream processing comprises everything prior to the cultivation process, vector construction, strain selection and media formulation, including the cultivation process while downstream processing follows the cultivation process and comprises product recovery and purification steps.

1.3 Upstream processing in *E. coli*

In *E. coli*, the product can be either expressed intracellularly in the cytoplasmic space, translocated from the cytoplasmic space into the periplasmic space or secreted into the medium. Protein expression in the cytoplasmic space might lead to aggregation into IBs. The accumulation into IBs might occur due to a lack of disulfide isomerases and chaperones in the cytoplasm that are necessary for correct protein folding[23]. Periplasmic or extracellular protein expression brings several advantages like simplified downstream processing, higher product stability since there are less proteases in the periplasmic space, enhanced biological activity due to proper disulfide bond

formation in the oxidizing environment of the periplasmic space and an authentic N-terminus of the protein as the signal sequence is cleaved off during the transport process[24], [25]. One important application of secretory protein expression in *E. coli* is the production of Fab fragments[26], currently one of the most important biopharmaceutical products[6]. However, major limitations are the production of not correctly folded or aggregated proteins and the inability of *E. coli* to carry out sufficient posttranslational modifications like glycosylation and proteolytic modification[25].

1.4 Downstream processing after expression in *E. coli*

Downstream processing is the most expensive part and major bottleneck in bacterial production processes as most products are expressed intracellularly and therefore many purification steps are required, and the more individual unit operations, the more product is lost. Purification steps are important to separate the product from host cell impurities and remove endotoxins embedded in the outer membrane of *E. coli*. Furthermore, compared to mammalian cells, *E. coli* is not capable of glycosylation and nearly all products relevant in the pharmaceutical industry are glycosylated, that is, such modifications need to be accomplished in DSP[22].

The first step in downstream processing is usually the separation of the biomass from the bulk by centrifugation. The subsequent steps are different, depending on the localisation of the product. Figure 3 shows a scheme for the downstream processing of products being expressed extracellularly, intracellularly or as Inclusion Bodies *E. coli*.

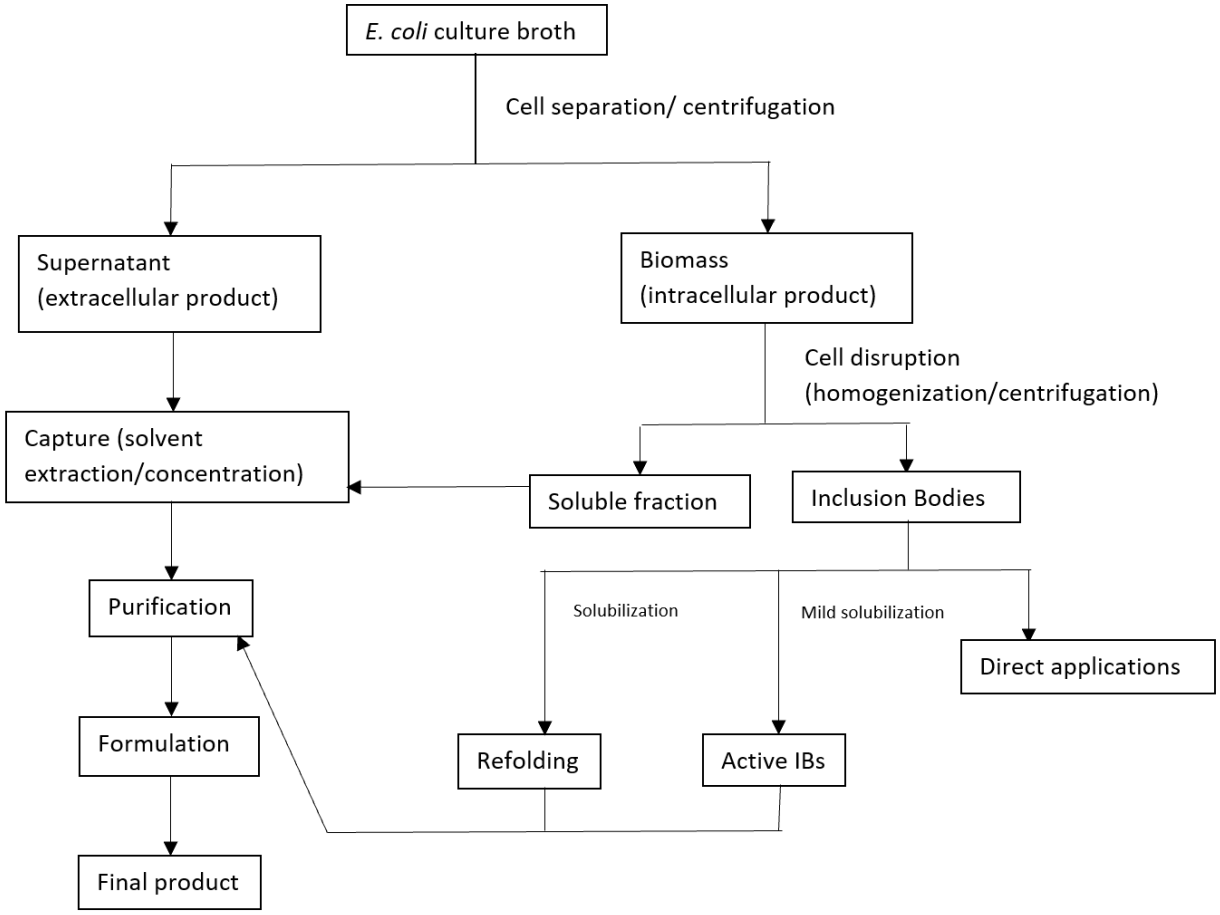

Figure 3. Downstream processing: First, the biomass is separated from the bulk by centrifugation. Intracellular products must be isolated by cell disruption. For the soluble fraction or products contained in the supernatant, subsequent steps involve capture of the product (removal of excess water and components having considerably different properties to the product), product purification (removal of contaminants with physical and chemical properties closely related to that of the product) and formulation (final step in order to stabilize the product for storage). In case of IBs, they must be solubilized and/or refolded after cell disruption to restore their native structure before purification. IBs with biological activity/ native-like protein structure can be used for direct applications.

If the product is expressed intracellularly, the purification is more demanding than for products secreted into the supernatant. To isolate the intracellular product, the cells must be disrupted. This is done either mechanically, chemically, by enzymatic treatment or by a combination of these. The product is then separated from the cells and impurities by centrifugation or filtration. After the separation step, the product is usually concentrated to remove excess water. Depending on the type and amount of product, common purification steps are concentration of the product, filtration,

adsorption, precipitation, solvent extraction, chromatography, and ultrafiltration. The latter is a very effective purification technique and usually the last step in purification for the removal of viruses. Finally, formulation is done to stabilize the product during storage and to maintain the biological activity[27].

The purification and recovery of Inclusion Bodies being misfolded aggregates is most sophisticated since the aggregated proteins must be solubilized after cell disruption and refolded[28]. The cells are broken apart mechanically, using ultrasonication, French press or high-pressure homogenization. After isolation, IBs undergo several washing steps to remove host impurities. Due to their compactness, IBs can be easily purified from cellular impurities by physical separation like centrifugation[3]. Afterwards, IBs are commonly solubilized using chaotropic reagents such as urea or guanidine hydrochloride, which in high concentrations might lead to product degradation, resulting in poor protein recovery yields[3]. In contrast, mild solubilization using organic solvents is suggested for IBs having native-like protein structure since the secondary protein structure can be preserved. This does not require refolding and thus leads to enhanced recovery yields[29].

Protein refolding of solubilized proteins, a crucial and time-consuming step, is commonly achieved by dilution in refolding buffer or by dialysis against a refolding buffer[30]. Furthermore, different chromatographic methods are available for refolding[29]. Using chromatographic beds, the refolding procedure can be coupled to the removal of solubilization agent and protein purification, which minimizes the purification steps and increases the refolding yield[31], but anyway these procedures implicate high costs and hence, their industrial application is limited[29].

A major drawback is the loss of biological activity during extensive protein recovery steps. However, this can be compensated by high expression levels and the enrichment of active protein in Inclusion Bodies[3], [25].

1.5 Inclusion Bodies and applications

Inclusion Bodies are insoluble protein aggregates, formerly considered to be waste products[32] until discovered that the accumulation of proteins occurs due to specific stress reactions like strong overexpression, high inducer concentrations, pH shifts, high temperatures and feeding rates, resulting in biologically inactive proteins[33]. Such IBs can be exploited for the production of toxic or unstable proteins that can be easily refolded in vitro[34]. Efficient refolding procedures are established today, but this time-consuming step to gain active protein for therapeutic use is a major drawback[32].

By the discovery that Inclusion Bodies contain a reasonable amount of correctly folded and thus biologically active protein, the misconception of IBs being inactive products composed of unfolded or misfolded proteins has changed in recent years[35], [36]. Showing high specific activities suggests an enrichment of active protein within IBs, making them important tools in the industrial biotechnological market and for biomedical applications[37], [38]. Catalytically active IBs (CatIBs) as carrier-free protein immobilizates are promising biomaterials for synthetic chemistry, biocatalysis and biomedicine[39].

Furthermore, the correctly folded polypeptides within IBs coexist with an amyloid like intermolecular beta-sheet structure conferring mechanical stability to IBs[40], [41]. Thus, IBs can be useful systems for therapeutic approaches studying pathologic protein deposition in amyloid diseases like Alzheimer's or Parkinson's disease, in which the accumulation of proteins initiates the pathogenic process[42]–[45].

IBs also unveil high potential in biomedical applications in vivo as delivery vehicles or 'nanopills' for prolonged drug release[46]–[49]. Active IBs as nanostructured amyloidal particles of 50-500 nm are considered as mimetics of the endocrine secretory granules as they naturally penetrate mammalian cells and release their protein in soluble and functional form under physiological

conditions[50]. Decorating 3D-scaffolds with bacterial IBs favouring mammalian cell surface colonization and stimulating proliferation, allows for penetration and intracellular delivery of functional protein in absence of cytotoxicity and hence, offers possibilities in tissue engineering and regenerative medicine[51]–[53]. However, IBs for the use in biomedicine are constrained by their bacterial origin and undefined composition. To overcome these constraints, the creation of artificial IBs resulting in homogenous protein reservoirs for prolonged in vivo delivery of tumour-targeted drugs has been reported lately[54].

1.6 The influence of upstream process parameters on IBs

Upstream process parameters including physical and chemical process parameters like temperature, pH, the media composition as well as the feeding strategy affect process variables. During a fed batch cultivation, physiological parameters are controlled based on the real-time values of specific growth rate, substrate consumption, temperature, pH, oxygen supply, and biomass production[13]. Amongst other factors, the formation of Inclusion Bodies is influenced by variation of upstream process parameters during the production phase. Stress factors leading to protein aggregation into IBs include high temperature, pH shifts and high physiological feeding rates. To increase productivity and activity, upstream process parameters need to be optimized for the individual product. Furthermore, optimization of the upstream process can have a positive influence on IB DSP[55], [56].

Using a DoE approach, critical process parameters (CPP) can be evaluated to assess the influence of variations in CPP on critical quality attributes of the product. These quality attributes are monitored during the production process and analysed in a time resolved manner and change during the cultivation process. These data are used to control upstream process parameters and thus QAs.

High temperature leads to strong overexpression which favors IB formation, but on the other side imposes stress on the cell which might lead to product degradation. In contrast, low temperature during the cultivation results in a higher amount of correctly folded protein within IBs and therefore reveals biological activity[36]. IB size and titer can be controlled by the specific substrate feeding rate. High feeding rate boosts titer and size of IBs early in the induction phase, but also leads to early sugar accumulation, increased number of dead cells and product degradation. Low $q_{s,C}$ values are recommended for the production of IBs with defined size as the sizes are longer stable throughout the induction phase, but also result in low IB titers. Using IPTG as inducer, IB size is highly dependent on the fed C-source ($q_{s,C}$)[57]. Furthermore, the pH of the medium influences the activity and stability of the protein. Previously, optimal pH to boost IB size was determined to 6.7 and using glycerol as C-source has a positive effect on the titer[56].

Since upstream process parameters have a great impact on the amount of native secondary structures within IBs and as the production of active IBs for direct application becomes more important, control of upstream process parameters and understanding of their influence on IB quality attributes gets more relevant[58].

1.7 Hyaluronidase of *Apis mellifera*

The enzyme hyaluronidase is a bee venom allergen that induces severe and fatal anaphylactic IgE-mediated reactions in humans[59]. In 2000, the 3D structure of *Apis mellifera* hyaluronidase was the first to be reported for this enzyme[60].

Hyaluronidases degrade hyaluronan, a high molecular weight glycosaminoglycan, by cleaving the ß-1,4 glycosidic bonds between N-acetylglucosamine and glucuronate, which results in tetrasaccharides. Hyaluronan is a ground substance of connective tissue and plays an important structural role in the extracellular matrix[59]. By cleaving hyaluronan, the penetration of other

toxins and drugs in the skin is facilitated and the diffusion rates and absorption of molecules up to 200 nm in diameter are increased[61].

Hyaluronan also promotes growth and spread of tumour cells. As hyaluronidases enhance the local diffusion of drugs into tissues and tumours, they have the potential for the development of anti-cancer drugs by degrading cancer-cell associated hyaluronan[62], [63]. Furthermore, recombinant hyaluronidases promote wound healing and reduce edema, they have an immunogenic potential in allergy diagnosis and immunotherapy, which makes them promising tools for the treatment of diseases[61].

Duran-Reynals et. al. were the first to identify hyaluronidase activity in 1928[64]. Another study showed that recombinant hyaluronidase produced in *E. coli* as inclusion body reached only 20 %-30 % of the activity of natural hyaluronidase[65].

1.8 Aim of this study and scientific questions

In this study we aimed for the expression of hyaluronidase from *Apis mellifera* as model enzyme for active Inclusion Bodies and for possible direct applications. For recombinant protein expression, *E. coli* BL21(DE3) was used as expression host in combination with the pET expression system and IPTG as inducing agent. Following scientific questions were raised during this thesis

- Has the hyaluronidase gene of *Apis mellifera* been successfully cloned into the pET28a(+) plasmid?
- Can the hyaluronidase of *Apis mellifera* be successfully expressed in *E. coli* BL21(DE3) as Inclusion Bodies?
- Can the hyaluronidase of *Apis mellifera* be used as model enzyme for active Inclusion Bodies and hence direct applications?

2 Materials and Methods

2.1 Strains

Hyaluronidase *E. coli* BL21(DE3) was used with the pET28a(+) plasmid system (kanamycin resistance) for recombinant protein production. Following 1155 kb gene long from *Apis mellifera* was codon optimized for *E. coli* and cloned at NdeI and XhoI into the pet plasmid by General Biosystems (NC, USA) and subsequently electroporated.

CAT
ATGAGCCGTCCGCTGGTTATTACCGAAGGCATGATGATTGGCGTTCTGCTGATGCTGGCACCGATTAATGCCCTGCTGCTGGGTTTT
GTTCAGAGCACCCCGGATAATAATAAGACCGTGCGTGAATTCAATGTGTATTGGAATGTGCCGACCTTTATGTGTCATAAATATGG
CCTGCGTTTTGAAGAAGTTAGCGAAAAATATGGTATCCTGCAGAATTGGATGGATAAATTTCGCGGTGAAGAAATTGCAATTCTGT
ATGATCCGGGCATGTTTCCGGCACTGCTGAAAGATCCGAATGGTAATGTTGTTGCCCGTAATGGTGGCGTGCCGCAGCTGGGTAAT
CTGACCAAACATCTGCAGGTGTTTCGCGATCATCTGATTAATCAGATTCCGGATAAAAGCTTTCCGGGTGTTGGTGTGATTGATTTT
GAAAGCTGGCGCCCGATTTTTCGCCAGAATTGGGCCAGTCTGCAGCCGTATAAAAAACTGAGTGTGGAAGTTGTTCGTCGCGAAC
ATCCGTTTTGGGATGATCAGCGTGTGGAACAGGAAGCCAAACGCCGTTTTGAAAAATATGGCCAGCTGTTTATGGAAGAAACCCT
GAAAGCCGCAAAACGCATGCGTCCGGCCGCCAATTGGGGCTATTATGCCTATCCGTATTGCTATAATCTGACCCCGAATCAGCCGA
GCGCCCAGTGTGAAGCAACCACCATGCAGGAAAATGATAAAATGAGTTGGCTGTTTGAAAGCGAAGATGTTCTGCTGCCGAGCGT
GTATCTGCGCTGGAATCTGACCAGTGGTGAACGTGTTGGCCTGGTTGGTGGTCGTGTTAAAGAAGCACTGCGCATTGCACGTCAGA
TGACCACCAGCCGCAAAAAAGTTCTGCCGTATTATTGGTATAAGTATCAGGATCGTCGCGATACCGATCTGAGCCGTGCAGATCTG
GAAGCAACCCTGCGCAAAATTACCGATCTGGGTGCAGATGGCTTTATTATTTGGGGTAGCAGTGATGATATTAATACCAAAGCCAA
ATGCCTGCAGTTTCGTGAATATCTGAATAATGAACTGGGCCCGGCCGTGAAACGCATTGCACTGAATAATAATGCCAATGATCGTC
TGACCGTGGATGTGAGCGTTGATCAGGTT
CTCGAG

E. coli BL21(DE3) was grown on LB agar plates[66]. For propagation, one colony from the plates was transferred into one mL LB broth, incubated at 37 °C overnight. 600 µL from this bacteria solution were further transferred into 44 mL LB broth in an Erlenmeyer flask and cultivated for two hours at 37 °C. For transfection, the plasmid (5 µg lyophilized) was dissolved in 50 µL ultrapure water (MQ) and diluted to a concentration of about 50 ng/µL. One mL of the bacteria solution was centrifuged and washed two times with ultrapure water. 20 µL of the competent cells were mixed with one µL plasmid in a cuvette and transformed via electroporation at 1342 V for 6.4 ms. The cells were transferred into one mL LB broth and incubated for two hours at 37 °C. To

check for the transformation, the cells were grown on LB agar plates containing 15 µg/µL kanamycin, using 50, 100 and 150 µL bacterial suspension, respectively. For the negative control, 100 µL bacterial suspension without plasmid were used. All plates were incubated at 32 °C overnight. Colonies grew on all plates except for the control plate. For further cultures 30 µg/µL kanamycin was used.

Single cultures were picked, and eight liquid cultures were prepared using two mL LB broth. Four were incubated at 37 °C and 30 °C, respectively. After 44 hours, three cultures incubated at 30 °C and two incubated at 37 °C showed growth. These were chosen to purify the plasmid DNA using GeneJET Plasmid Miniprep Kit from Thermo Scientific, resulting in 30 µL plasmid DNA. The plasmid concentrations were determined via NanoDrop spectrophotometer (Thermo Scientific, Waltham, MA, USA).

(Another five liquid cultures were prepared using five mL LB broth with five µL of the respective bacteria solutions. After incubation, the plasmid DNA was purified again (using MQ instead of elution buffer) and the concentrations were determined.) The bacteria culture having the highest plasmid DNA concentration (211.9 ng/µL) was chosen to be sequenced using the primer pET-up (Microsynth, Switzerland). The sequences are shown below.

Primer pET-up sequence

ATGCGTCCGGCGTAG

Aligned blast sequence of hyaluronidase gene

ATGAGCCGTCCGCTGGTTATTACCGAAGGCATGATGATTGGCGTTCTGCTGATGCTGGCACCGATTAATGCCCTGCTGCTGGGTTTT
GTTCAGAGCACCCCGGATAATAATAAGACCGTGCGTGAATTCAATGTGTATTGGAATGTGCCGACCTTTATGTGTCATAAATATGT
TTGAAGAAGTTAGCGAAAAATATGGTATCCTGCAGAATTGGATGGATAAATTTCGCGGTGAAGAAATTGCAATTCTGTATGATCCG
GGCATGTTTCCGGCACTGCTGAAAGATCCGAATGGTAATGTTGTTGCCCGTAATGGTGGCGTGCCGCAGCTGGGTAATCTGACCAA
ACATCTGCAGGTGTTTCGCGATCATCTGATTAATCAGATTCCGGATAAAAGCTTTCCGGGTGTTGGTGTGATTGATTTTGAAAGCTG
GCGCCCGATTTTTCGCCAGAATTGGGCCAGTCTGCAGCCGTATAAAAAACTGAGTGTGGAAGTTGTTCGTCGCGAACATCCGTTTT
GGGATGATCAGCGTGTGGAACAGGAAGCCAAACGCCGTTTTGAAAAATATGGCCAGCTGTTTATGGAAGAAACCCTGAAAGCCGC
AAAACGCATGCGTCCGGCCGCCAATTGGGGCTATTATGCCTATCCGTATTGCTATAATCTGACCCCGAATCAGCCGAGCGCCCAGT
GTGAAGCAACCACCATGCAGGAAAATGATAAAATGAGTTGGCTGTTTGAAAGCGAAGATGTTCTGCTGCCGAGCGTGTATCTGCG
CTGGAATCTGACCAGTGGTGAACGTGTTGGCCTGGTTGGTGGTCGTGTTAAAGAAGCACTGCGCATTGCACGTCAGATGACCACCA

GCCGCAAAAAAGTTCTGCCGTATTATTGGTATAAGTATCAGGATCGTCGCGATACCGATCTGAGCCGTGCAGATCTGGAAGCAACC
CTGCGCAAAATTACCGATCTGGGTGCAGATGGCTTTATTATTTGGGGTAGCAGTGATGATATTAAT-AATGCCTGCAGTTTCNTGAA

Finally, Cryos were prepared by mixing one mL bacteria solution with 175 µL 75 % Glycerol each and stored at -80°C as starting material for fermentations.

2.2 Bioreactor cultivations

All bioreactor and preculture cultivations were carried out using the strain *E. coli* BL21(DE3) together with the pET28a(+) plasmid system consisting of the hyaluronidase gene of *Apis mellifera*. A defined minimal medium referred to DeLisa et al. (1999)[67] was used throughout all cultivations. As carbon source, glycerol was used. Batch media and the preculture media had the same composition with different amounts of glycerol - 8 g/L for the preculture, 20 g/L for the batch phase. The feed for uninduced and induced fed-batch had a concentration of 400 g/L glycerol.

Table 1. DeLisa Media composition of preculture, batch and fed batch cultivation.

	Preculture	Batch	Fed Batch
Medium components	*Final conc. [g/L]*		
Glycerol	8.00	20.00	400
KH_2PO_4	13.30	13.30	-
$(NH_4)_2HPO_4$	4.00	4.00	-
Citric acid	1.70	1.70	-
Trace elements	*Stock add. [mL/L]*		
$MgSO_4$ * 7 H_2O (stock 500x)	2.00	2.00	16.67
Fe(III) citrate (stock 100x)	10.00	10.00	2.00
EDTA (stock 100x)	10.00	10.00	7.74
$Zn(CH_3COO)_2$ * 2 H_2O (stock 200x)	5.00	5.00	3.08
TE (stock 200x)	5.00	5.00	7.27
Thiamine HCl (stock 1000x)	1.00	1.00	-
Kanamycin (stock 500x)	2.00	2.00	-

The DeLisa media were autoclaved together with the sugar solutions, trace element solutions were autoclaved separately. After the solutions had cooled down, the trace elements were added to the medium under sterile conditions. Antibiotic was added throughout all fermentations, resulting in a final concentration of 0.02 g/L of kanamycin. All precultures were performed using 500 mL high yield flasks. They were inoculated with 1.5 mL of bacteria solution stored in cryos at -80 °C and subsequently cultivated for 20 h at 230 rpm in an Infors HR Multitron shaker (Infors, Bottmingen Switzerland) at 37 °C. IPTG was added once to start induction and had a final concentration of 0.5 mM inside the reactor.

Screening for recombinant protein production was performed in a DASGIP Mini bioreactor-4-parallel fermenter system (max. working volume: 2.5 L; Eppendorf, Hamburg, Germany). Cultivation offgas was analyzed by gas sensors - IR for CO_2 and ZrO_2 based for O_2 (Blue Sens Gas analytics, Herten, Germany).

Process control was established using the DAS-GIP-control system, DASware-control, which logged the process parameters. During batch-phase and fed-batch phase pH was kept constant at 6.7 and controlled with base only (12.5 % NH_4OH), while acid (5 % H_3PO_4) was added manually, when necessary. The pH was monitored using an EasyFerm Plus pH-sensor (Hamilton, Reno, NV, USA). The reactors were continuously stirred at 1400 rpm and aerated using a mixture of pressurized air and pure oxygen at 2 vvm. Dissolved oxygen (dO_2) was always kept higher than 30 % by increasing the ratio of oxygen in the ingas. The dissolved oxygen was monitored using a fluorescence dissolved oxygen electrode Visiferm DO (Hamilton, Reno, NV, USA) The fed batch phase for biomass generation was followed by an induction phase.

2.3 Cultivation scheme

All DASGIP bioreactors contained 1 L batch medium. DeLisa medium [67] and glycerol were sterilized by autoclavation in the bioreactor and trace elements were added after sterile filtration. The bioreactors were inoculated with 100 mL preculture showing an OD_{600} between 6 and 9. The batch process was run at 37 °C and took around 8 hours, a drop in the CO_2 signal indicates the end of the batch. After the batch, OD_{600} was measured to calculate the biomass concentration needed to adapt growth rate μ and feeding rate $q_{s,C}$ for the non-induced fed batch process which was run overnight. The biomass concentration after the batch was about 10 g/L, μ was set between 0.08-0.09 1/h to gain a biomass of about 30 g/L after non-induced fed batch.

Prior to induction, $q_{s,C}$ and temperature were adjusted. The feeding strategy used was an exponential feed forward approach. To control and maintain a constant $q_{s,C}$, the feed rate was adapted according to equation 1[68]:

$$F(t) = \frac{q_{s,C} * X(t) * \rho_f}{c_f} \qquad \text{Equation 1}$$

with F being the feed rate [g/h], $q_{s,C}$ the specific glycerol uptake rate [g/g/h], X the absolute biomass [g], ρ_f the feed density [g/L] and c_f the feed concentration [g/L], respectively.

IB production was triggered in the induction phase. The fed batch was induced using 1.3 mL IPTG of 1000x stock resulting in a final concentration of 0.5 mM inside the reactor. Specific substrate feeding rate ($q_{s,C}$) and temperature in the induction phase were adapted according to the design of experiments (DoE) given in Figure 4. $q_{s,C}$ was altered between 0.1 g/g/h and 0.5 g/g/h and temperature between 25 °C and 35 °C. The center point at 30 °C and 0.3 g/g/h was cultivated four times to assess statistical experimental error.

Induction phase lasted 8 hours, samples were taken every 2 hours.

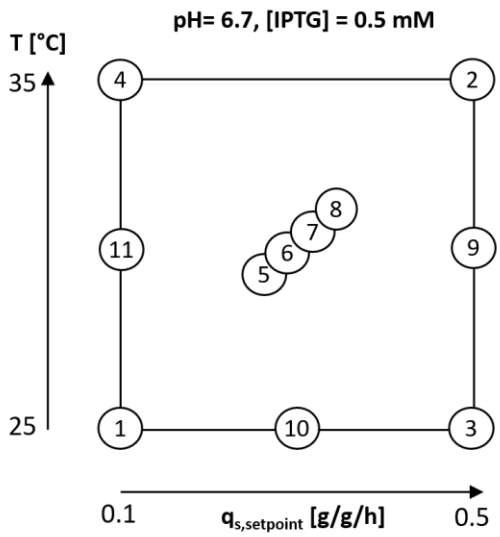

Figure 4. DoE for process optimization to produce recombinant Hyaluronidase. Experiments 1 -7 were performed in a full factorial design. Additional experiments 8-11 were subsequently performed to screen for quadratic interactions in the region of interest.

2.4 Cultivation Analytics

2.4.1 Biomass

For dry cell weight (DCW) measurements 1 mL of the cultivation broth was centrifuged at 9000 g, subsequently washed with 0.9 % NaCl solution and centrifuged again under the same conditions. After drying the cells at 105 °C for 48 h the pellet was evaluated gravimetrically. DCW measurements were performed in three replicates and the mean error for DCW was about 3 %. Offline OD_{600} measurements were performed in duplicates in a UV/VIS photometer Genisys 20 (Thermo Scientific, Waltham, MA, US).

2.4.2 Sugar analytics

Glycerol and acetate concentrations in the filtered fermentation broth were determined using a Supelco C-610H HPLC column (Supelco, Bellefonte, PA, USA) on an Ultimate 300 HPLC system (Thermo Scientific, Waltham, MA, US) using 0.1 % H_3PO_4 as running buffer at 0.5 mL/min or an

Aminex HPLC column (Biorad, Hercules; CA, USA) on an Agilent 1100 System (Agilent Systems, Santa Clara, CA, USA) with 4 mM H_2SO_4 as running buffer at 0.6 mL/min. Data were analyzed using Chromeleon software. To determine the concentrations, glycerol, and acetate calibration standards within a concentration range of 1-50 g/L were used.

2.4.3 Cell viability

Cell viability during induction phase was measured using flow cytometry (FCM). The principle of FCM is demonstrated in figure 5[69].

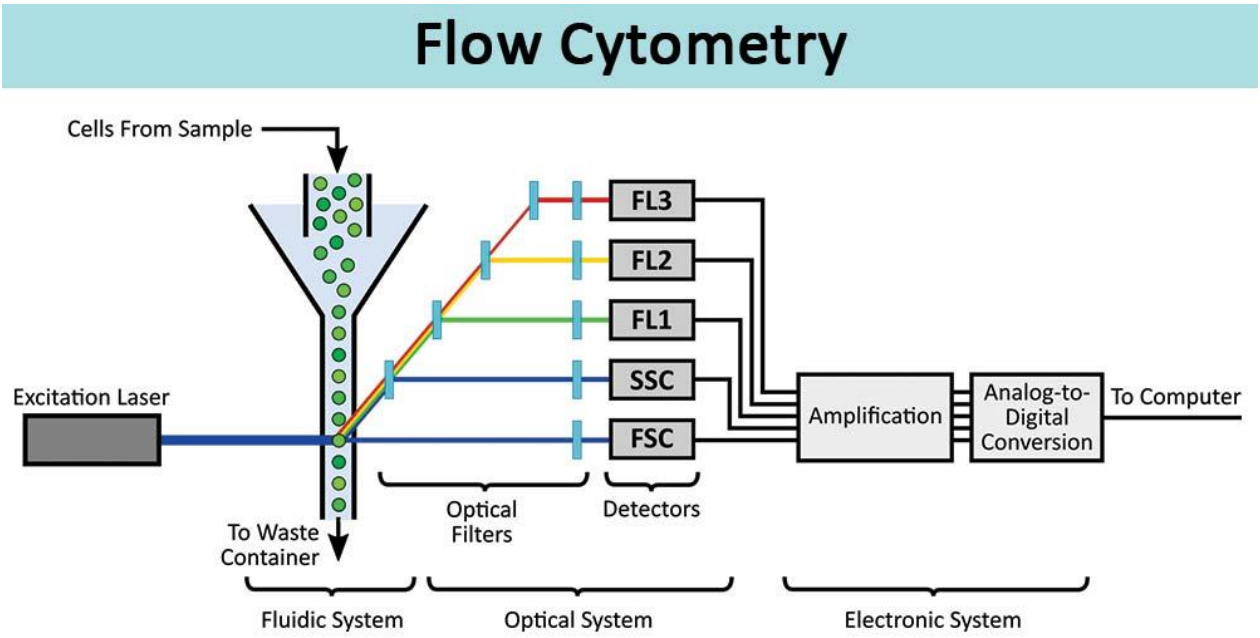

Figure 5. FCM principle. A mixture of suspended fluorescent tagged cells passes through a laser-detector system that monitors the fluorescent and light scatter characteristics. The fluorescent emission is related to the amount of fluorescent probe bound to the cell. FSC (forward scatter) is proportional to cell size; SSC (side scatter) indicates cell granularity. Fluorescence patterns of each subpopulation, combined with FSC and SSC data, are used to identify which cells are present in a sample.

The cultivation broth was diluted 1:100 with filtered 0.9 % NaCl solution and stored at 4 °C. Before measurement, the samples were diluted further according to their OD_{600} (dilution – OD_{600} x 100).

The software Cube 8 (Sysmex, Partec, Görlitz, Germany) according to Langemann et al.[70] was used.

DiBAC4 (Bis-(1,3-Dibutylbarbituric Acid)Trimethine Oxonol) and RH414 (*N*-(3-Triethylammoniumpropyl)-4-(4-(4-(Diethylamino)phenyl)Butadienyl)Pyridinium Dibromide) were used to stain the cells. The membrane potential-sensitive fluorescent dye DiBAC4 enters depolarized membranes and binds to intracellular proteins and membranes, which makes it possible to distinguish between living and dead cells. The second dye, RH414, which stains all plasma membranes, is used to exclude non-cellular background. Stock solutions of 0.5 mM DiBAC4 and 2 mM RH414 were prepared in DMSO and stored at -20 °C. For measurements, 1.5 µL of each dye were added to 1 mL diluted cultivation broth. Data was evaluated using the software FCS express V4. For analysis, data are defined by a gate set after the batch process, where cells inside the gate indicate for dead cells. Dead cells (%) were calculated as follows:

$$\frac{dead\ cells}{all\ cells - dirt} * 100 \qquad \text{Equation 2}$$

2.4.4 IB Preparation

5 mL fermentation broth samples were centrifuged at 4800 rpm at 4 °C. The supernatant was discarded, and the pellet was resuspended using an Ultra-Turrax to a DCW of about 4 g/L in lysis buffer (100 mM Tris, 10 mM EDTA at pH = 7.4). Afterwards the sample was homogenized using a high-pressure homogenizer at 1500 bar for 10 passages (PandaPLUS, Gea AG, Germany). After centrifugation at 10000 rpm and 4 °C the supernatant was discarded and the resulting IB pellet was washed twice with ultrapure water and aliquoted into pellets à 2 mL broth, centrifuged (14000 rpm, 10 min 4 °C) and stored at -20 °C.

2.4.5 IB Size

Washed and aliquoted IB samples were resuspended in ultrapure water. 100 µL of appropriate dilution of the suspension were pipetted on a gold-sputtered (10 - 50 nm) polycarbonate filter (Millipore-Merck, Darmstadt, Germany) using reusable syringe filter holders with a diameter of 13 mm (Sartorius, Göttingen, Germany). 100 µL of ultrapure water were added and pressurized air was used for subsequent filtration. Additional 200 µL of ultrapure water were used for washing. The wet filters were fixed on a SEM sample holder using graphite adhesive tape and subsequently sputtered with gold to increase the contrast of the sample. SEM was performed using a QUANTA FEI SEM (Thermo Fisher, Waltham, MA, US) with a secondary electron detector[71]. The acceleration voltage of the electron beam was set between 3 to 5 kV. To determine the diameter of the IBs, 50 IBs on SEM pictures were measured using the ImageJ plugin Fiji (Laboratory for Optical and Computational Instrumentation (LOCI), University of Wisconsin-Madison, US).

2.4.6 IB Titer

For titer measurements IB pellets were solubilized using solubilization buffer (7.5 M guanidine hydrochloride, 62 mM Tris at pH = 8). The filtered samples were quantified by HPLC analysis. The HPLC was equipped with a BioResolve RP mAb Polyphenyl column (dimensions 100 x 3 mm, particle size 2.7 µm) which is designed for mAb and large protein analyses (Waters Corporation, MA, USA). To prolong column lifetime, a pre-column (3.9 *5 mm, 2.7 µm) was used. The mobile phase was composed of ultrapure water (=MQ, eluent A) and acetonitrile (eluent B) both supplemented with 0.10 % (v/v) trifluoroacetic acid. The injection volume was set to 2.0 µL. The flow rate and the column temperature of the final method were 0.4 mL/min and 70 °C, respectively.

For evaluation, the areas under the peaks in the chromatogram were identified and the protein concentration was determined using a BSA standard calibration with BSA standards prepared in

ultrapure water containing 0.1 % (v/v) formic acid ranging from 5-50 mg/L. Details on the measurement methodology is given in 'Development of a generic reversed-phase liquid chromatography method for protein quantification using analytical quality-by-design principles'[72].

2.4.7 IB activity

2.4.7.1 Activity assay

To determine the activity, a turbidimetric activity assay according to SigmaAldrich (Enzymatic Assay of Hyaluronidase (3.2.1.35)) was used. Washed IB pellets were resuspended in 100 µL ultrapure water and mixed with 71 µL Enzyme diluent (20 mM Sodium Phosphate with 77 mM Sodium Chloride and 0.01% (w/v) Bovine Serum Albumin at pH 7.0), the respective suspension was incubated for 10 min at 230 rpm in an Infors HR Multitron shaker (Infors, Bottmingen Switzerland) at 37 °C. Then, 171 µL hyaluronic acid solution (0.03 % (w/v) in 300 mM Sodium phosphate buffer at pH 5.35) was added and the mixed samples were incubated again at 230 rpm at 37 °C, for 45 minutes. To stop the reaction, 150 µL of the sample solution were transferred into cuvettes containing 750 µL acidic albumin solution (24 mM Sodium Acetate, 79 mM Acetic Acid with 0.1% (w/v) bovine serum albumin at pH 3.75), mixed by inversion and incubated for 10 min at RT. After 10 minutes, % transmittance at 600 nm was measured using a UV/VIS photometer Genisys 20 (Thermo Scientific, Waltham, MA, US). The activity (U/mL) was calculated using a calibration curve generated with a commercial hyaluronidase of bovine testes (SigmaAldrich). The enzymatic reaction upon hyaluronan degradation is given in equation 3:

$$HA + Hya \rightarrow Di - and\ monosaccharides + smaller\ HA\ fragments \qquad \text{Equation 3}$$

2.4.7.2 FT-IR spectroscopy

For FT-IR measurements, IB pellets were concentrated via centrifugation and resuspended in ultrapure water according to the dilution needed. FT-IR absorption measurements of IB activity monitoring was performed using a Bruker Vertex 70V FT-IR spectrometer (Ettlingen, Germany) equipped with a Bruker Optics Platinum ATR module (diamond crystal, 1 mm^2 area with single reflection) and a liquid nitrogen cooled HgCdTe (mercury cadmium telluride) detector. To start the enzymatic reaction, 15 µL of IB at different concentrations were mixed with 15 µL hyaluronan (sodium salt from *Streptococcus equi*, bacterial glycosaminoglycan polysaccharide, No. 53747, Sigma Aldrich) with a concentration of 1, 2.5 and 5 mg/mL respectively and thoroughly vortexed. The sample solution was then placed on the ATR crystal and covered with a cap to prevent solvent evaporation during spectra acquisition. ATR-FT-IR spectra were collected every minute for a time period of 40 minutes. For IB concentration determination, commercially obtained hyaluronidase type I-S from bovine testes (No. H3506, Sigma Aldrich) was used for calibration and the amide II band height was evaluated. Spectra were acquired with a spectral resolution of 4 cm^{-1} in double-sided acquisition mode; the mirror velocity was set to 80 kHz. A total of 450 scans were averaged per spectrum, which was calculated using a Blackman-Harris 3-term apodization function and a zero-filling factor of 2. All spectra were acquired at 25 °C. Spectra were analyzed using the software package OPUS 8.1 (Bruker, Ettlingen, Germany).

3 Results and Discussion

The goal of this study was to investigate how the IB QAs titer, size and activity can be influenced by altering the upstream process parameters temperature and specific substrate uptake rate ($q_{s,C}$) during the induced fed batch cultivation. In a DoE, the QAs titer and size were monitored as a function of induction time and analyzed in a time-resolved manner. As IB QAs strongly depend on

upstream process conditions, the aim was to find optimal temperature and $q_{s,C}$ in order to boost size, activity and titer.

Temperature and pH effect the biological activity of IBs, especially during the induction phase. As a pH of 6.7 has already been validated for optimal IB QAs[56], we investigated the impact of temperature, by varying it between 25 and 35 °C. Furthermore, IB QAs depend on the specific uptake rate of the C-source. We used glycerol as C-source because it is reported to increase the specific IB productivity[73]. The specific substrate uptake rate was altered between 0.1 and 0.5 g/g/h. For statistical evaluation, four center points were measured at 30 °C and 0.3 g/g/h.

There is a strong correlation between induction strength and IB size and titer. High $q_{s,C}$ increased titer and size early in the induction phase, but lead to sugar accumulation and therefore an increased number of dead cells. During the cultivation, the viable cell concentration was determined via FCM to control the stability of the process. Furthermore, according to previous studies, low temperature seems to be beneficial to produce IBs.

Production of hyaluronidase IBs within *E. coli* was induced with IPTG and the induction phase lasted for 12 hours. Samples were taken every 2 hours during the induction phase and analyzed as described in the Material and Methods part.

For statistical evaluation, MODDE 12 was used. The experimental runs with maximum titer, specific titer, glycerol, acetate production and mean productivity are listed in Table 2.

Table 2. List of experimental runs in DoE. 11 runs with T and $q_{s,C}$ alternated according to the DoE were carried out. Maximum titer, specific titer, glycerol, acetate production and the mean productivity are listed in the table.

Exp No	Temperature [°C]	qs.C [g/g/h]	titer max [g/L]	max glycerol [g/L]	max acetate [g/L]	qp mean [g/g/h]	spec titer max [g/g]
1	25	0.1	$17.0*10^{-2}$	-	-	$5.21*10^{-4}$	$14.2*10^{-4}$
2	35	0.1	$10.7*10^{-2}$	-	0.1	$3.05*10^{-4}$	$32.8*10^{-4}$
3	25	0.5	$16.8*10^{-2}$	142.3	7.8	$2.68*10^{-4}$	$68.1*10^{-4}$
4	35	0.5	$2.5*10^{-2}$	161.6	15.5	$0.70*10^{-4}$	$9.6*10^{-4}$
5	30	0.3	$4.0*10^{-2}$	64.9	7.9	$1.81*10^{-4}$	$13.2*10^{-4}$
6	30	0.3	$13.2*10^{-2}$	73.7	15.3	$3.65*10^{-4}$	$66.0*10^{-4}$
7	30	0.3	$8.6*10^{-2}$	87.2	8.5	$1.32*10^{-4}$	$28.6*10^{-4}$
8	30	0.3	$8.9*10^{-2}$	32.5	27.7	$1.85*10^{-4}$	$22.3*10^{-4}$
9	25	0.3	$9.7*10^{-2}$	65.7	1.5	$2.66*10^{-4}$	$31.2*10^{-4}$
10	30	0.1	$1.0*10^{-2}$	1.5	5.3	$5.04*10^{-4}$	$35.1*10^{-4}$
11	30	0.5	$7.1*10^{-2}$	98.9	7.7	$2.74*10^{-4}$	$25.0*10^{-4}$

3.1 Hyaluronidase IB titer

Hyaluronidase IB titers were measured with RP-HPLC and determined via BSA standard calibration.

High $q_{s,C}$ increased the specific titer at early induction times, meaning high feeding rates favored product formation in the beginning of the production phase, but also lead to sugar accumulation early in the induction phase and therefore product degradation. Figure 6a shows high specific titers early in the induction phase and high sugar accumulation for a cultivation at 35 °C and $q_{s,C}$ of 0.5 g/g/h.

Figure 6b shows 3 different cultivations. At lowest T and $q_{s,C}$ set point, the titer was highest in the beginning and decreased afterwards, but remained relatively stable in the end due to nearly no sugar accumulation and consequently less product degradation. For high $q_{s,C}$ (0.5 g/g/h) and low T (25 °C), the titer was very high in the beginning and quickly decreased after 4h induction time. At the highest setpoints, the specific titers were low compared to the other two cultivations given in the figure 6b.

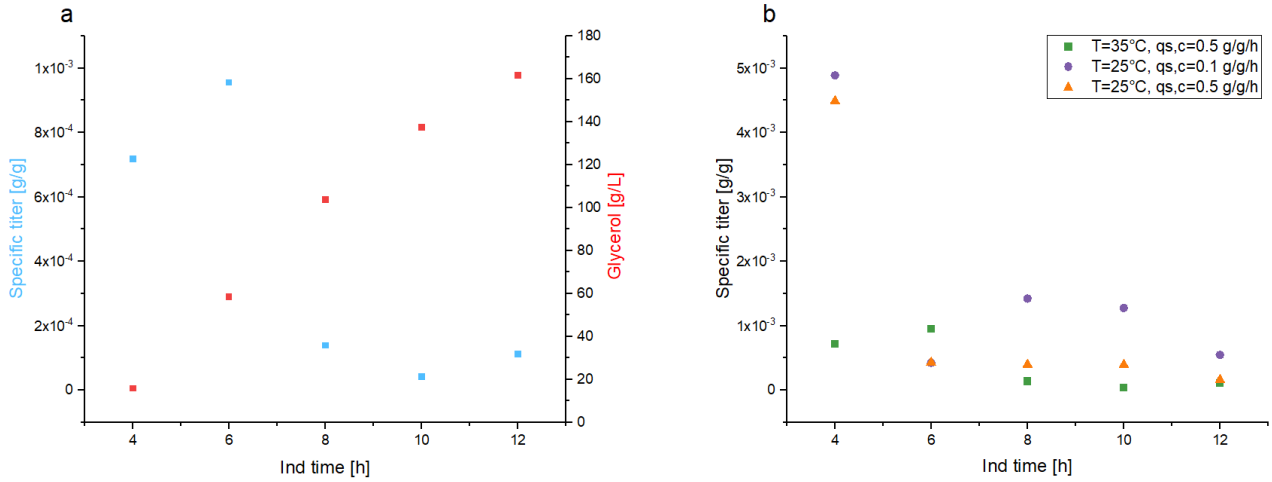

Figure 6.**a)** specific titer and glycerol concentration over induction time for a cultivation at T = 35 °C and $q_{s,C}$ = 0.5 g/g/h. Blue spots indicate for the specific titer, red spots indicate for glycerol concentration; **b)** Effect of applied $q_{s,C}$ and temperature on the specific titer over induction time.

Time-dependent cultivation responses for all center point cultivations are given in figure 7, including standard deviations.

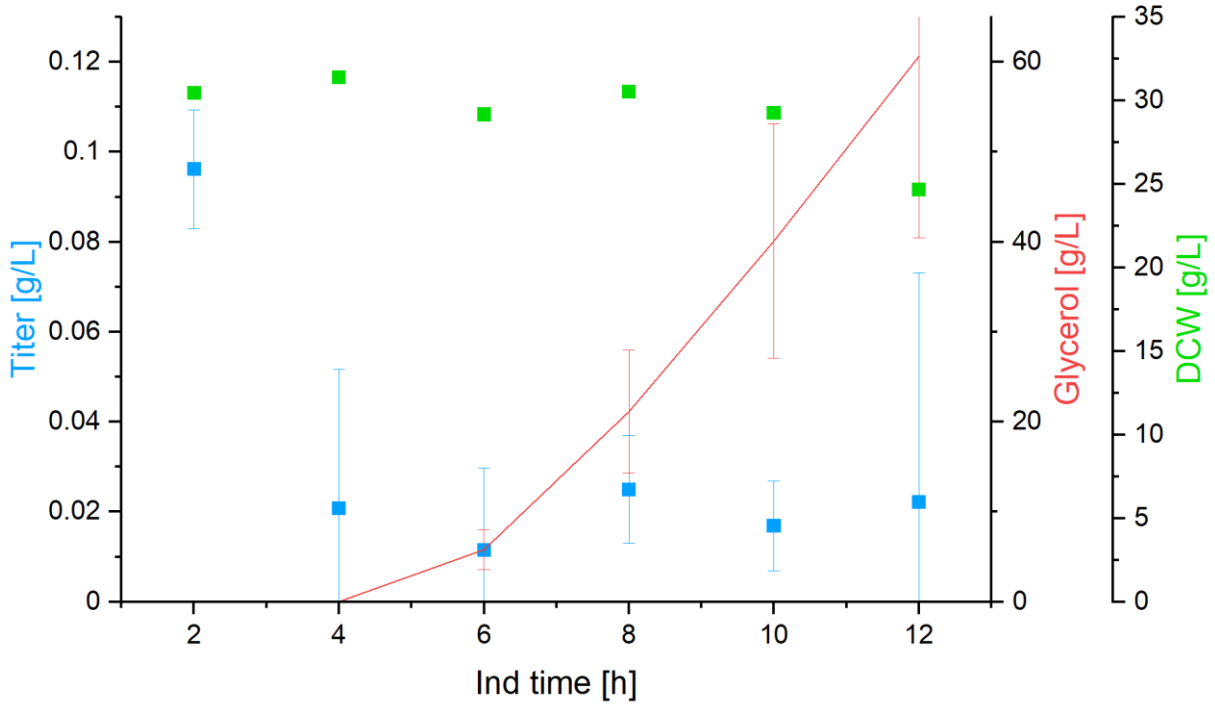

Figure 7. Mean values for the four center point cultivations (T=30 °C, $q_{s,C}$ =0.3 g/g/h). Titer, glycerol, and biomass over induction time with error bars for titer and glycerol.

The mean values and standard deviations for titer and glycerol uptake were calculated. The biomass remained relatively constant during the induction phase within a range of 25-30 g/L DCW. The titer was highest in the beginning and decreased after 2 h induction time but was stable towards the end. Sugar accumulation increased with time and had rather high standard deviations towards the end of induction phase. However, the overall trend of hyaluronidase expression could be clearly dedicated from the center point runs. Expression maximum was in the beginning, at 2-4 h induction time and quickly dropped afterwards due to a high metabolic burden imposed to the cells upon hyaluronidase production.

Summing up, hyaluronidase IBs can only be produced in a low amount. Low expression rates can be explained by cell stress resulting in a decreased specific growth rate. This further lead to glycerol and acetate accumulation since the $q_{s,C}$ was applied constantly over the whole induction time. High acetate concentrations inhibit cell growth and recombinant protein expression. With high $q_{s,C}$ and T , high specific titers could be found early in the induction phase, but increased cell stress resulted in product degradation and cell death at later induction times. That implicates that time-dependent analysis of the QA titer is very important for the determination of the harvest time point.

The enzyme with a molecular weight of about 43 kDa is rather big and therefore production of recombinant hyaluronidase might not be efficient in *E. coli*[74]. Since the hyaluronidase was classified unstable[75], this could also be a possible explanation for low expression yields.

Therefore, we hypothesize that specific titers of IB based products can be improved by applying low temperatures and low $q_{s,C}$ during the induction phase. Furthermore, time dependent monitoring of QAs can be used to optimize upstream process parameters T and $q_{s,C}$.

The highest titers were achieved at a temperature of 25 °C, during the first 4 hours of induction phase, being around 0.17 g/L. After 6 hours, the titers decreased due to ongoing product degradation given the high metabolic burden as the enzyme is hard to express for the cells.

With higher induction time, more sugar accumulated and lead to a drop in the specific growth rate and specific substrate uptake rate. Consequently, the production of hyaluronidase is tunable until 4 hours of induction and as titer and biomass strongly decrease afterwards due to product degradation, induction phase can be stopped after 4 hours.

3.2 Statistical evaluation

Giving the contour plots in Figure 8, glycerol and acetate production strongly depends on the specific substrate uptake rate. Due to a high metabolic burden upon hyaluronidase production, high

sugar uptake lead to early accumulation inside the cells and therefore degradation of the product. The mean specific productivity increased towards the lowest temperature, meaning it only depends on the temperature, not $q_{s,C}$. Evaluation of the specific titer was done at 4 hours induction as it was seen that the titer strongly increased within 4 hours of induction and decreased with higher induction time due to the high metabolic burden as the hyaluronidase was hard to express for *E. coli*.

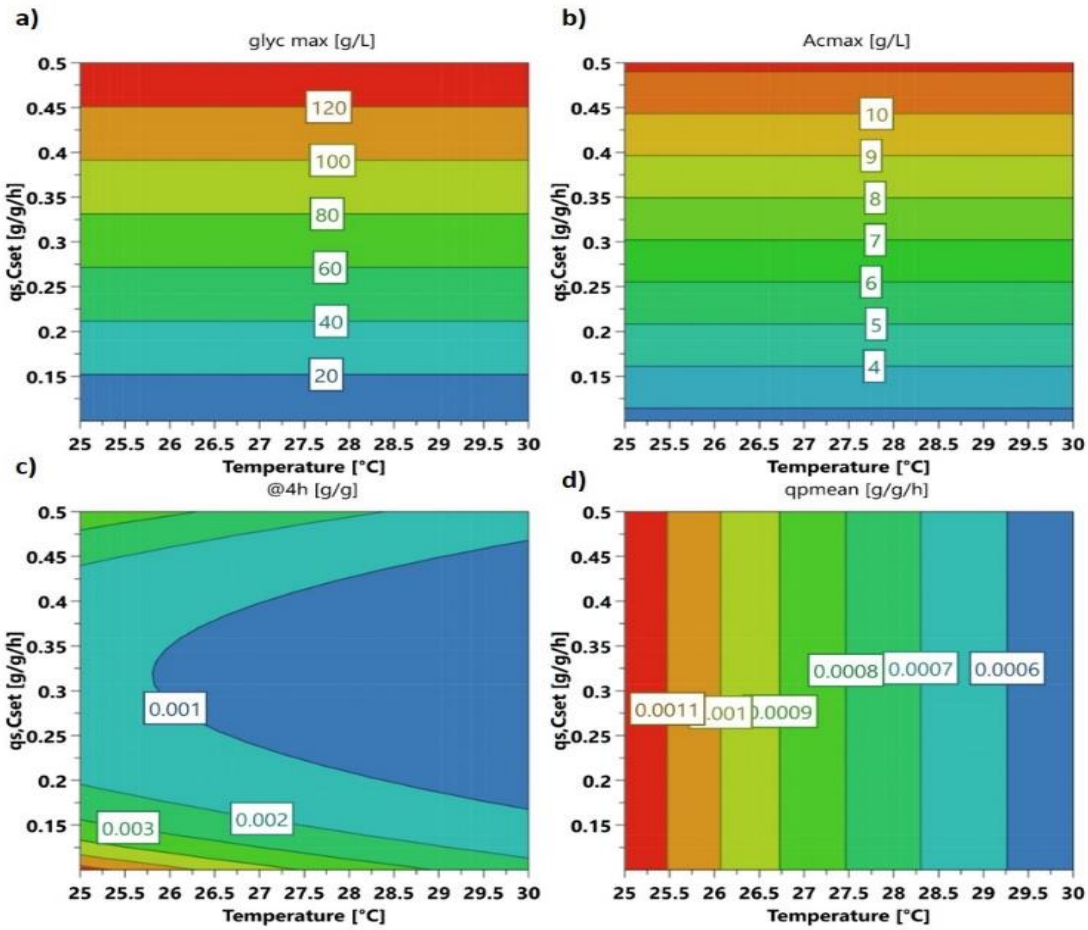

Figure 8. Contour plots. **a)** maximum glycerol concentration in broth; **b)** maximum acetate concentration in broth; **c)** specific hyaluronidase IB titer at 4-hour induction time; **d)** mean specific productivity over the whole induction time.

Taking the contour plots, highest titers after 4 hours were achieved at lowest temperature, which is in accordance with the mean productivity. Due to almost no sugar accumulation at lower $q_{s,C}$ rates,

lower points are beneficial for the specific titer, which was highest at 0.1 g/g/h. Considering the plots, the DoE reveals best conditions at T=25 °C and $q_{s,C}$=0.1 g/g/h, at the lowest points measured. To optimize the production of the hyaluronidase further, the DoE could be extended towards a lower T and $q_{s,C}$ range. According to the model evaluation plots in Figure 9, the mean productivity over the whole induction time is only linear depended on the temperature, the $q_{s,C}$ term was included to increase the model quality.

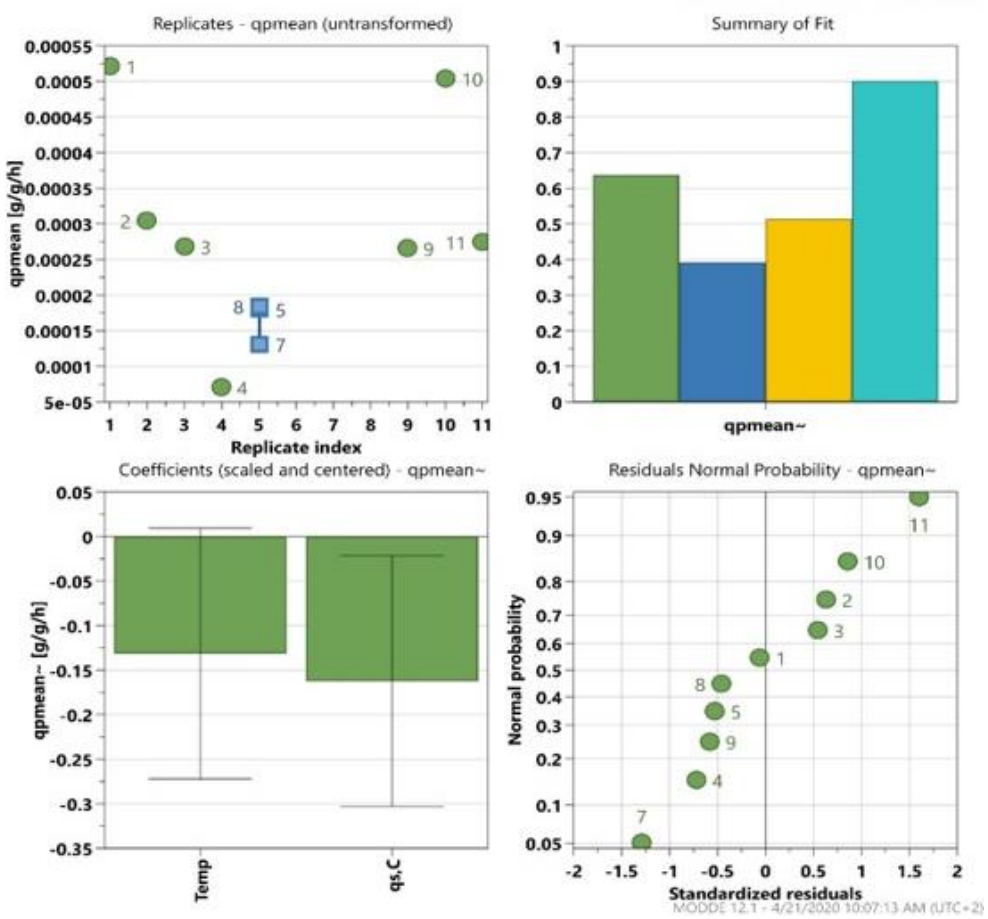

Figure 9. Model evaluation by MODDE 12 for Contour plots; mean productivity.

For the statistical evaluation, only positive values were considered, and product degradation was not taken into account. High $q_{s,C}$ boosted productivity, but resulted in early product degradation whereas low $q_{s,C}$ allowed for stable production. Highest productivities were achieved at lowest temperature, stating that lower temperature is favorable to produce hyaluronidase IBs. Looking at

the plots in Figure 10, the linear temperature term and the quadratic term for $q_{s,C}$ are significant for the specific titer. The linear $q_{s,C}$ term is close to significance, but was included to increase the model quality. Given an overall uncertainty of the titers measured, low temperature and low substrate uptake rate seem to be optimal to achieve highest specific titers for the hyaluronidase IBs.

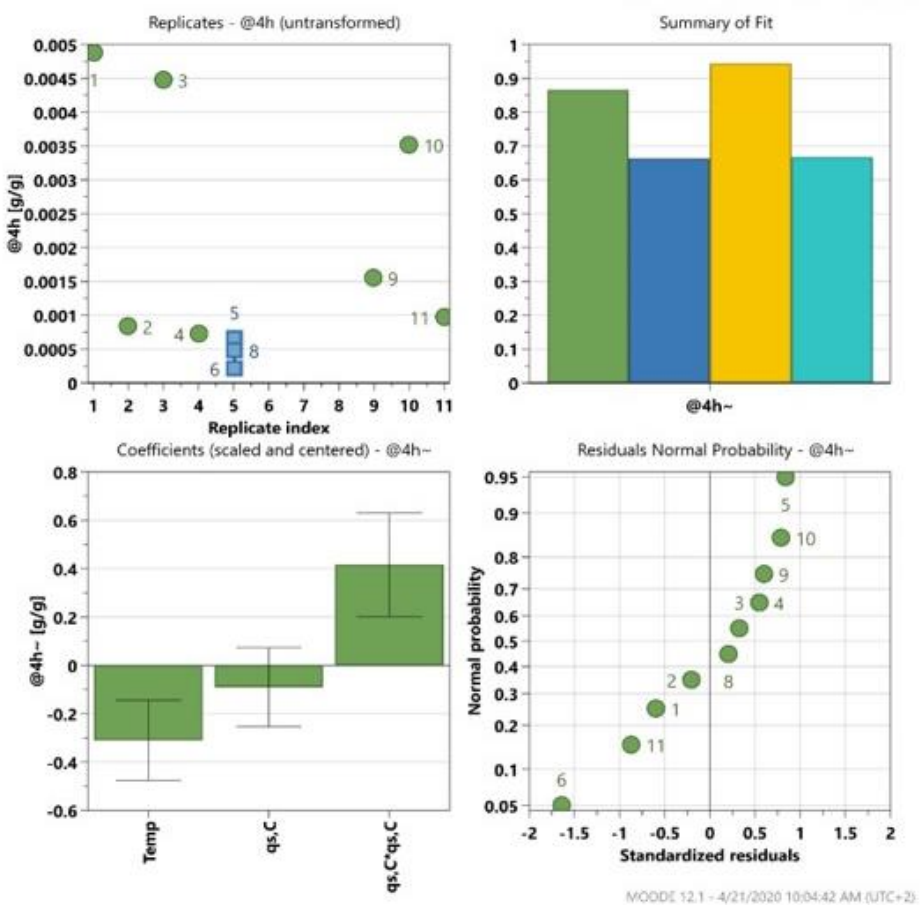

Figure 10. Model evaluation by MODDE 12 for Contour plots; specific titer at 4 hours induction.

As seen in Figure 11, for maximum glycerol production, only the linear $q_{s,C}$ term is significant, meaning the glycerol production only depends on the specific substrate uptake rate and not on the temperature. Furthermore, the maximum glycerol concentrations of the center points fit together quite well. Highest accumulations were found at highest $q_{s,C}$ rates and impose a high metabolic burden to the host. As there was almost no accumulation at lower $q_{s,C}$ rates, the lowest points are best for the production of hyaluronidase leading to no product degradation. Therefore, specific

glycerol uptake rates of 0.1 g/g/h are recommended to successfully express the hyaluronidase, preventing metabolic burden and early cell death.

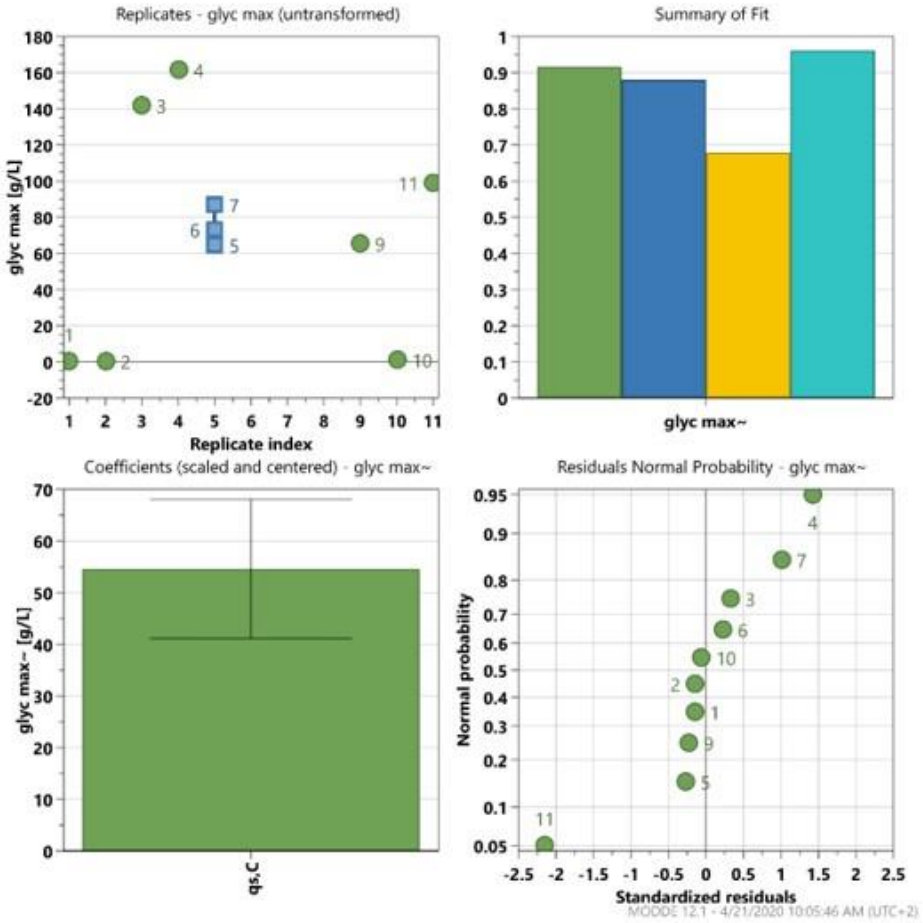

Figure 11. Model evaluation by MODDE 12 for Contour plots; maximum glycerol production.

Looking at Figure 12, acetate production is only dependent on the specific substrate feeding rate as only the $q_{s,C}$ term is significant. Given the replications of the center point cultivations, there is one outlier, which might be due to fluctuations during the cultivation. However, such high acetate production is unexpected in BL21, as this strain is regarded as a low acetate former[8]. These high acetate concentrations indicate enormous metabolic stress levels upon production of recombinant hyaluronidase.

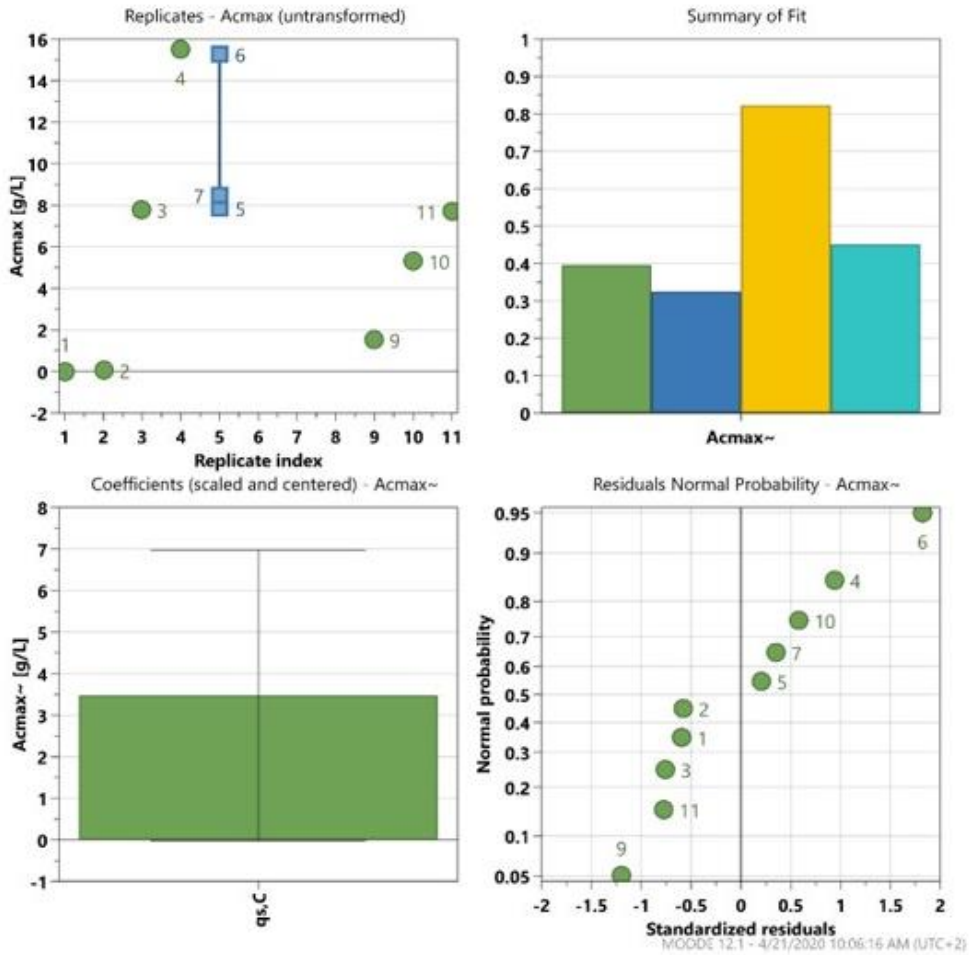

Figure 12. Model evaluation by MODDE 12 for Contour plots; maximum acetate production.

3.3 Hyaluronidase IB bead size

IB bead size was analyzed via scanning electron microscopy, for cultivations and induction times with the highest titers. To determine the average IB bead size, 50 IBs on the SEM picture were measured using Fiji (ImageJ, software package) and the mean values were considered. The mean IB bead size for highest titer (4h and 6h induction time) was in the range of 270 nm. At late induction times and lower titers, the mean IB bead size was in the range of 230 nm. However, with about 10 % standard deviations, no statistical significance between the induction times can be observed, indicating overall identical size.

The IB bead size can be controlled by upstream process parameters and is important for DSP in the pharmaceutical industry. IB bead size is dependent on the harvest time during cultivation. The effects of upstream process parameters pH and temperature on IB bead size as a function of the induction time have already been investigated in previous studies[56]. Knowledge about IB bead size is also important in applications of IBs as nanomaterials or biocatalysts.

In this study, hyaluronidase was expressed as IBs with the goal to control the IB bead size based on the specific substrate feeding rate. Figure 13 shows a SEM picture of hyaluronidase IBs at a center point cultivation.

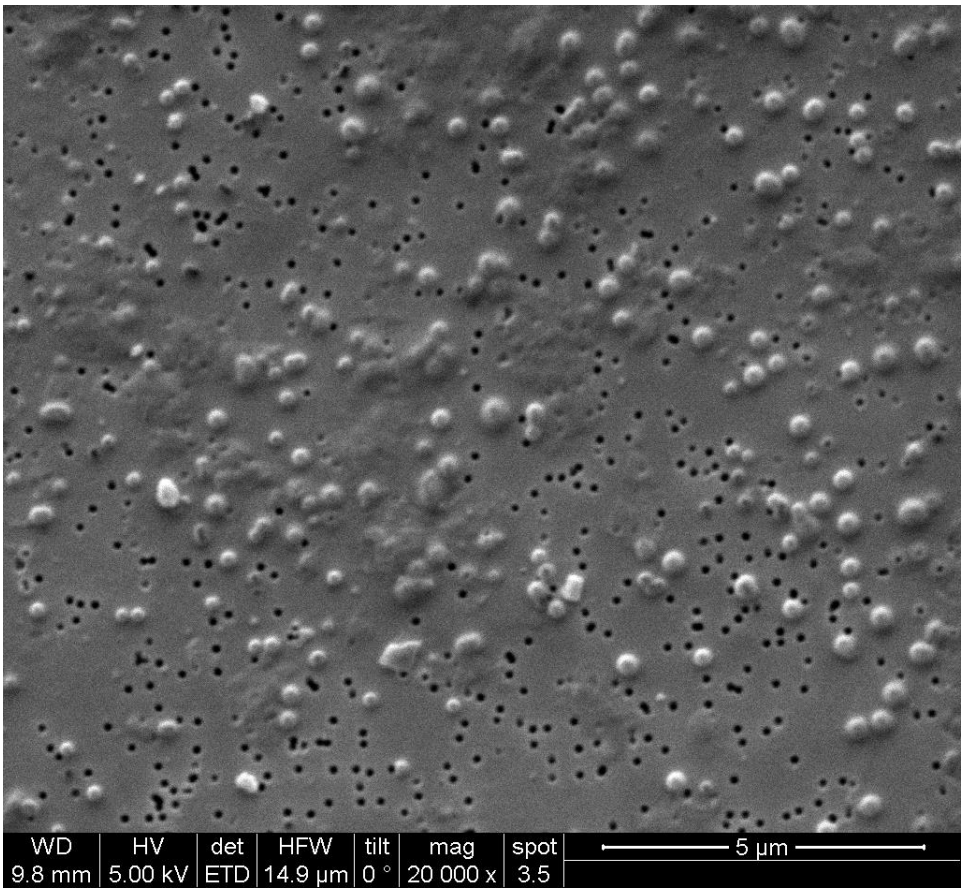

Figure 13. IB bead size for a center point cultivation (30 °C, 0.3 g/g/h) at 2 h induction time after homogenization and washing with ultrapure water; bright spots indicate for IBs; dark spots are host cell related impurities.

According to previous studies, large IBs show high purity, which is favorable for direct applications[56]. IB bead size increased over time and strongly depended on the amount of fed C-

source ($q_{s,C}$), while temperature and pH were kept constant during the induction phase. Decrease in IB size indicates for cell death and sugar accumulation. Changes in IB size are based on the harvest time during the cultivation. Therefore, we wanted to find optimal $q_{s,C}$ for stable IB size and low $q_{s,C}$ rates indicate for defined IB bead sizes.

Furthermore, IB bead size is strongly product and induction dependent. The IB bead size is tunable by adjusting the inducer concentration. Using IPTG as inducer, the IB size is highly dependent on the amount of fed C-source[56].

Due to exceptionally low titers of the hyaluronidase, we got rather small IBs, with maximum mean bead sizes of 280-295 nm at highest titer. In this study, no increase in IB size can be observed after 6 hours induction time, that is no new IBs are produced after 6 hours induction. Given Figure 14, maximum IB bead size was determined to be at 4 hours induction time and decreased afterwards due to product degradation and cell death.

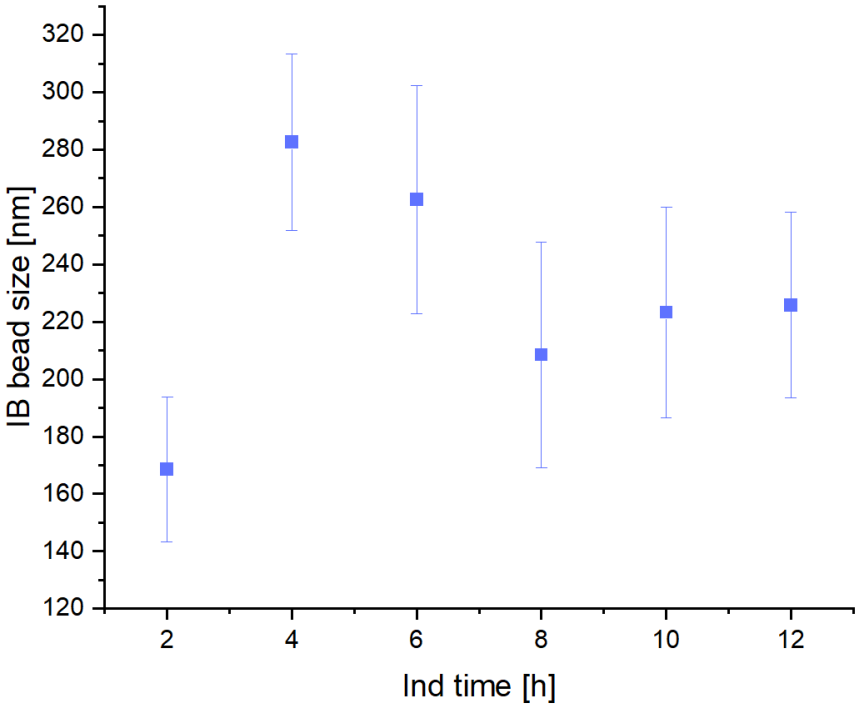

Figure 14. Mean IB bead size at T = 25°C and $q_{s,C}$ = 0.1 g/g/h over induction time with mean standard deviations.

Due to uncertainties of the measurement method for the Inclusion Body size and since it was not possible to get rid of all impurities contained in the sample making it difficult to measure the size precisely, the standard deviations were relatively high. However, compared to the specific titers, the data fit together well as the IB bead size increased linearly with the specific titer.

Low $q_{s,C}$ values are recommended for the production of IBs with defined size. Small sizes were observed at the beginning, after 2 h induction phase, highest after 4 h and 6 h and more stable sizes at later induction phase. At low $q_{s,C}$ values, IB bead sizes were stable at late induction times due to high viable cell concentration.

In earlier studies it was also shown that the IB bead size strongly correlates with the IB titer[56], [57]. Although the standard deviations were high, generally, the IB bead size is linear dependent on the specific IB titer. Both increased over induction time. At high $q_{s,C}$ and T, highest titer and biggest sizes were detected early in the induction phase, but as already denoted, lead to product degradation and no stable IB production over time. Such a linear correlation between IB bead size and specific titer can be seen in Figure 15.

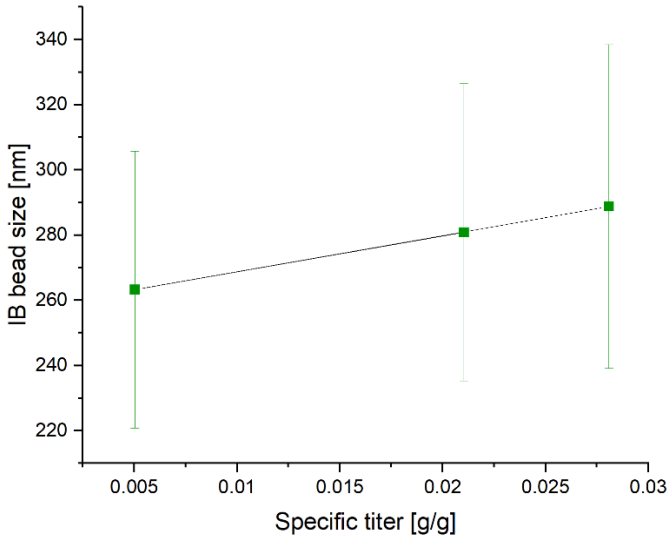

Figure 15. IB bead size – specific titer correlation for 3 cultivations at 4h induction time.

3.4 Hyaluronidase IB activity assay

The biological activity of hyaluronidase IBs was determined using a turbidimetric activity assay. The % transmittance was measured via photometer and converted into U/mg.

For calibration, a commercial hyaluronidase type I-S from bovine testes (No. H3506, Sigma Aldrich) with a concentration of 5.56 U/mL was measured at pH 7 in triplicates and the mean % transmittance was calculated.

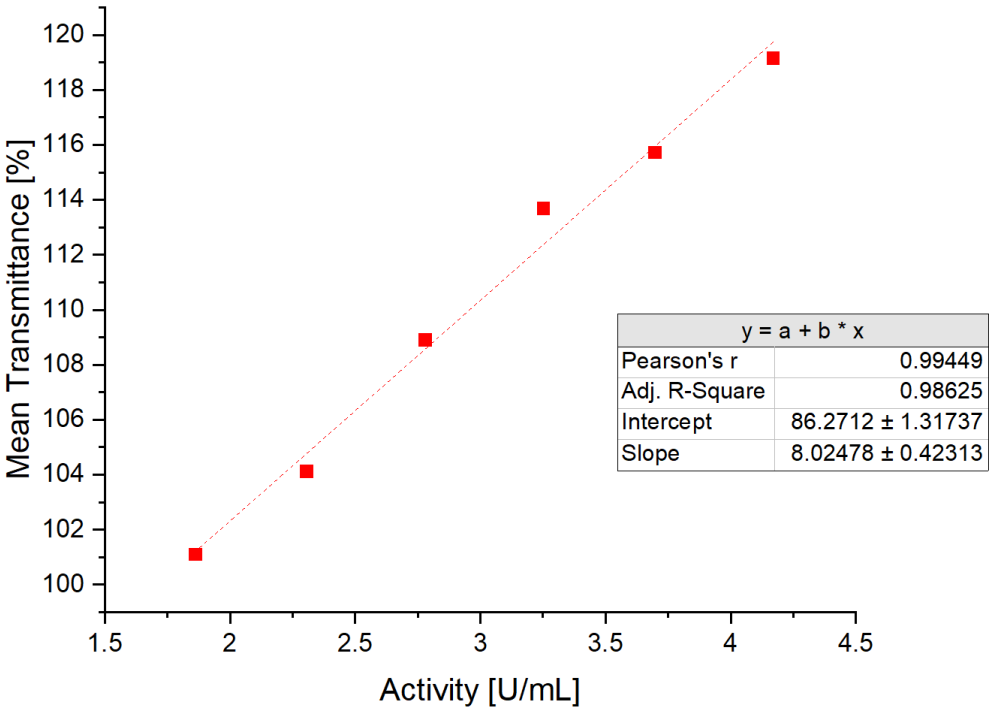

Figure 16. Calibration of commercial hyaluronidase activity using the photometric assay method.

Turbidimetric assays for hyaluronidase activity require large amounts of enzymes and are relatively inaccurate[59]. As little protein was produced, it was difficult to determine the hyaluronidase activity using this method.

Unfortunately, it was not possible to quantify the biological activity using this assay as such turbidimetric assays often lack specificity and sensitivity[76]. Reasons for fluctuations in the assay might be low titer concentrations and the instability of the hyaluronidase IBs.

Figure 17 shows fluctuations of the measured IB activity according to the titer.

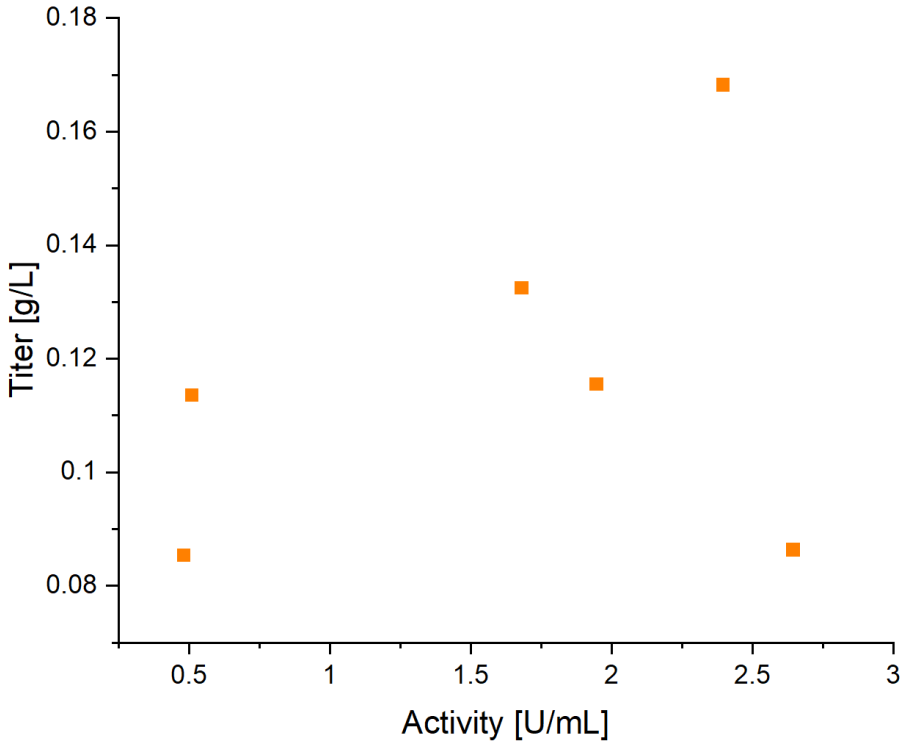

Figure 17. Biological activity of hyaluronidase inclusion bodies vs titer

However, we already saw activity using our IBs during these first measurements, while quantification was problematic. According to the results, there are biologically active hyaluronidase IBs, but no significant results could be achieved for the activity of hyaluronidase IBs using this turbidimetric assay. Therefore, we tried to determine the activity with FT-IR spectroscopy.

3.5 Hyaluronidase IB activity using FT-IR spectroscopy

FT-IR spectroscopy is a low-resolution technique used to study protein structures and monitor dynamic changes of protein structures[77]. FT-IR measurements requires high enzyme concentrations and since the IB titers were relatively low, the enzyme activity was only analyzed for one experimental point in the DoE. Therefore, hyaluronidase IBs were produced at what we found to be optimal conditions. At a temperature of 25 °C and $q_{s,C}$ of 0.1 g/g/h, 4 L broth was harvested after 4 h induction. The resulting IB pellets were centrifuged and resuspended as described in the material and methods part.

For activity determination, the enzymatic reaction of hyaluronidase IBs with its native substrate hyaluronan was monitored. Hyaluronan (HA) is a multifunctional high molecular weight linear glycosaminoglycan composed of repeating disaccharide units, D-glucuronic acid and N-acetyl glucosamine, linked by alternating β (1,3) and β (1,4) glycosidic bonds. Hyaluronidases turnover hyaluronan by cleaving the β (1,4) glycosidic bonds resulting in tetrasaccharides (GlcA-GlcNAc-GlcA-GlcNAc)[60].

The enzymatic activity is affected by ionic strength and substrate concentration. At high substrate concentrations and under low ionic strength, there is a strong inhibition of the hyaluronan hydrolysis catalyzed by hyaluronidase. Low ionic strength favours the electrostatic interactions between HA and hyaluronidase, leading to the formation of non-specific HA-Hyase complexes which inhibit the catalytic activity of the hyaluronidase[78]–[80]. This results in an atypical Michaelis-Menten behaviour. Other contributions to the atypical kinetics may include the high viscosity of highly concentrated HA solutions and therefore, the steric exclusion of hyaluronidase from hyaluronan solutions[81].

A series of experiments was performed by measuring the initial reaction rate of IB-substrate solutions with different hyaluronidase IB concentrations ranging from 1.5 – 30 mg/mL and a HA

concentration of 1 mg/mL as there is a lower limit for the substrate concentration due to the sensitivity of the FT-IR spectroscopy.

Figure 18 shows a representative spectrum of the progression of the enzymatic reaction in the spectral region where the changes of the substrate HA occur.

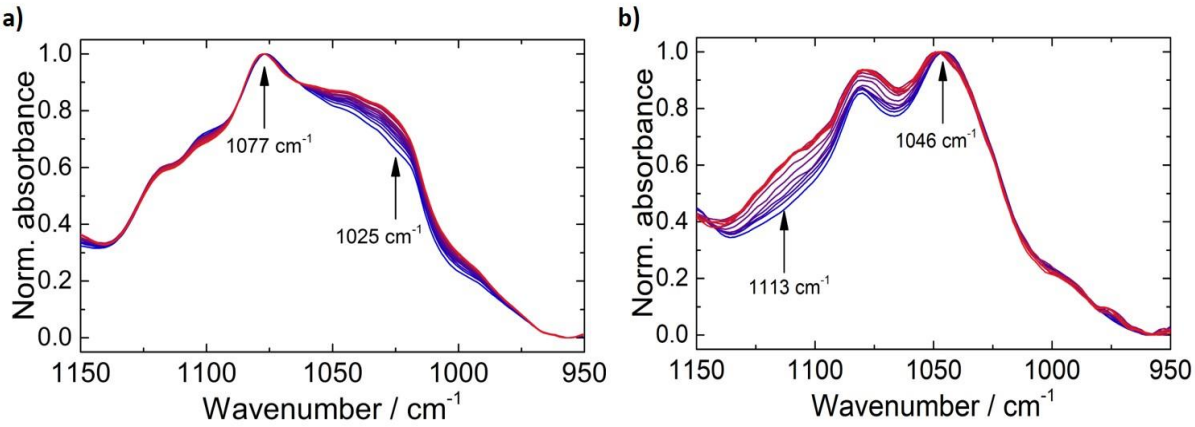

Figure 18. FT-IR spectra of the enzymatic reaction after 1 minute (blue) and after 40 minutes (red). **a)** FT-IR spectra of the enzymatic reaction with hyaluronidase IB at an IB concentration of 12.6 mg/mL **b)** analyzed IR bands for degradation of hyaluronan with commercial hyaluronidase at a concentration of 30 mg/mL; different bands showed high changes compared to IBs.

The band at 1077 cm^{-1} was assigned to the $\nu_{C\text{-}O\text{-}C}$ ring mode and the band at 1025 cm^{-1} could be attributed to the $\nu_{C\text{-}OH}$ modes of alcohols[82], [83]. The band height of these two bands was evaluated and then the ratio was calculated. This normalization step was necessary, because the viscosity of the solution changed during the measurement[84], which lead to a changing baseline and varying absorbance across the entire spectrum.

For further analysis, the band height ratios were plotted versus the reaction time (Figure 19a).

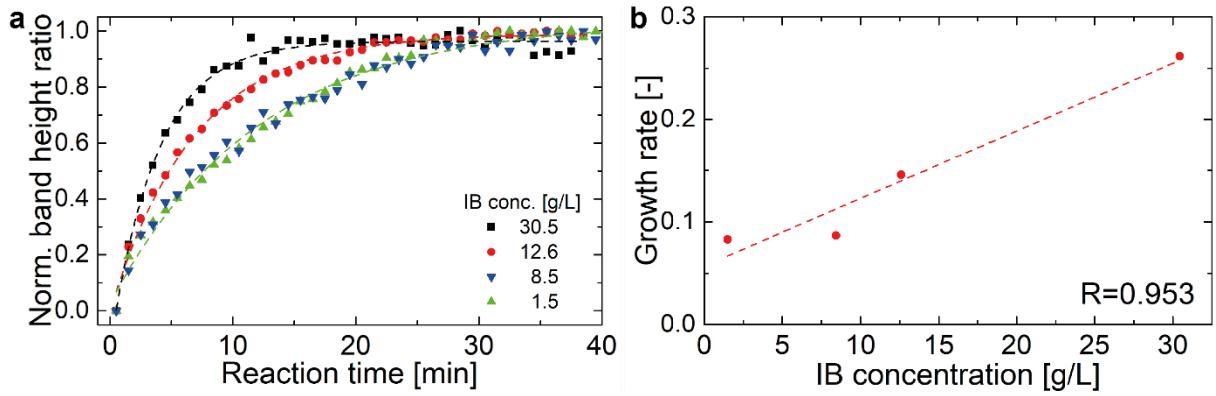

Figure 19. **a)** Progression of the normalized band ratio with time of four investigated IB concentrations. **b)** Growth rate vs IB concentration shows linear relationship.

The obtained temporal progression was then fitted using a one-phase exponential grow function with time offset (with a high coefficient of determination, R^2>0.98) and the growth rate was calculated as the inverse time constant. The growth rate shows a linear correlation to the IB concentration as visualized in Figure 19b, which demonstrates the activity of our hyaluronidase IBs. Due to the applied normalization step, no quantitative information about the reaction rate can be obtained, however, it is shown that spectral changes caused by the enzymatic reaction can be related to a biological activity of the hyaluronidase IBs.

As the degradation of HA catalysed by hyaluronidases increases the permeability of connective tissues and is involved in the spread of toxins and venoms, and cancer progression, inhibition of HA degradation may be crucial in reducing disease progression and spread of venom/toxins. Therefore, hyaluronidase inhibitors could potentially be used as contraceptives and anti-tumour agents and furthermore, HA and hyaluronidases can be used as pharmacological tools to study their physiological and pathophysiological role[85].

Hyaluronidases play an important role in cancer development as they hydrolyse long HA chains with anti-angiogenic properties into short HA-chains with angiogenic properties. Thus it is very

important to control the hyaluronidase activity as it may control the balance between hyaluronan and oligosaccharides[79], [81].

4. Conclusions and Outlook

In many fields, applications of IBs become increasingly interesting as protein can be enriched in IBs, the expression of toxic proteins is possible, and they can be directly used for some applications. Especially in the pharmaceutical industry, active IBs are of great importance, such as to produce antibody fragments.

Within this study, the enzyme hyaluronidase of *Apis mellifera* was recombinantly produced as IBs in the genetically modified strain *E. coli* BL21(DE3) using the pET expression system. We tried to increase the IB productivity in the induction phase by controlling the process parameters T and $q_{s,C}$. The alternation of classical process parameters in the induction phase influences IB quality attributes. Peternel et al., already showed that IB properties strongly depend on cultivation conditions[55]. We aimed to control IB quality attributes, titer, size, and activity with upstream process parameters. The specific substrate feeding rate strongly influences the quality attributes, although high $q_{s,C}$ boosted the titer early in the induction phase, it lead to early sugar accumulation and thus, product degradation. Low $q_{s,C}$ allowed for a stable production process indicated by higher viable cell concentration at late induction times as there was almost no sugar accumulation. Additionally, at high substrate feeding rates, we observed acetate formation during the production phase, which is unexpected in the strain *E. coli* BL21. The reason might be, that the hyaluronidase imposes an enormous metabolic burden to the cells. However, due to acetate production, cell growth and recombinant protein production was inhibited resulting in low expression yields.

High T imposes stress to the cells while low T favors the formation of IBs, but the temperature has no significant effect on the product titer. Furthermore, highest productivities for this fed batch

cultivation are found after 4 hours induction, hence, the production can be stopped afterwards since no increase in product yield can be observed.

The performed cultivations showed high impact on analyzed IB QAs titer and size based on process parameters T and $q_{s,C}$ tested in the DoE approach. Results showed that specific titer and IB bead size are strongly dependent on the amount of the specific substrate uptake rate. High $q_{s,C}$ boosted titer and size early in the induction phase, but lead to high glycerol and acetate accumulation, while low $q_{s,C}$ did not impose a metabolic burden to the cell, but IB production was low. A similar dependence was found for temperature.

Low $q_{s,C}$ values and temperatures are recommended for IBs with defined sizes since IB bead sizes are longer stable at lower values. Largest IBs could be found in the beginning of induction, however, with a standard deviation of about 10 % for analyzed IB bead sizes, no significant impact of the induction time on IB size can be observed.

Furthermore, the QAs titer and size are strongly product dependent[56]. The primary sequence of the protein and the hydrophobicity influence the IB bead size.

Activity measurements using FT-IR spectroscopy, showed promising results of hyaluronidase IB activity, seen in spectral changes of the substrate hyaluronan that can be related to the enzymatic activity of hyaluronidase IBs. Since the QA activity was only analyzed for one cultivation at T=25 °C and $q_{s,C}$=0.1 g/g/h and no quantitative information could be obtained, a dependence for variations in T and specific substrate feeding rate during the induction phase on the amount of active protein within IBs could not be determined.

However, already shown in different studies, lower temperature seems to increase the activity of IBs. For further activity information, the enzymatic reaction would have to be measured in a time dependent manner.

All in all, lower temperatures and substrate feeding rates seem to have a positive impact on all QAs.

4.1 Has the hyaluronidase gene of *Apis mellifera* been successfully cloned into the pET28a(+) plasmid?

For recombinant protein expression in *E. coli*, the hyaluronidase gene of *Apis mellifera* has been codon optimized and cloned into the pET plasmid by General Biosystems (NC, USA). While the first experiments, including transformation of *E. coli* with the plasmid and subsequent cultivation, were disappointing as only few colonies of *E. coli* were growing, the plasmid was sent to Microsynth, Switzerland, for sequencing, which was not possible suggesting our plasmid had a nick in the DNA strand. However, subsequent cultivation experiments turned out well and the plasmid DNA was purified using GeneJET Plasmid Miniprep Kit from Thermo Scientific and due to sequencing, successful cloning of the hyaluronidase gene into the plasmid was confirmed.

4.2 Can the hyaluronidase of *Apis mellifera* be successfully expressed in *E. coli* BL21(DE3) as Inclusion Bodies?

Prior to the microbial cultivation, the hyaluronidase from *Apis mellifera* was analyzed with ExPASy analysis tool ProtParam to obtain physicochemical properties deduced from the protein sequence[75]. The estimated half-life of the protein in *E. coli* is > 10 hours. More interesting, the hyaluronidase is classified as unstable with an instability index of 44.30. Aanalysis of the hyaluronidase with the Disulfind server[86] predicts two disulfide bonds with high probability. Since the hyaluronidase lacks the signal sequence for translocation from the cytoplasmic space into the periplasmic space and disulfide bonds can only hardly

be correctly formed in the environment of the cytoplasmic space, expression of the hyaluronidase as IBs is highly favored.

Upon recombinant expression in *E. coli*, only low expression rates of recombinant hyaluronidase were achieved. Therefore, we alternated the specific substrate feeding rate and the temperature in a DoE approach based on previous results[56].

The hyaluronidase was successfully expressed as IBs, but the titers achieved are low. Highest titers and largest IB bead sizes could be achieved after 4 hours of induction. With higher indication time, titers strongly decrease due to the high metabolic burden as the hyaluronidase is hard to express for *E. coli*.

Various factors impose a metabolic burden to the cells upon recombinant protein production. High temperatures and IPTG cause stress to the cells[87], and high substrate concentrations minimize the growth rate[88], leading to glycerol accumulation and acetate production. Acetate accumulation results in cell growth inhibition and inhibits recombinant protein production. Although high acetate formation is unusual in *E. coli* strain BL21[89], our cultivations resulted in high acetate concentrations leading to the assumption that recombinant hyaluronidase expression imposes tremendous metabolic stress to the cells. Hence, low temperatures and specific substrate feeding rates of 0.1 g/g/h are recommended for successful expression of hyaluronidase IBs.

4.3 Can the hyaluronidase of *Apis mellifera* be used as model enzyme for active inclusion bodies?

Active hyaluronidase IBs may be useful tools in pharmaceutical production since hyaluronidases play an important role in cancer development. In tumours, hyaluronidases are found together with high concentrations of their native substrate, hyaluronan. Long hyaluronan chains having anti-angiogenic properties are degraded into short chains

promoting angiogenesis and suppression of tumour growth. Biological hyaluronidase activity might control the balance between hyaluronan and oligosaccharides. Therefore, controlling the hyaluronidase activity is important when it comes to cancer research[79], [81]. To be a useful tool in cancer chemotherapy, hyaluronan fragments of defined sizes need to be produced because certain biological functions have been assigned to specific oligosaccharides[90]. Since hyaluronidase IBs are mechanically stable and have native-like protein structure conferring residual activity, they could be exploited for the degradation of hyaluronan into defined oligosaccharide structures.

The biological activity of recombinant hyaluronidase from *Apis mellifera* expressed as IBs in *E.coli* has already been determined, but reached only 20 % to 30 % of the activity of natural bee venom hyaluronidase after refolding[65]. In this study we successfully expressed the hyaluronidase as IBs in *E. coli* and sought to determine the protein activity which turned out to be complex.

Using an enzymatic activity assay based on the degradation of hyaluronic acid measuring the turbidity using UV/VIS spectroscopy[37], [90], [91], no quantitative results could be achieved for the hyaluronidase IBs. Thus, we tried to determine the protein activity using FT-IR spectroscopy. The linear correlation of the growth rate to the IB concentration demonstrates the activity of hyaluronidase IBs[92]. However, because of the applied normalization steps, no quantitative information about the enzyme velocity can be obtained. Nevertheless, enzymatic activity can be derived from the obtained spectra depicting spectral changes of the substrate hyaluronan caused by hydrolyzation of the substrate by hyaluronidases.

4.4 Outlook

Instead of performing a fed batch cultivation process, one could aim to express the hyaluronidase as IB in *E.coli* performing a continuous cascade of two stirred tank reactors, one for biomass production and the other for recombinant protein expression, recently reported to boost the productivity and space/time yields for IB production[93].

Moreover, using another inducer might be advantageous since IPTG imposes enormous metabolic stress to the cells[87]. Lactose could be an alternative when it comes to continuous processing[93], however, regulatory issues may arise using animal derived products.

Interestingly, biologically active hyaluronidases mediate the degradation of hyaluronan into oligosaccharides in tumours. The hydrolysis into defined hyaluronan oligosaccharides is mandatory to be a counteract against tumour progression. Therefore, the production of mechanically stable and biologically active hyaluronidase IBs could be beneficial for cancer therapies since such active IBs would facilitate the degradation of hyaluronan into defined fragments[85].

Planned improvements of this experimental approach, such as a temperature-controlled ATR manifold, will pave the way for a fully IR-based activity characterization of IBs and enzymes *in situ*. Alternatively, as IR spectroscopy was proven to be an excellent tool for in-line monitoring of bioprocesses by using fiber optic probes[94], [95], IB activity measurements could also be performed in-line directly in an reactor vessel.

4.5 Literature

[1] F. Baneyx, 'Recombinant protein expression in Escherichia coli', *Curr Opin Biotechnol*, vol. 10, no. 5, pp. 411–21, Oct. 1999, doi: 10.1016/s0958-1669(99)00003-8.

[2] C. Huang, H. Lin and X. Yang, 'Industrial production of recombinant therapeutics in Escherichia coli and its recent advancements', *J. Ind. Microbiol. Biotechnol.*, vol. 39, no. 3, pp. 383–399, Jan. 2012, doi: doi:10.1007/s10295-011-1082-9.

[3] S. Sahdev, S. K. Khattar and K. S. Saini, 'Production of active eukaryotic proteins through bacterial expression systems: a review of the existing biotechnology strategies', *Mol. Cell. Biochem.*, vol. 307, no. 1, pp. 249–264, Sep. 2007, doi: doi:10.1007/s11010-007-9603-6.

[4] G. Walsh, 'Biopharmaceutical benchmarks 2010', *Nat Biotechnol*, vol. 28, no. 9, pp. 917–24, Sep. 2010, doi: 10.1038/nbt0910-917.

[5] M. N. Baeshen, A. M. Al-Hejin, R. S. Bora, M. M. M. Ahmed, H. A. I. Ramadan, K. S. Saini, N. A. Baeshen and E. M. Redwan, 'Production of Biopharmaceuticals in E. coli: Current Scenario and Future Perspectives', *J Microbiol Biotechnol*, vol. 25, no. 7, pp. 953–62, Jul. 2015, doi: 10.4014/jmb.1412.12079.

[6] O. Spadiut, S. Capone, F. Krainer, A. Glieder, and C. Herwig, 'Microbials for the production of monoclonal antibodies and antibody fragments', in *Trends Biotechnol*, vol. 32, 2014, pp. 54–60.

[7] F. W. Studier and B. A. Moffatt, 'Use of bacteriophage T7 RNA polymerase to direct selective high-level expression of cloned genes', *J Mol Biol*, vol. 189, no. 1, pp. 113–30, May 1986, doi: 10.1016/0022-2836(86)90385-2.

[8] J. S. Michele van de Walle, 'Proposed mechanism of acetate accumulation in two recombinant Escherichia coli strains during high density fermentation - van de Walle - 1998 - Biotechnology and Bioengineering - Wiley Online Library', 1998, doi: 10.1002/(SICI)1097-0290(19980105)57:1<71::AID-BIT9>3.0.CO;2-S.

[9] J. W. Dubendorff and F. W. Studier, 'Controlling basal expression in an inducible T7 expression system by blocking the target T7 promoter with lac repressor', *J Mol Biol*, vol. 219, no. 1, pp. 45–59, May 1991, doi: 10.1016/0022-2836(91)90856-2.

(10) R. Steen, A. E. Dahlberg, B.N. Lade, F.W. Studier and J.J. Dunn, T7 RNA Polymerase Directed Expression of the Escherichia Coli RrnB Operon. | The EMBO Journal. *EMBO J* **1986**, *5* (5), 1099–1103. https://doi.org/10.1002/j.1460-2075.1986.tb04328.x.

[11] R. C. Mierendorf, B. B. Morris, B. Hammer and R. E. Novy, 'Expression and Purification of Recombinant Proteins Using the pET System', *Methods Mol. Med.*, vol. 13, 1998, doi: 10.1385/0-89603-485-2:257.

[12] D. J. Wurm, L. Veiter, S. Ulonska, B. Eggenreich, C. Herwig, and O. Spadiut, 'The E. coli pET expression system revisited-mechanistic correlation between glucose and lactose uptake', *Appl Microbiol Biotechnol*, vol. 100, no. 20, pp. 8721–9, Oct. 2016, doi: 10.1007/s00253-016-7620-7.

[13] S. H. EL Moslamy, 'Application of Fed-Batch Fermentation Modes for Industrial Bioprocess Development of Microbial Behaviour', *Ann Biotechnol Bioeng*, vol. 2019;1(1): 1001, 2019.

[14] R. Carlson, 'Estimating the biotech sector's contribution to the US economy', *Nat. Biotechnol.*, vol. 34, no. 3, pp. 247–255, Mar. 2016, doi: doi:10.1038/nbt.3491.

[15] E. National Academies of Sciences, Division on Earth and Life Studies, Board on Chemical Sciences and Technology, Board on Agriculture and Natural Resources, Board on Life Sciences, and Committee on Future Biotechnology Products and Opportunities to Enhance Capabilities of the Biotechnology Regulatory System, 'Emerging Trends and Products of Biotechnology', Jun. 2017, doi: https://www.ncbi.nlm.nih.gov/books/NBK442203/.

[16] B. S. Kim, S. C. Lee, S. Y. Lee, Y. K. Chang, and H. N. Chang, 'High cell density fed-batch cultivation of Escherichia coli using exponential feeding combined with pH-stat', *Bioprocess Biosyst. Eng.*, vol. 26, no. 3, pp. 147–150, Feb. 2004, doi: doi:10.1007/s00449-003-0347-8.

[17] W. Johnston, R. Cord-Ruwisch and M. J. Cooney, 'Industrial Control of Recombinant E. Coli Fed-Batch Culture: New Perspectives on Traditional Controlled Variables', *Bioprocess Biosyst. Eng.*, vol. 25, no. 2, Jun. 2002, doi: 10.1007/s00449-002-0287-8.

[18] L. Yee and H. W. Blanch, 'Recombinant Protein Expression in High Cell Density Fed-Batch Cultures of Escherichia Coli', *Bio/Technology*, vol. 10, no. 12, pp. 1550–1556, 1992, doi: doi:10.1038/nbt1292-1550.

[19] R. Poontawee and S. Limtong, 'Feeding Strategies of Two-Stage Fed-Batch Cultivation Processes for Microbial Lipid Production from Sugarcane Top Hydrolysate and Crude Glycerol by the Oleaginous Red Yeast Rhodosporidiobolus fluvialis', in *Microorganisms*, vol. 8, 2020.

[20] G. N. Vemuri, M. A. Eiteman and E. Altman, 'Succinate production in dual-phase Escherichia coli fermentations depends on the time of transition from aerobic to anaerobic conditions', *J. Ind. Microbiol. Biotechnol.*, vol. 28, no. 6, Jun. 2002, doi: 10.1038/sj/jim/7000250.

[21] J. Lee and S. Y. Lee, 'Control of fed-batch fermentations - ScienceDirect', 1999.

[22] K. G. Clarke, *Bioprocess Engineering: An Introductory Engineering and Life Science Approach*. Elsevier Science, 2013.

[23] J. Skórko-Glónekv and A. Sobiecka, '[Periplasmatic Disulfide Oxidoreductases From Bacterium Escherichia Coli--Their Structure and Function]', *Postepy Biochem.*, vol. 51, no. 4, 2005.

[24] A. Berlec and B. Štrukelj, 'Current state and recent advances in biopharmaceutical production in Escherichia coli , yeasts and mammalian cells', *J. Ind. Microbiol. Biotechnol.*, vol. 40, no. 3, pp. 257–274, Feb. 2013, doi: doi:10.1007/s10295-013-1235-0.

[25] National Research Council (US) Committee on Bioprocess Engineering, 'Current Bioprocess Technology, Products, and Opportunities', 1992, doi: https://www.ncbi.nlm.nih.gov/books/NBK236005/.

[26] M. Luo, M. Zhao, C. Cagliero, H. Jiang, Y. Xie, J. Zhu, H. Yang, M. Zhang, Y. Zheng, Y. Yuan, Z. Du and H. Lu, 'A general platform for efficient extracellular expression and purification of Fab from Escherichia coli', *Appl. Microbiol. Biotechnol.*, vol. 103, no. 8, pp. 3341–3353, Mar. 2019, doi: doi:10.1007/s00253-019-09745-8.

[27] 'Stages in Downstream Processing: 5 Stages', Sep. 2015, doi: https://www.biologydiscussion.com/biotechnology/downstream-processing/stages-in-downstream-processing-5-stages/10160.

[28] P. T. Wingfield, I. Palmer and S. M. Liang, 'Folding and Purification of Insoluble (Inclusion Body) Proteins From Escherichia Coli', *Curr. Protoc. Protein Sci.*, vol. 78, Mar. 2014, doi: 10.1002/0471140864.ps0605s78.

[29] A. Singh, V. Upadhyay, A. K. Upadhyay, S. M. Singh, and A. K. Panda, 'Protein recovery from inclusion bodies of Escherichia coli using mild solubilization process', in *Microb Cell Fact*, vol. 14, 2015.

[30] K. Tsumoto, D. Ejima, I. Kumagai, and T. Arakawa, 'Practical considerations in refolding proteins from inclusion bodies', *Protein Expr Purif*, vol. 28, no. 1, pp. 1–8, Mar. 2003, doi: 10.1016/s1046-5928(02)00641-1.

[31] A. Jungbauer, W. Kaar and R. Schlegl, 'Folding and Refolding of Proteins in Chromatographic Beds', *Curr. Opin. Biotechnol.*, vol. 15, no. 5, Oct. 2004, doi: 10.1016/j.copbio.2004.08.009.

[32] E. García-Fruitós, E. Vázquez, C. Díez-Gil, J. L. Corchero, J. Seras-Franzoso, I. Ratera, J. Veciana and A. Villaverde, 'Bacterial inclusion bodies: making gold from waste', *Trends Biotechnol.*, vol. 30, no. 2, pp. 65–70, Feb. 2012, doi: 10.1016/j.tibtech.2011.09.003.
[33] A. Villaverde and M. M. Carrió, 'Protein aggregation in recombinant bacteria: biological role of inclusion bodies', *Biotechnol. Lett.*, vol. 25, no. 17, pp. 1385–1395, 2003, doi: doi:10.1023/A:1025024104862.
[34] F. Baneyx and M. Mujacic, 'Recombinant protein folding and misfolding in Escherichia coli', *Nat. Biotechnol.*, vol. 22, no. 11, pp. 1399–1408, Nov. 2004, doi: doi:10.1038/nbt1029.
[35] S. Ventura and A. Villaverde, 'Protein quality in bacterial inclusion bodies', *Trends Biotechnol.*, vol. 24, no. 4, pp. 179–185, Apr. 2006, doi: 10.1016/j.tibtech.2006.02.007.
[36] Š. Peternel, J. Grdadolnik, V. Gaberc-Porekar, and R. Komel, 'Engineering inclusion bodies for non denaturing extraction of functional proteins', in *Microb Cell Fact*, vol. 7, 2008, p. 34.
[37] E. García-Fruitós, 'Inclusion bodies: a new concept', in *Microb Cell Fact*, vol. 9, 2010, p. 80.
[38] S. Peternel and R. Komel, 'Active protein aggregates produced in Escherichia coli', *Int J Mol Sci*, vol. 12, no. 11, pp. 8275–87, 2011, doi: 10.3390/ijms12118275.
[39] U. Krauss, V. D. Jager, M. Diener, M. Pohl, and K. E. Jaeger, 'Catalytically-active inclusion bodies-Carrier-free protein immobilizates for application in biotechnology and biomedicine', *J Biotechnol*, vol. 258, pp. 136–147, Sep. 2017, doi: 10.1016/j.jbiotec.2017.04.033.
[40] M. Carrio, N. Gonzalez-Montalban, A. Vera, A. Villaverde, and S. Ventura, 'Amyloid-like properties of bacterial inclusion bodies', *J Mol Biol*, vol. 347, no. 5, pp. 1025–37, Apr. 2005, doi: 10.1016/j.jmb.2005.02.030.
[41] M. Morell, R. Bravo, A. Espargaró, X. Sisquella, F. X. Avilés, X. Fernàndez-Busquets, and S. Ventura, 'Inclusion bodies: specificity in their aggregation process and amyloid-like structure', *Biochim Biophys Acta*, vol. 1783, no. 10, pp. 1815–25, Oct. 2008, doi: 10.1016/j.bbamcr.2008.06.007.
[42] M. M. Carrio and A. Villaverde, 'Protein aggregation as bacterial inclusion bodies is reversible', *FEBS Lett*, vol. 489, no. 1, pp. 29–33, Jan. 2001, doi: 10.1016/s0014-5793(01)02073-7.
[43] N. S. de Groot, R. Sabate, and S. Ventura, 'Amyloids in bacterial inclusion bodies', *Trends Biochem. Sci.*, vol. 34, no. 8, pp. 408–416, Aug. 2009, doi: 10.1016/j.tibs.2009.03.009.
[44] W. Wu, L. Xing, B. Zhou, and Z. Lin, 'Active protein aggregates induced by terminally attached self-assembling peptide ELK16 in Escherichia coli', *Microb. Cell Factories*, vol. 10, no. 1, pp. 1–8, Feb. 2011, doi: doi:10.1186/1475-2859-10-9.
[45] B. Zhou, L. Xing, W. Wu, X. Zhang, and Z. Lin, 'Small surfactant-like peptides can drive soluble proteins into active aggregates', *Microb. Cell Factories*, vol. 11, no. 1, pp. 1–8, Jan. 2012, doi: doi:10.1186/1475-2859-11-10.
[46] K. Talafová, E. Hrabárová, D. Chorvát, and J. Nahálka, 'Bacterial inclusion bodies as potential synthetic devices for pathogen recognition and a therapeutic substance release', in *Microb Cell Fact*, vol. 12, 2013, p. 16.
[47] E. Vázquez, J. L. Corchero, J. F. Burgueño, J. Seras-Franzoso, A. Kosoy, R. Bosser, R. Mendoza, J. M. Martínez-Láinez, U. Rinas, E. Fernández, L. Ruiz-Avila, E. García-Fruitós, and A. Villaverde, 'Functional inclusion bodies produced in bacteria as naturally occurring nanopills for advanced cell therapies', *Adv Mater*, vol. 24, no. 13, pp. 1742–7, Apr. 2012.
[48] M. Liovic, M. Ozir, A. B. Zavec, S. Peternel, R. Komel, and T. Zupancic, 'Inclusion bodies as potential vehicles for recombinant protein delivery into epithelial cells', in *Microb Cell Fact*, vol. 11, 2012, p. 67.
[49] F. Rueda, O. Cano-Garrido, U. Mamat, K. Wilke, J. Seras-Franzoso, E. García-Fruitós, and A. Villaverde, 'Production of functional inclusion bodies in endotoxin-free Escherichia coli',

Appl. Microbiol. Biotechnol., vol. 98, no. 22, pp. 9229–9238, Aug. 2014, doi: doi:10.1007/s00253-014-6008-9.

[50] E. Vázquez and A. Villaverde, 'Microbial biofabrication for nanomedicine: biomaterials, nanoparticles and beyond', *https://doi.org/10.2217/nnm.13.164*, Nov. 2013, doi: 10.2217/nnm.13.164.

[51] J. Seras-Franzoso, C. Steurer, M. Roldan, M. Vendrell, C. Vidaurre-Agut, A. Tarruella, L. Saldana, N. Vilaboa, M. Parera, E. Elizondo, I. Ratera, N. Ventosa, J. Veciana, A. J. Campillo-Fernandez, E. Garcia-Fruitos, E. Vazquez, A. Villaverde, 'Functionalization of 3D scaffolds with protein-releasing biomaterials for intracellular delivery', *J Control Release*, vol. 171, no. 1, pp. 63–72, Oct. 2013, doi: 10.1016/j.jconrel.2013.06.034.

[52] M. V. Céspedes, Y. Fernández, U. Unzueta, R. Mendoza, J. Seras-Franzoso, A. Sánchez-Chardi, P. Álamo, V. Toledo-Rubio, N. Ferrer-Miralles, E. Vázquez, S. Schwartz, I. Abasolo, J. L. Corchero, R. Mangues, A. Villaverde, 'Bacterial mimetics of endocrine secretory granules as immobilized in vivo depots for functional protein drugs', in *Sci Rep*, vol. 6, 2016.

[53] U. Unzueta, J. Seras-Franzoso, M. V. Cespedes, P. Saccardo, F. Cortes, F. Rueda, E. Garcia-Fruitos, N. Ferrer-Miralles, R. Mangues, E. Vazquez, and A. Villaverde, 'Engineering tumor cell targeting in nanoscale amyloidal materials', *Nanotechnology*, vol. 28, no. 1, p. 015102, Jan. 2017, doi: 10.1088/0957-4484/28/1/015102.

[54] J. M. Sánchez, H. López-Laguna, P. Álamo, N. Serna, A. Sánchez-Chardi, V. Nolan, O. Cano-Garrido, I. Casanova, U. Unzueta, E. Vazquez, R. Mangues, and A. Villaverde, 'Artificial Inclusion Bodies for Clinical Development', in *Adv Sci (Weinh)*, vol. 7, 2020.

[55] S. Peternel, S. Jevsevar, M. Bele, V. Gaberc-Porekar, and V. Menart, 'New properties of inclusion bodies with implications for biotechnology', *Biotechnol Appl Biochem*, vol. 49, no. Pt 4, pp. 239–46, Apr. 2008, doi: 10.1042/ba20070140.

[56] C. Slouka, J. Kopp, S. Hutwimmer, M. Strahammer, D. Strohmer, E. Eitenberger, A. Schwaighofer, and C. Herwig, 'Custom made inclusion bodies: impact of classical process parameters and physiological parameters on inclusion body quality attributes', *Microb. Cell Factories*, vol. 17, no. 1, pp. 1–15, Sep. 2018, doi: doi:10.1186/s12934-018-0997-5.

[57] J. Kopp, C. Slouka, D. Strohmer, J. Kager, O. Spadiut, and C. Herwig, 'Inclusion Body Bead Size in E. coli Controlled by Physiological Feeding', in *Microorganisms*, vol. 6, 2018.

[58] C. Slouka, J. Kopp, O. Spadiut, and C. Herwig, 'Perspectives of inclusion bodies for bio-based products: curse or blessing?', in *Appl Microbiol Biotechnol*, vol. 103, 2019, pp. 1143–53.

[59] R. Stern and M. J. Jedrzejas, 'The Hyaluronidases: Their Genomics, Structures, and Mechanisms of Action', *Chem Rev*, vol. 106, no. 3, pp. 818–39, Mar. 2006, doi: 10.1021/cr050247k.

[60] Z. Marković-Housley, G. Miglierini, L. Soldatova, P. J. Rizkallah, U. Müller, and T. Schirmer, 'Crystal Structure of Hyaluronidase, a Major Allergen of Bee Venom', *Structure*, vol. 8, no. 10, pp. 1025–1035, Oct. 2000, doi: 10.1016/S0969-2126(00)00511-6.

[61] K. C. F. Bordon, G. A. Wiezel, F. G. Amorim, and E. C. Arantes, 'Arthropod venom Hyaluronidases: biochemical properties and potential applications in medicine and biotechnology', *J. Venom. Anim. Toxins Trop. Dis.*, vol. 21, no. 1, pp. 1–12, Oct. 2015, doi: doi:10.1186/s40409-015-0042-7.

[62] S. Shuster, G. I. Frost, A. B. Csoka, B. Formby, and R. Stern, 'Hyaluronidase reduces human breast cancer xenografts in SCID mice', *Int J Cancer*, vol. 102, no. 2, pp. 192–7, Nov. 2002, doi: 10.1002/ijc.10668.

[63] E. J. Menzel and C. Farr, 'Hyaluronidase and its substrate hyaluronan: biochemistry, biological activities and therapeutic uses', *Cancer Lett*, vol. 131, no. 1, pp. 3–11, Sep. 1998, doi: 10.1016/s0304-3835(98)00195-5.

[64] F. Duran-Reynals, 'Exaltation de l'activité de virus vaccinal par les extraits de certains organs', *Compt Rend Soc Biol*, vol. 9, pp. 6–7, 1928.

[65] L. N. Soldatova, R. Crameri, M. Gmachl, D. M. Kemeny, M. Schmidt, M. Weber, and U. R. Mueller, 'Superior biologic activity of the recombinant bee venom allergen hyaluronidase expressed in baculovirus-infected insect cells as compared with Escherichia coli', *J. Allergy Clin. Immunol.*, vol. 101, no. 5, pp. 691–698, May 1998, doi: 10.1016/S0091-6749(98)70179-4.

[66] G. Sezonov, D. Joseleau-Petit, and R. D'Ari, 'Escherichia coli Physiology in Luria-Bertani Broth ▿ ', in *J Bacteriol*, vol. 189, 2007, pp. 8746–9.

[67] M. P. DeLisa, J. Li, G. Rao, W. A. Weigand, and W. E. Bentley, 'Monitoring GFP-operon fusion protein expression during high cell density cultivation of Escherichia coli using an on-line optical sensor', *Biotechnol Bioeng*, vol. 65, no. 1, pp. 54–64, Oct. 1999.

[68] M. Choi, S. M. Al-Zahrani, and S. Y. Lee, 'Kinetic model-based feed-forward controlled fed-batch fermentation of Lactobacillus rhamnosus for the production of lactic acid from Arabic date juice', *Bioprocess Biosyst. Eng.*, vol. 37, no. 6, Jun. 2014, doi: 10.1007/s00449-013-1071-7.

[69] A. Sapkota, 'Flow Cytometry-Definition, Principle, Parts, Steps, Types, Uses', May 2020, doi: https://microbenotes.com/flow-cytometry/.

[70] T. Langemann, U. B. Mayr, A. Meitz, W. Lubitz, and C. Herwig, 'Multi-parameter flow cytometry as a process analytical technology (PAT) approach for the assessment of bacterial ghost production', *Appl Microbiol Biotechnol*, vol. 100, no. 1, pp. 409–18, Jan. 2016, doi: 10.1007/s00253-015-7089-9.

[71] P. Dvorak, L. Chrast, P. I. Nikel, R. Fedr, K. Soucek, M. Sedlackova, R. Chaloupkova, V. de Lorenzo, Z. Prokop, and J. Damborsky, 'Exacerbation of substrate toxicity by IPTG in Escherichia coli BL21(DE3) carrying a synthetic metabolic pathway', *Microb Cell Fact*, vol. 14, p. 201, Dec. 2015, doi: 10.1186/s12934-015-0393-3.

[72] J. Kopp, F. B. Zauner, A. Pell, J. Hausjell, D. Humer, J. Ebner, C. Herwig, O. Spadiut, C. Slouka, and R. Pell, 'Development of a Generic Reversed-Phase Liquid Chromatography Method for Protein Quantification Using Analytical Quality-By-Design Principles', *J. Pharm. Biomed. Anal.*, vol. 188, Apr. 2020, doi: 10.1016/j.jpba.2020.113412.

[73] J. Kopp, C. Slouka, S. Ulonska, J. Kager, J. Fricke, O. Spadiut, and C. Herwig, 'Impact of Glycerol as Carbon Source onto Specific Sugar and Inducer Uptake Rates and Inclusion Body Productivity in E. coli BL21(DE3)', in *Bioengineering (Basel)*, vol. 5, 2018.

[74] H. Abtahi, A. Moradkhani, and I. Pakzad, 'Cloning and Expression of the Streptococcus pyogenes Hyaluronidase Gene in E.coli', *Aust. J. Basic* Appl. *Sci.*, vol. 6, pp. 95–99, 2012, doi: https://www.researchgate.net/publication/286195624_Cloning_and_expression_of_the_Streptococcus_pyogenes_hyaluronidase_gene_in_Ecoli.

[75] M. R. Wilkins, E. Gasteiger, A. Bairoch, J. C. Sanchez, K. L. Williams, R. D. Appel, and D. F. Hochstrasser, 'Protein Identification and Analysis Tools in the ExPASy Server', *Methods Mol. Biol. Clifton NJ*, vol. 112, 1999, doi: 10.1385/1-59259-584-7:531.

[76] K. P. Vercruysse, A. R. Lauwers, and J. M. Demeester, 'Absolute and Empirical Determination of the Enzymatic Activity and Kinetic Investigation of the Action of Hyaluronidase on Hyaluronan Using Viscosimetry', *Biochem. J.*, vol. 306 (Pt 1), no. Pt 1, Feb. 1995, doi: 10.1042/bj3060153.

[77] A. Schwaighofer, M. R. Alcaráz, C. Araman, H. Goicoechea, and B. Lendl, 'External cavity-quantum cascade laser infrared spectroscopy for secondary structure analysis of proteins at low concentrations', *Sci. Rep.*, vol. 6, no. 1, pp. 1–10, Sep. 2016, doi: doi:10.1038/srep33556.
[78] J. C. Vincent and H. Lenormand, 'How Hyaluronan-Protein Complexes Modulate the Hyaluronidase Activity: The Model', *Biophys. Chem.*, vol. 145, no. 2–3, Dec. 2009, doi: 10.1016/j.bpc.2009.09.010.
[79] H. Lenormand, B. Deschrevel, and JC. Vincent, 'How electrostatic interactions can change the kinetic behaviour of a Michaelis-Menten type enzyme. Application to the hyaluronan/hyaluronidase system', 2007, doi: http://www.amsi.ge/jbpc/40707/40702.html.
[80] B. Deschrevel, H. Lenormand, F. Tranchepain, N. Levasseur, T. Astériou, and JC. Vincent, 'Hyaluronidase Activity Is Modulated by Complexing With Various Polyelectrolytes Including Hyaluronan', *Matrix Biol. J. Int. Soc. Matrix Biol.*, vol. 27, no. 3, Apr. 2008, doi: 10.1016/j.matbio.2007.11.002.
[81] T. Astériou, JC. Vincent, F. Tranchepain, and B. Deschrevel, 'Inhibition of Hyaluronan Hydrolysis Catalysed by Hyaluronidase at High Substrate Concentration and Low Ionic Strength', *Matrix Biol. J. Int. Soc. Matrix Biol.*, vol. 25, no. 3, Apr. 2006, doi: 10.1016/j.matbio.2005.11.005.
[82] K. Haxaire, Y. Maréchal, M. Milas, and M. Rinaudo, 'Hydration of hyaluronan polysaccharide observed by IR spectrometry. II. Definition and quantitative analysis of elementary hydration spectra and water uptake - Haxaire - 2003 - Biopolymers - Wiley Online Library', 2003, doi: 10.1002/bip.10342.
[83] R. Gilli, M. Kacuráková, M. Mathlouthi, L. Navarini, and S. Paoletti, 'FTIR studies of sodium hyaluronate and its oligomers in the amorphous solid phase and in aqueous solution', *Carbohydr. Res.*, vol. 263, no. 2, Oct. 1994, doi: 10.1016/0008-6215(94)00147-2.
[84] N. S. El-Safory, A. E. Fazary, and C. K. Lee, 'Hyaluronidases, a group of glycosidases: Current and future perspectives', *Carbohydr. Polym.*, vol. 81, no. 2, pp. 165–181, Jun. 2010, doi: 10.1016/j.carbpol.2010.02.047.
[85] K. S. Girish and K. Kemparaju, 'The Magic Glue Hyaluronan and Its Eraser Hyaluronidase: A Biological Overview', *Life Sci.*, vol. 80, no. 21, Jan. 2007, doi: 10.1016/j.lfs.2007.02.037.
[86] A. Ceroni, A. Passerini, A. Vullo, and P. Frasconi, 'DISULFIND: a disulfide bonding state and cysteine connectivity prediction server', *Nucleic Acids Res*, vol. 34, no. Web Server issue, pp. W177-81, Jul. 2006, doi: 10.1093/nar/gkl266.
[87] F. T. Haddadin and S. W. Harcum, 'Transcriptome Profiles for High-Cell-Density Recombinant and Wild-Type Escherichia Coli', *Biotechnol. Bioeng.*, vol. 90, no. 2, Apr. 2005, doi: 10.1002/bit.20340.
[88] P. Malakar and K. V. Venkatesh, 'Effect of substrate and IPTG concentrations on the burden to growth of Escherichia coli on glycerol due to the expression of Lac proteins', *Appl. Microbiol. Biotechnol.*, vol. 93, no. 6, pp. 2543–2549, Oct. 2011, doi: doi:10.1007/s00253-011-3642-3.
[89] J. Shiloach and R. Fass, 'Growing E. Coli to High Cell Density--A Historical Perspective on Method Development', *Biotechnol. Adv.*, vol. 23, no. 5, Jul. 2005, doi: 10.1016/j.biotechadv.2005.04.004.
[90] M. Oettl, J. Hoechstetter, I. Asen, G. Bernhardt, and A. Buschauer, 'Comparative Characterization of Bovine Testicular Hyaluronidase and a Hyaluronate Lyase From Streptococcus Agalactiae in Pharmaceutical Preparations', *Eur. J. Pharm. Sci. Off. J. Eur. Fed. Pharm. Sci.*, vol. 18, no. 3–4, Mar. 2003, doi: 10.1016/s0928-0987(03)00022-8.

[91] T. Takahashi, M. Ikegami-Kawai, R. Okuda, and K. Suzuki, 'A Fluorimetric Morgan-Elson Assay Method for Hyaluronidase Activity', *Anal. Biochem.*, vol. 322, no. 2, Nov. 2003, doi: 10.1016/j.ab.2003.08.005.
[92] H. Bisswanger, 'Enzyme assays', *Perspect. Sci.*, vol. 1, no. 1, pp. 41–55, May 2014, doi: https://doi.org/10.1016/j.pisc.2014.02.005.
[93] J. Kopp, A. M. Kolkmann, P. G. Veleenturf, O. Spadiut, C. Herwig, and C. Slouka, 'Boosting Recombinant Inclusion Body Production—From Classical Fed-Batch Approach to Continuous Cultivation', *Front Bioeng Biotechnol*, vol. 7, 2019, doi: 10.3389/fbioe.2019.00297.
[94] C. Koch, M. Brandstetter, P. Wechselberger, B. Lorantfy, M. Plata, S. Radel, C. Herwig, and B. Lendl, 'Ultrasound-Enhanced Attenuated Total Reflection Mid-infrared Spectroscopy In-Line Probe: Acquisition of Cell Spectra in a Bioreactor', *Anal Chem*, vol. 87, no. 4, pp. 2314–20, Feb. 2015, doi: 10.1021/ac504126v.
[95] C. Koch, A. E. Posch, C. Herwig, and B. Lendl, 'Comparison of Fiber Optic and Conduit Attenuated Total Reflection (ATR) Fourier Transform Infrared (FT-IR) Setup for In-Line Fermentation Monitoring', *Appl. Spectrosc.*, vol. 70, no. 12, Dec. 2016, doi: 10.1177/0003702816662618.

4.6 Figures

Figure 1. Principle of pET expression system: Expression of T7 RNA polymerase upon induction with lactose or an analogue of it which displaces the lac repressor from the lac promotor. The T7 RNA polymerase in turn activates the T7 promotor on the plasmid leading to the transcription of the target gene. 11
Figure 2. Simplified fed batch cultivation scheme for our cultivation; with X being the biomass concentration [g/L], S the substrate concentration [g/L] and P the product concentration [g/L]...12
Figure 3. Downstream processing: First, the biomass is separated from the bulk by centrifugation. Intracellular products must be isolated by cell disruption. For the soluble fraction or products contained in the supernatant, subsequent steps involve capture of the product (removal of excess water and components having considerably different properties to the product), product purification (removal of contaminants with physical and chemical properties closely related to that of the product) and formulation (final step in order to stabilize the product for storage). In case of IBs, they must be solubilized and/or refolded after cell disruption to restore their native structure before purification. IBs with biological activity/ native-like protein structure can be used for direct applications.....15

Figure 4. DoE for process optimization to produce recombinant Hyaluronidase. Experiments 1 -7 were performed in a full factorial design. Additional experiments 8-11 were subsequently performed to screen for quadratic interactions in the region of interest. 26
Figure 5. FCM principle. A mixture of suspended fluorescent tagged cells passes through a laser-detector system that monitors the fluorescent and light scatter characteristics. The fluorescent emission is related to the amount of fluorescent probe bound to the cell. FSC (forward scatter) is proportional to cell size; SSC (side scatter) indicates cell granularity. Fluorescence patterns of each subpopulation, combined with FSC and SSC data, are used to identify which cells are present in a sample.....27
Figure 6.**a)** specific titer and glycerol concentration over induction time for a cultivation at T = 35 °C and $q_{s,C}$ = 0.5 g/g/h. Blue spots indicate for the specific titer, red spots indicate for glycerol concentration; **b)** Effect of applied $q_{s,C}$ and temperature on the specific titer over induction time. 34
Figure 7. Mean values for the four center point cultivations (T=30 °C, $q_{s,C}$ =0.3 g/g/h). Titer, glycerol, and biomass over induction time with error bars for titer and glycerol. 35
Figure 8. Contour plots. **a)** maximum glycerol concentration in broth; **b)** maximum acetate concentration in broth; **c)** specific hyaluronidase IB titer at 4-hour induction time; **d)** mean specific productivity over the whole induction time. 37
Figure 9. Model evaluation by MODDE 12 for Contour plots; mean productivity. 38
Figure 10. Model evaluation by MODDE 12 for Contour plots; specific titer at 4 hours induction. 39
Figure 11. Model evaluation by MODDE 12 for Contour plots; maximum glycerol production. 40
Figure 12. Model evaluation by MODDE 12 for Contour plots; maximum acetate production. ..41
Figure 13. IB bead size for a center point cultivation (30 °C, 0.3 g/g/h) at 2 h induction time after homogenization and washing with ultrapure water; bright spots indicate for IBs; dark spots are host cell related impurities. 42
Figure 14. Mean IB bead size at T = 25°C and $q_{s,C}$ = 0.1 g/g/h over induction time with mean standard deviations. 43
Figure 15. IB bead size – specific titer correlation for 3 cultivations at 4h induction time. 44
Figure 16. Calibration of commercial hyaluronidase activity using the photometric assay method. 45
Figure 17. Biological activity of hyaluronidase inclusion bodies vs titer 46

Figure 18. FT-IR spectra of the enzymatic reaction after 1 minute (blue) and after 40 minutes (red). **a)** FT-IR spectra of the enzymatic reaction with hyaluronidase IB at an IB concentration of 12.6 mg/mL **b)** analyzed IR bands for degradation of hyaluronan with commercial hyaluronidase at a concentration of 30 mg/mL; different bands showed high changes compared to IBs. 48
Figure 19. **a)** Progression of the normalized band ratio with time of four investigated IB concentrations. **b)** Growth rate vs IB concentration shows linear relationship. 49

5. Paper: Production of active recombinant Hyaluronidase Inclusion Bodies from *Apis mellifera* in *E. coli* Bl21(DE3) and characterization by FT-IR Spectroscopy

International Journal of
Molecular Sciences

MDPI

Article

Production of Active Recombinant Hyaluronidase Inclusion Bodies from *Apis mellifera* in *E. coli* Bl21(DE3) and characterization by FT-IR Spectroscopy

Andreas Schwaighofer [1], Sarah Ablasser [2], Laurin Lux [1], Julian Kopp [2], Christoph Herwig [2], Oliver Spadiut [3], Bernhard Lendl [1] and Christoph Slouka [3,*]

1 FG Environmental Analytics, Process Analytics and Sensors, Institute of Chemical Technology and Analytics, Vienna University of Technology, Getreidemarkt 9/164, 1060 Wien, Austria; andreas.schwaighofer@tuwien.ac.at (A.S.); laurin.lux@tuwien.ac.at (L.L.); bernhard.lendl@tuwien.ac.at (B.L.)
2 FG Bioprocess Technology, ICEBE, Vienna University of Technology, Gumpendorferstrasse 1a, 1060 Vienna, Austria; sarah.ablasser@hotmail.com (S.A.); julian.kopp@tuwien.ac.at (J.K.); christoph.herwig@tuwien.ac.at (C.H.)
3 FG Integrated Bioprocess Development, ICEBE, Vienna University of Technology, Gumpendorferstrasse 1a, 1060 Vienna, Austria; oliver.spadiut@tuwien.ac.at
* Correspondence: christoph.slouka@tuwien.ac.at; Tel.: +43-699-12971472

Received: 26 April 2020; Accepted: 27 May 2020; Published: 29 May 2020

check for updates

Abstract: The bacterium *E. coli* is one of the most important hosts for recombinant protein production. The benefits are high growth rates, inexpensive media, and high protein titers. However, complex proteins with high molecular weight and many disulfide bonds are expressed as inclusion bodies (IBs). In the last decade, the overall perception of these IBs being not functional proteins changed, as enzyme activity was found within IBs. Several applications for direct use of IBs are already reported in literature. While fluorescent proteins or protein tags are used for determination of IB activity to date, direct measurements of IB protein activity are scacre. The expression of recombinant hyaluronidase from *Apis mellifera* in *E. coli* BL21(DE3) was analyzed using a face centered design of experiment approach. Hyaluronidase is a hard to express protein and imposes a high metabolic burden to the host. Conditions giving a high specific IB titer were found at 25 °C at low specific substrate uptake rates and induction times of 2 to 4 h. The protein activity of hyaluronidase IBs was verified using (Fourier transform) FT-IR spectroscopy. Degradation of the substrate hyaluronan occurred at increased rates with higher IB concentrations. Active recombinant hyaluronidase IBs can be immediately used for direct degradation of hyaluronan without further down streaming steps. FT-IR spectroscopy was introduced as a method for tracking IB activity and showed differences in degradation behavior of hyaluronan dependent on the applied active IB concentration.

Keywords: *Escherichia coli*; active inclusion body; recombinant protein production; upstream process development; FT-IR spectroscopy

1. Introduction

The bacterium *Escherichia coli* (*E. coli*) is one of the most extensively used prokaryotic organisms for recombinant protein production [1]. Being an expression host of choice for a long time, the genetic basis of *E. coli* is well characterized, and many manipulation tools are available [2]. Although *E. coli* lacks the post-translational machinery, advantages, like fast growth to high cell densities on comparatively inexpensive media, high biomass yields and simple scale-up, make the bacterium favorable [3]. Today, various eukaryotic expression systems are used to produce recombinant proteins, but *E. coli* accounts for the production of nearly 40% of all approved biopharmaceuticals [4]. Monoclonal antibodies

and antibody fragments are currently the most important biopharmaceutical products. This further expands the use of *E. coli* as production host, as fragmented antigen binding antibodies (Fabs) can be successfully expressed [5,6].

The *E. coli* strain BL21(DE3), created by Studier and Moffatt back in 1986 [7], is often used for industrial production as it allows for high replication rates and shows low acetate formation [8]. In combination with the pET expression system, high transcriptional rates can be achieved [9]. Using such strong expression systems combined with harsh inducers, like IPTG, leads to high product yields, but also causes a high metabolic burden to the cells, often resulting in intracellular protein aggregates, called inclusion bodies (IBs). Inclusion bodies are insoluble protein aggregates, formerly considered as waste products [10]. Proteins accumulate due to specific stress reactions, like strong overexpression, high inducer concentrations, pH shifts, high temperatures and uptake rates, resulting in biologically inactive proteins [11]. Such IBs can be exploited for the production of toxic or unstable proteins that can subsequently be refolded in vitro [12]. Efficient refolding procedures are established today, but this time-consuming step to gain active protein for therapeutic use is a major drawback.

However in recent years, it was discovered that IBs contain a reasonable amount of correctly folded and thus biologically active protein and the misconception of IBs being inactive products composed of unfolded or misfolded proteins has changed [13–15]. Showing high specific activities suggests enrichment of active protein within IBs, making them important tools in the industrial biotechnological market and for biomedical applications [10,16,17]. Catalytically active IBs (CatIBs) as carrier-free protein immobilisates are promising biomaterials for synthetic chemistry, biocatalysis and biomedicine [18,19]. Furthermore, the correctly folded polypeptides within IBs coexist with an amyloid-like intermolecular beta-sheet structure conferring mechanical stability to IBs [20,21]. Thus, IBs can be useful systems for therapeutic approaches studying pathologic protein deposition in amyloid diseases, like Alzheimer's or Parkinson's disease, in which the accumulation of proteins initiates the pathogenic process [22–25].

Inclusion bodies also unveil high potential in biomedical applications in vivo as delivery vehicles or 'nanopills' for prolonged drug release [26–29]. Active IBs, as nanostructured amyloidal particles of 50-500 nm, are considered as mimetics of the endocrine secretory granules because they naturally penetrate mammalian cells and release their protein in soluble and functional form under physiological conditions [30]. It was shown, that decorating 3D-scaffolds with bacterial IBs favored mammalian cell surface colonization and stimulating proliferation and allowed the penetration and intracellular delivery of functional protein in absence of cytotoxicity and hence, offers possibilities in tissue engineering and regenerative medicine [31–33]. However, IBs are constrained for the use in biomedicine by their bacterial origin and undefined composition. To overcome these constraints, the creation of artificial IBs resulting in homogenous protein reservoirs for prolonged in vivo delivery of tumor-targeted drugs has been reported recently [34]. As new approaches emerge and the production of active IBs gains more interest, the impact of upstream process parameters on IB attributes becomes more important as they highly affect the amount of active protein within IBs [35].

Fourier transform-infrared (FT-IR) spectroscopy is a powerful analytical technique that provides molecule specific qualitative and quantitative information in a nondestructive and label-free manner by probing molecular vibrations [36]. It is a commonly used method for the analysis of biological samples, in particular proteins [37] and carbohydrates [38]. IR spectroscopy was successfully employed for monitoring enzyme activity by evaluating spectral changes of the substrate triggered by the enzymatic reaction [39–41]. Most recently, it was applied for secondary structure characterization of IBs [42–45]. To the best of our knowledge, this is the first report of assessing CatIB activity by IR spectroscopy.

Hyaluronidase is an important enzyme for oncological care. The enzyme itself is known for rendering tissues more permeable for drug absorption (spreading effect) [46]. It is further used for defined production of hyaluronan oligosaccharides, which play crucial roles in different cellular responses. One of the main applications is tumor suppression and angiogenesis–formation of new blood vessels in tissues [47,48]. The goal of this study was the production of a high amount of active IBs

of a hyaluronidase from *Apis mellifera* for direct application in the production of defined hyaluronan. Our hypotheses were (1) that adjustment of process parameters during the upstream process does not only affect productivity but also IB activity, and (2) that IR spectroscopy can be used to measure IB activity. For recombinant protein expression, *E. coli* BL21(DE3) was used as expression host in combination with the pET expression system and IPTG as inducing agent. In a fed batch cultivation, IB production was triggered in the induction phase. The upstream process parameters temperature and specific substrate uptake rate were altered using design of experiments (DoE) approaches and the IB size, and titer were analyzed. For activity assessment FT-IR analysis was used, and we showed that the produced hyaluronidase IBs exhibited reasonable activity and were able to degrade hyaluronan in situ.

2. Results

2.1. Variation of Specific Substrate Uptake Rate and Temperature Using a DoE Approach

In order to check for multivariate dependencies, we cultivated *E. coli* harboring the target protein in a classical fed batch approach and altered temperature and specific substrate uptake rate ($q_{s,C}$) in the induction phase based on the design in the Materials Part. Expression of recombinant hyaluronidase in *E. coli* led to a very high metabolic burden. Time-dependent cultivation responses are given in Figure 1. The four center point cultivations were compared in terms of volumetric recombinant protein titer and glycerol accumulation in the broth. Titer had a rather high standard deviation as starting biomass before induction differed in a range of approx. 25–30 g/L dry cell weight (DCW), however, the overall trend of recombinant protein expression could be clearly dedicated from the center point runs. Expression maximum was at very early induction times of approx. 2 to 4 h, with titers of 100 mg/L recombinant IBs. Longer expression led to high metabolic burden, which resulted in massive accumulation of the carbon source in the broth. This also resulted in a pronounced drop in specific growth rate and carbon uptake rate, often seen during harsh induction using IPTG [49]. Hence, biomass was only slowly growing during the induction phase and stopped after 2–4 h completely (Figure 1). In Figure 2 the statistical evaluation of different process and product parameters is presented. Figure 2a shows the maximal glycerol concentration in the broth in the induction phase. Irrespective of temperature, high accumulation occurred at medium to high specific substrate uptake set points, as growth rates decreased. A very similar dependence was found for acetate production (Figure 2b), which is only dependent on the applied $q_{s,C}$.

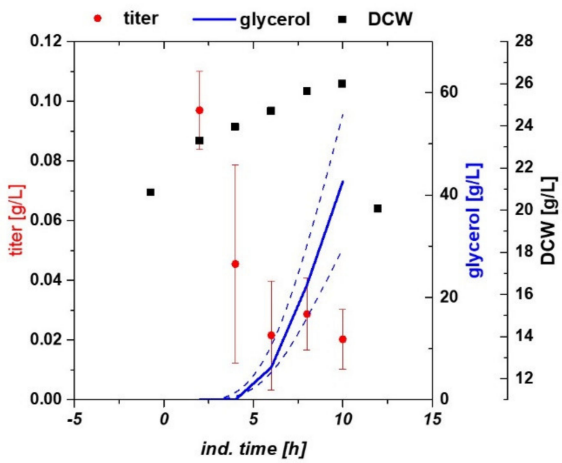

Figure 1. Centerpoint cultivations of *E. coli* expressing recombinant hyaluronidase. Recombinant protein expression is the highest at early induction times. As the protein is obviously hard to express, biomass growth decreases and glycerol accumulates in the broth over induction time.

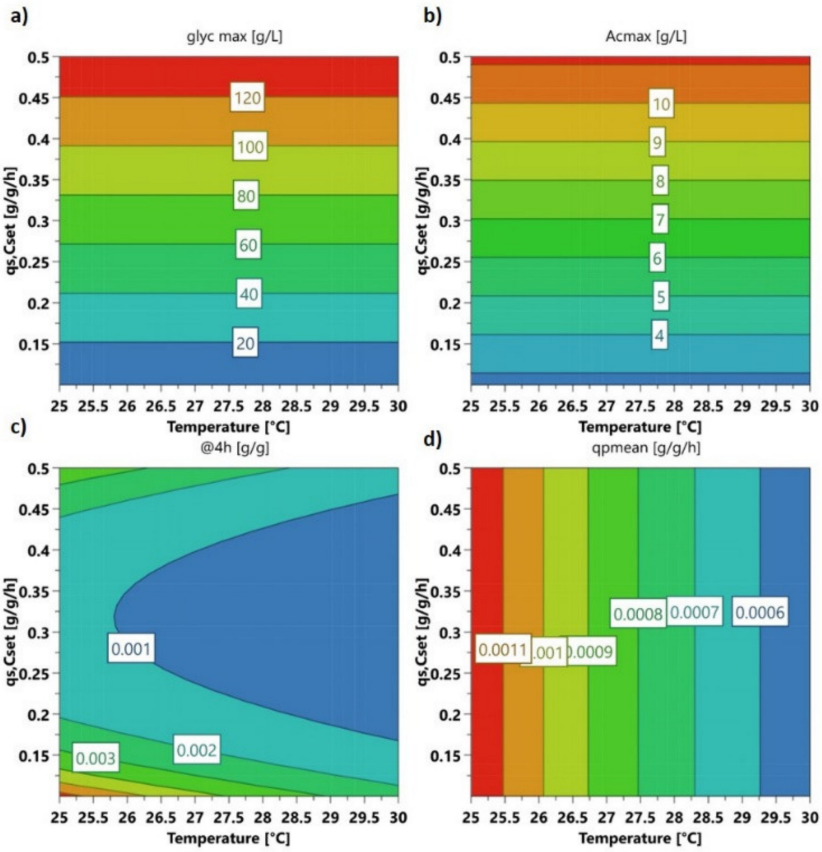

Figure 2. Contour plots. (**a**) maximum glycerol concentration in broth; (**b**) maximum acetate concentration in broth; (**c**) specific hyaluronidase IB titer at 4-h induction time; (**d**) mean specific productivity over the whole induction time.

Analogue responses were found for the protein titer after 4 h of induction (Figure 2c). This response was chosen, because the highest specific IB titers were found after 4 h of induction. Low specific substrate uptake rates in combination with low temperatures seem to be the optimal conditions for a high specific IB titer. Linear terms for temperature and quadratic terms for $q_{s,C}$ are significant in the model. The linear $q_{s,C}$ term is only close to significance, but kept in the model to increase the quality of the fit. Quadratic interaction could only be roughly estimated through this DoE model and did not reflect absolute values (compare to Supplementary Figure S1).

The averaged specific IB productivity ($q_{p,mean}$) over the entire induction time showed only dependence on temperature (Figure 2d). Only positive values were considered, and degradation of the product was not taken into account. Considering the overall uncertainty of these values based on titer values/divided by biomass per time, the best induction strategy for production of recombinant hyaluronidase IBs is at low temperatures at a low specific substrate uptake rate for a maximum of 4 h of induction. The statistical evaluation can be found in Supplementary Figure S1.

We also analyzed IB bead size using scanning electron microscopy (SEM), for cultivations and induction times with the highest IB titers. 50 individual IB beads were measured on different images. It was found that the bead size was 230 nm throughout the analyzed cultivation with about 15% standard deviation. It was shown in recent studies by our group that IB size is strongly related to the IB titer during cultivation [44,50]. Both results indicate no new recombinant protein production after 4 h as also no increase in IB size could be observed. Figure 3a shows a representative SEM picture of hyaluronidase IBs of a centerpoint cultivation. Grey parts are host cell impurities, while bright spots are actual IBs. For purity determination we performed SDS-Page of two cultivation runs to compare purity during expression. The corresponding gel is given in Figure 3b. First line is the ladder, line 2 to 5 a commercially available BSA standard and lines 6 to 15 hyaluronidase samples. Titers of the IBs

are below 0.5 g/L and therefore in good accordance with HPLC results. The MW of hyaluronidase is about 43 kDa with the clearly visible double peak as already known in literature [51]. The purity differs between 30 to 45% for the analyzed samples. As the IBs were only washed with ultrapure water, several host cell proteins can still be found in the pellet (which are also visible in the SEM). An extensive washing procedure with buffers including detergents like Triton X 100 may increase purity further as water insoluble host cell impurities will be solved.

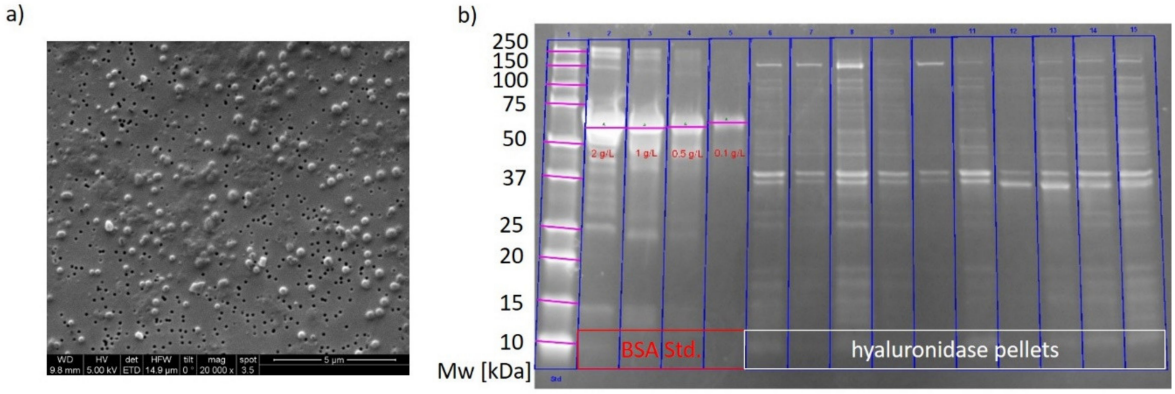

Figure 3. (**a**) SEM of hyaluronidase IBs. The bright spots are IB beads, while dark gray spots are host cell related impurities after the washing procedure; (**b**) SDS-PAGE of two hyaluronidase cultivations. Lane 1 is the molecular weight ladder, lane 2 to 5 the BSA standard, lane 6–10 and lane 11–15 two respective IB samples from two cultivations with sampling times of 4, 6, 8, 10 and 12 h of induction

2.2. Hyaluronidase IB Activity Measured by FT-IR Spectroscopy

As IR measurements demand higher overall concentration of recombinant protein, activity could not be analyzed of all experimental points of the DoE based on the relatively low titer. In order to produce high amounts of IBs, we used the optimal condition of 4 h induction at 25 °C and a $q_{s,C}$ of 0.1 g/g/h and cultivated and harvested about 4 L of broth. IBs were centrifuged and re-suspended for IR measurements. The activity of the produced hyaluronidase IBs was tested by monitoring the enzymatic reaction with its native substrate, hyaluronan, by FT-IR spectroscopy. Hyaluronan is a polysaccharide of high molecular weight composed of repeating disaccharide units of D-glucuronic acid–β(1,3)-*N*-acetyl-D-glucosamine linked by β(1,4) glycosidic bonds. The hyaluronidase produced by *Apis mellifera* hydrolyses the glycosidic bonds in the β(1,4) position [45]. It was found that hyaluronidase exhibits an atypical Michaelis-Menten behavior at high substrate concentrations potentially because of non-specific complexes between hyaluronan and hyaluronidase based on electrostatic interactions. [52] Furthermore, the high viscosity of highly concentrated hyaluronan close to the solubility limit of 5 mg/mL may contribute to the atypical behavior due to steric exclusions of hyaluronidase from hyaluronan solution. Regarding the sensitivity of FT-IR spectroscopy, there is also a lower limit for the substrate concentration. For this reason, a hyaluronan concentration of 1 mg/mL was chosen for all IB activity test measurements.

The reaction of the IB-substrate solutions at IB concentrations between 1.5 and 30 mg/mL was monitored by FT-IR spectroscopy. Supplementary Figure S2a) shows a representative spectrum of the progression of the enzymatic reaction in the spectral region where the changes of the substrate occur. The band at 1077 cm^{-1} was assigned to the $\nu_{C\text{-}O\text{-}C}$ ring mode and the band at 1025 cm^{-1} could be attributed to the $\nu_{C\text{-}OH}$ modes of alcohols [53,54]. The band height of these two bands was evaluated and then the ratio was calculated. This normalization step was necessary, because the viscosity of the solution changed during the measurement, which lead to a changing baseline and varying absorbance across the entire spectrum [45]. For further analysis, the band height ratios were plotted versus the reaction time (Figure 4a). The obtained temporal progression was then fitted using a one-phase exponential grow function with time offset (with a high coefficient of determination, $R^2 > 0.98$) and the

growth rate was calculated as the inverse time constant. The growth rate shows a linear correlation to the IB concentration as visualized in Figure 4b.

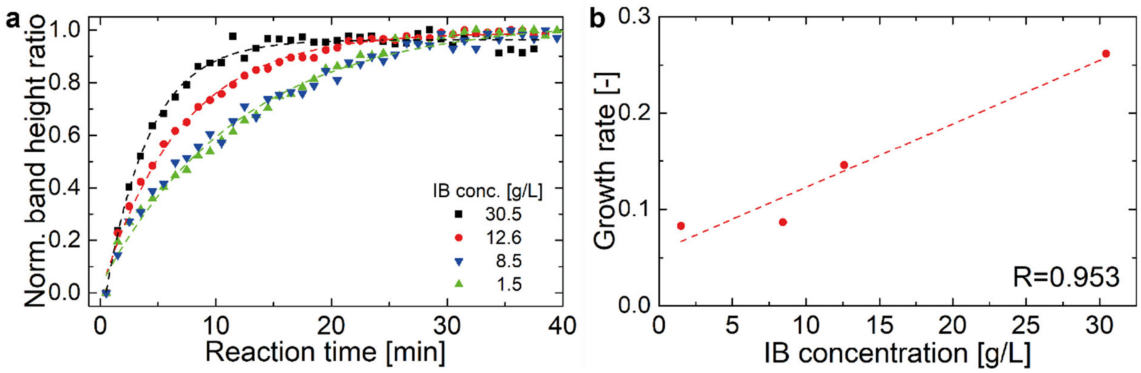

Figure 4. (**a**) Progression of the normalized band ratio with time of four investigated IB concentrations. (**b**) Growth rate vs IB concentration shows linear relationship.

3. Discussion

Hyaluronan oligosaccharides stimulate angiogenesis and suppress the growth of tumors [47]. Production of defined hyaluronan oligosaccharides is mandatory to fulfill this task. Active IBs of hyaluronidase are partly misfolded proteins, but exhibit residual protein activity, and are stable and easy to immobilize [55]. Such active IBs would facilitate degradation of hyaluronan to defined structures. Therefore, we cultivated *E. coli* expressing recombinant hyaluronidase, which shows rather low expression rates in *E. coli*. In order to increase the production of active IBs, we alternated the specific substrate uptake rate and induction temperature in a DoE design based on previous results [44]. We analyzed the expression in a small-scale system and expressed the protein in a larger scale to produce sufficient amounts of IB to comply with the sensitivity requirements of FT-IR spectroscopy, which we used to measure the activity of the IBs. Before cultivation we analyzed hyaluronidase from *Apis mellifera* with Expasy ProtPrameter server [56] and Disulfind server [57]. ProtParameter characterizes hyaluronidase as unstable with a computed instability index of 44.3 and Disulfind predicts two disulfide bonds with high probability. As the protein does not have a signal sequence for translocation into the periplasm, expression as IB is highly favored for this protein as disulfide bonds often cannot be correctly expressed in the cytoplasm. Recent works expressed hyaluronidase in *E. coli* as IBs in a shake flask-based approach with complex media. However, no upstream production in a controlled bioreactor system was performed [47,51,58]. The results of our cultivations showed expected expression as IBs, however, only in low concentrations. Cell stress is often the bottleneck for high protein expression in bacterial hosts. Recent studies marked several reasons for the so called metabolic burden upon recombinant protein expression [59–64]. Markers for metabolic burden during cultivation are a decrease of the specific growth rate (μ), resulting in glycerol accumulation and acetate formation.

However, such high acetate production is unexpected in BL21, as this strain is regarded as a low acetate former. This is based on an highly active glyoxylate shunt, which is generally inactive in the high acetate producing strain [65,66]. High acetate concentrations inhibit cell growth and recombinant protein production, which may be also the case in our cultivation. These high acetate concentrations indicate enormous metabolic stress levels upon production of recombinant hyaluronidase. Therefore, high uptake rates must be omitted. Low temperatures and specific glycerol uptake rates of 0.1 g/g/h fulfilled this task and were, therefore, well-chosen process parameters to successfully express hyaluronidase.

Measurement of IB activity can be complex procedure depending on the protein of interest. Many groups use marker proteins, like GFP related fluorescence proteins, or protein activity assays to get insight into protein activity [10,11,67]. Within this work, initial tests of photometric assays using hyaluronan based upon sedimentation of particles or initial turbidity of the sample mix did only show significant results for commercial hyaluronidase, but not for the produced IBs (Sigma Aldrich

test No: 3.2.1.35). Therefore, we aimed for an alternative measurement method for activity testing based on IR spectroscopy. As depicted in Figure 4b), the growth rate shows a linear correlation to the IB concentration, demonstrating and verifying the activity of the produced IB [68]. However, because of the applied normalization steps, no quantitative information about the enzyme velocity can be obtained. Comparison to commercially available hyaluronidase showed similar degradation behavior in FT-IR, given in Figure 5a. However different bands were evaluated for commercial enzyme compared to IBs. Details on the spectral information are given in Supplementary Figure S2b. For the commercial enzyme bands at 1113 cm^{-1} as $\nu_{C\text{-}O\text{-}C}$ glycosidic vibration and 1046 cm^{-1} as $\nu_{C\text{-}OH}$ vibration were used. Similar dependence on degradation behavior based on protein concentration is found for IBs and commercially available enzyme. However, absolute quantification based on the degradation curve is challenging, compare to Figure 5b.

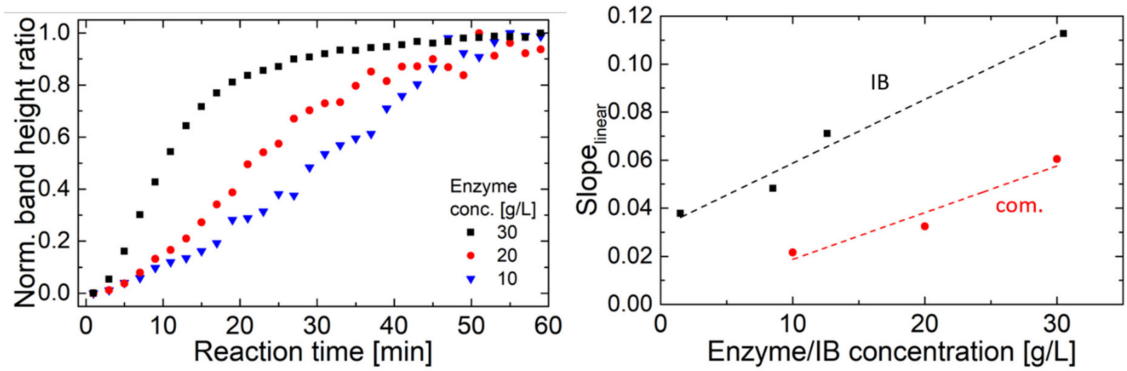

Figure 5. (**a**) degradation behavior of commercially available enzyme, (**b**) linear part of the slopes of the degradation curves vs. concentration of the enzymes.

Due to normalization of band changes absolute values are tricky to obtain and enzymatic activity depends on several parameters, such as pH and ionic strength [69,70]. However, based on a first photometric measurement, commercially derived enzymes seem to inherit a higher activity than the IB beads. For detailed enzymatic activity, the reaction products would have to be measured in a time dependent matter.

Nevertheless, it is shown that spectral changes caused by the enzyme reaction can be directly related to the enzyme activity, thus eliminating the need for further reaction steps that are usually required in conventional activity assays to obtain a reaction product detectable by UV/VIS spectroscopy. Planned improvements of this experimental approach, such as a temperature-controlled ATR manifold, will pave the way for a fully IR-based activity characterization of IBs and enzymes in situ. Alternatively, as IR spectroscopy was proven to be an excellent tool for in-line monitoring of bioprocesses by using fiber optic probes [71,72], IB activity measurements could also be performed in-line directly in an reactor vessel.

4. Materials and Methods

4.1. Strains

E. coli BL21(DE3) was used with the pET28a plasmid system (kanamycin resistance) for recombinant protein production. A 1155 kb gene from *Apis mellifera* was codon optimized for *E. coli* and cloned at *Nde*I and *Xho*I into the pET plasmid by General Biosystems (Durham, NC, USA) and subsequently electroporated. Details on state-of-the-art cloning procedure are given in the Supplementary Part.

4.2. Bioreactor Cultivations

All preculture and bioreactor cultivations were carried out using a defined minimal medium referred to DeLisa et al. (1999) [73]. Batch media and the preculture media had the same composition

with different amounts of glycerol—8 g/L for the preculture, 20 g/L for the batch phase. The feed for uninduced and induced fed-batch had a concentration of 400 g/L glycerol. Antibiotic was added throughout all fermentations in batch, resulting in a final concentration of 0.02 g/L of kanamycin. All precultures were performed using 500 mL high yield flasks. They were inoculated with 1.5 mL of bacteria solution stored in cryo stocks at −80 °C and subsequently cultivated for 20 h at 230 rpm in an Infors HR Multitron shaker (Infors, Bottmingen Switzerland) at 37 °C. IPTG was added once to start induction and had a final concentration of 0.5 mM. Recombinant protein production was performed in a DASGIP Mini bioreactor-4-parallel fermenter system (max. working volume: 2.5 L; Eppendorf, Hamburg, Germany). Cultivation offgas was analyzed by gas sensors-IR for CO_2 and ZrO_2 based for O_2 (Blue Sens Gas analytics, Herten, Germany). For analytics, protein was produced in a stainless-steel Sartorius Biostat Cplus bioreactor (Sartorius, Göttingen, Germany) with 10 L working volume.

Process control was established using the PIMS Lucullus and the DAS-GIP-control system, DASware-control, which logged the process parameters. During batch-phase and fed-batch phase pH was kept constant at 6.7 and controlled with base only (12.5% NH_4OH), while acid (5% H_3PO_4) was added manually, when necessary. The pH was monitored using an EasyFerm Plus pH-sensor (Hamilton, Reno, NV, USA). The reactors were continuously stirred at 1400 rpm and aerated using a mixture of pressurized air and pure oxygen at 2 vvm. Dissolved oxygen (dO_2) was always kept higher than 30% by increasing the ratio of oxygen in the ingas. The dissolved oxygen was monitored using a fluorescence dissolved oxygen electrode Visiferm DO (Hamilton, Reno, NV, USA) The fed-batch phase for biomass generation was followed by an induction phase. Specific substrate uptake rate ($q_{s,C}$) and temperature in the induction phase was adapted according to the DoE given in Figure 6. The specific substrate uptake rate was altered between 0.1 g/g/h and 0.5 g/g/h and temperature between 25 °C and 35 °C. The center point at 30 °C and 0.3 g/g/h was cultivated four times in order to assess the statistical experimental error.

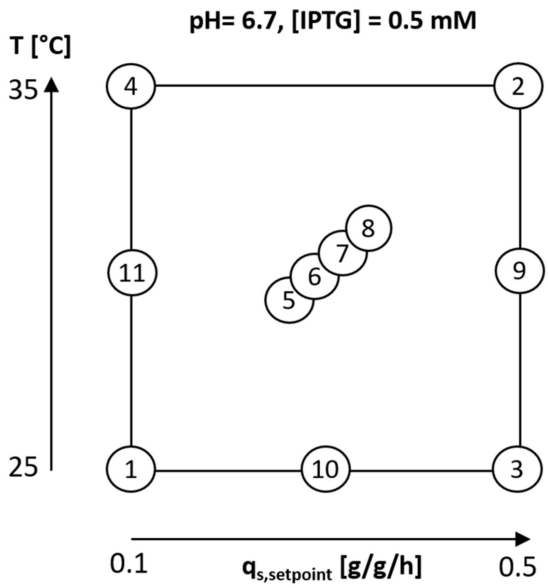

Figure 6. DoE for process optimization to produce active recombinant hyaluronidase IBs. Experiments 1–7 were performed in a modified CCF design. Additional experiments 9–11 were subsequently performed to analyze for quadratic interactions in the region of interest.

4.3. Cultivation Analytics

4.3.1. Biomass

For dry cell weight (DCW) measurements 1 mL of the cultivation broth was centrifuged at 9000× *g*, subsequently washed with 0.9% NaCl solution and centrifuged again under the same conditions. After

drying the cells at 105 °C for 48 h, the pellet was evaluated gravimetrically. DCW measurements were performed in five replicates and the mean error for DCW was approx. 3%. Offline OD_{600} measurements were performed in duplicates in a UV/VIS photometer Genisys 20 (Thermo Scientific, Waltham, MA, USA).

4.3.2. Sugar Analytics

Sugar concentrations in the filtered fermentation broth were determined using a Supelco C-610H HPLC column (Supelco, Bellefonte, PA, USA) on an Ultimate 3000 HPLC system (Thermo Scientific, Waltham, MA, US) using 0.1% H_3PO_4 as running buffer at 0.5 mL/min or an Aminex HPLC column (Biorad, Hercules; CA, USA) on an Agilent 1100 System (Agilent Systems, Santa Clara, CA, USA) with 4 mM H_2SO_4 as running buffer at 0.6 mL/min.

4.4. Product Analytics

4.4.1. IB Preparation

5 mL fermentation broth samples were centrifuged at 4800 rpm at 4 °C for 10 min. The supernatant was discarded and the pellet was resuspended to a DCW of about 4 g/L in lysis buffer (100 mM Tris, 10 mM EDTA at pH = 7.4). Afterwards the sample was homogenized using a high-pressure homogenizer at 1500 bar for 10 passages (PandaPLUS, Gea AG, Germany). After centrifugation at 10,000 rpm and 4 °C the supernatant was discarded and the resulting IB pellet was washed twice with ultrapure water and aliquoted into pellets of 2 mL broth, centrifuged (14,000 rpm, 10 min 4 °C) and stored at −20 °C.

4.4.2. IB Size

Washed and aliquoted IB samples were resuspended in ultrapure water. 100 µL of appropriate dilution of the suspension were pipetted on a gold-sputtered (10–50 nm) polycarbonate filter (Millipore-Merck, Darmstadt, Germany) using reusable syringe filter holders with a diameter of 13 mm (Sartorius, Göttingen, Germany). 100 µL of ultrapure water were added and pressurized air was used for subsequent filtration. Additional 200 µL of ultrapure water were used for washing. The wet filters were fixed on a SEM sample holder using graphite adhesive tape and subsequently sputtered with gold to increase the contrast of the sample. SEM was performed using a QUANTA FEI SEM (Thermo Fisher, Waltham, MA, USA) with a secondary electron detector [60]. The acceleration voltage of the electron beam was set between 3 to 5 kV. To determine the diameter of the IBs, 50 IBs on SEM pictures were measured using the ImageJ plugin Fiji (Laboratory for Optical and Computational Instrumentation (LOCI), University of Wisconsin-Madison, USA). SEM analytics of two different time points for both strains are given in Figure 2.

4.4.3. IB Titer

For titer measurements, IB pellets were solubilized using solubilization buffer (7.5 M guanidine hydrochloride, 62 mM Tris at pH = 8). The filtered samples were quantified by HPLC analysis. The HPLC was equipped with a BioResolve RP mAb Polyphenyl column (dimensions 100 × 3 mm, particle size 2.7 µm) which is designed for mAb and large protein analyses (Waters Corporation, MA, USA). To prolong column lifetime, a pre-column (3.9 × 5mm, 2.7 µm) was used. The mobile phase was composed of ultrapure water (=MQ, eluent A) and acetonitrile (eluent B) both supplemented with 0.10% (*v/v*) trifluoroacetic acid. The injection volume was set to 2.0 µL. The flow rate and the column temperature of the final method were 0.4 mL/min and 70 °C, respectively. Details on the measurement methodology is given in [74].

4.4.4. SDS-PAGE

For the SDS-page Mini-PROTEAN® TGX Stain-Free™ (BioRad, Hercules, CA, USA) was used. 4× Laemmli sample buffer (BioRad) containing 200 µL ß-mercaptoethanol was diluted 2 times with ultrapure water for the soluble samples and 4 times in order to dissolve the IB pellets. BSA standard with concentrations of 2, 1, 0.5, 0.1 g/L were mixed 1:1 with Laemmli buffer. The IB pellets were dissolved with 500 µL Laemmli buffer. All samples were denatured for 5 min at 95 °C and subsequently spun down. 5 µL protein standard (precision plus protein standard dual color, BioRad) and 10 µL of each sample were loaded onto the gel and it was run for 30 min at 180V. Afterwards the gel was stained for about an h using Coomassie brilliant blue (BioRad).

4.4.5. FT-IR Spectroscopy

FT-IR absorption measurements of IB activity monitoring was performed using a Bruker Vertex 70V FT-IR spectrometer (Ettlingen, Germany) equipped with a Bruker Optics Platinum ATR module (diamond crystal, 1 mm^2 area with single reflection) and a liquid nitrogen cooled HgCdTe (mercury cadmium telluride) detector. To start the enzymatic reaction, 15 µL of IB at different concentrations were mixed with 15 µL of 1 mg/mL hyaluronan (sodium salt from *Streptococcus equi*, bacterial glycosaminoglycan polysaccharide, No. 53747, Sigma Aldrich) and thoroughly vortexed. The sample solution was then placed on the ATR crystal and covered with a cap to prevent solvent evaporation during spectra acquisition. ATR-FT-IR spectra were collected every minute for a time period of 40 min. For IB concentration determination, commercially obtained hyaluronidase type I-S from bovine testes (No. H3506, Sigma Aldrich) was used for calibration and the amide II band height was evaluated. Spectra were acquired with a spectral resolution of 4 cm^{-1} in double-sided acquisition mode; the mirror velocity was set to 80 kHz. A total of 450 scans were averaged per spectrum, which was calculated using a Blackman-Harris 3-term apodization function and a zero-filling factor of 2. All spectra were acquired at 25 °C. Spectra were analyzed using the software package OPUS 8.1 (Bruker, Ettlingen, Germany).

5. Conclusions

Here we present a cultivation strategy to obtain a high specific titer of active hyaluronidase from *Apis mellifera* IBs in *E. coli* as well as a novel tool to determine their catalytic activity by using ATR FT-IR spectroscopy. We demonstrated that active hyaluronidase IB can be used for degradation of hyaluronan. Further evaluation of critical quality attributes will be necessary, but these active IBs may be a useful tool for pharmaceutical applications.

Supplementary Materials: Supplementary materials can be found at http://www.mdpi.com/1422-0067/21/11/3881/s1.

Author Contributions: C.S. and A.S. designed the study. C.S., J.K. and S.A. conducted the bioreactor experiments and analyzed the data. A.S., L.L. and S.A. conducted the FT-IR measurements. A.S. analyzed FT-IR data. C.S., S.A. and A.S. drafted the manuscript. C.H. and B.L. proofread the manuscript, O.S. supervised the work and gave valuable input. All authors have read and agreed to the published version of the manuscript.

Funding: This work has received financial support by the Austrian Science Fund FWF (project no. P32644-N).

Acknowledgments: Open Access Funding by the Austrian Science Fund (FWF). Furthermore, we also thank COMET Center CHASE (project No 868615) for funding. CHASE is funded within the framework of COMET (Competence Centers for Excellent Technologies) by BMVIT, BMDW, and the Federal Provinces of Upper Austria and Vienna. The COMET program is run by the Austrian Research Promotion Agency (FFG).

Conflicts of Interest: The authors declare no conflict of interest.

Abbreviations

DCW	Dry cell weight
dO_2	Dissolved oxygen
DoE	Design of experiments
CCF	Face centered composite design
IB	Inclusion Body
IPTG	isopropyl β-D-1 thiogalactopyranoside
FT-IR	Fourier Transformed – Infrared (Spectroscopy)
MQ	Ultrapure water
$q_{s,C}$ [g/g/h]	specific substrate uptake rate
q_P [g/g/h]	Specific production rate
SEM	Scanning electron microscopy

References

1. Baneyx, F. Recombinant protein expression in Escherichia coli. *Curr. Opin. Biotechnol.* **1999**, *10*, 411–421. [CrossRef]
2. Huang, C.-J.; Lin, H.; Yang, X. Industrial production of recombinant therapeutics in Escherichia coli and its recent advancements. *J. Ind. Microbiol. Biotechnol.* **2012**, *39*, 383–399. [CrossRef] [PubMed]
3. Sahdev, S.; Khattar, S.K.; Saini, K.S. Production of active eukaryotic proteins through bacterial expression systems: A review of the existing biotechnology strategies. *Mol. Cell. Biochem.* **2007**, *307*, 249–264. [CrossRef] [PubMed]
4. Walsh, G. Biopharmaceutical benchmarks 2010. *Nat. Biotechnol.* **2010**, *28*, 917–924. [CrossRef] [PubMed]
5. Baeshen, M.N.; Al-Hejin, A.M.; Bora, R.S.; Ahmed, M.M.; Ramadan, H.A.; Saini, K.S.; Baeshen, N.A.; Redwan, E.M. Production of Biopharmaceuticals in *E. coli*: Current Scenario and Future Perspectives. *J. Microbiol. Biotechnol.* **2015**, *25*, 953–962. [CrossRef]
6. Spadiut, O.; Capone, S.; Krainer, F.; Glieder, A.; Herwig, C. Microbials for the production of monoclonal antibodies and antibody fragments. *Trends Biotechnol.* **2014**, *32*, 54–60. [CrossRef]
7. Studier, F.W.; Moffatt, B.A. Use of bacteriophage T7 RNA polymerase to direct selective high-level expression of cloned genes. *J. Mol. Biol.* **1986**, *189*, 113–130. [CrossRef]
8. Kopp, J.; Slouka, C.; Ulonska, S.; Kager, J.; Fricke, J.; Spadiut, O.; Herwig, C. Impact of Glycerol as Carbon Source onto Specific Sugar and Inducer Uptake Rates and Inclusion Body Productivity in *E. coli* BL21(DE3). *Bioengineering* **2018**, *5*, 1. [CrossRef]
9. Dubendorff, J.W.; Studier, F.W. Controlling basal expression in an inducible T7 expression system by blocking the target T7 promoter with lac repressor. *J. Mol. Biol.* **1991**, *219*, 45–59. [CrossRef]
10. García-Fruitós, E. Inclusion bodies: A new concept. *Microb. Cell Fact.* **2010**, *9*, 80. [CrossRef]
11. García-Fruitós, E.; Arís, A.; Villaverde, A. Localization of functional polypeptides in bacterial inclusion bodies. *Appl. Environ. Microbiol.* **2007**, *73*, 289–294. [CrossRef] [PubMed]
12. Baneyx, F.; Mujacic, M. Recombinant protein folding and misfolding in Escherichia coli. *Nat. Biotechnol.* **2004**, *22*, 1399–1408. [CrossRef] [PubMed]
13. Ventura, S.; Villaverde, A. Protein quality in bacterial inclusion bodies. *Trends Biotechnol.* **2006**, *24*. [CrossRef] [PubMed]
14. Peternel, Š.; Grdadolnik, J.; Gaberc-Porekar, V.; Komel, R. Engineering inclusion bodies for non denaturing extraction of functional proteins. *Microb. Cell Fact.* **2008**, *7*, 34. [CrossRef]
15. Rinas, U.; Garcia-Fruitós, E.; Corchero, J.L.; Vázquez, E.; Seras-Franzoso, J.; Villaverde, A. Bacterial inclusion bodies: Discovering their better half. *Trends Biochem. Sci.* **2017**, *42*, 726–737. [CrossRef]
16. Peternel, S.; Komel, R. Active protein aggregates produced in Escherichia coli. *Int. J. Mol. Sci.* **2011**, *12*, 8275–8287. [CrossRef]
17. De Marco, A.; Ferrer-Miralles, N.; Garcia-Fruitós, E.; Mitraki, A.; Peternel, S.; Rinas, U.; Trujillo-Roldán, M.A.; Valdez-Cruz, N.A.; Vázquez, E.; Villaverde, A. Bacterial inclusion bodies are industrially exploitable amyloids. *FEMS Microbiol. Rev.* **2019**, *43*, 53–72. [CrossRef]

18. Krauss, U.; Jager, V.D.; Diener, M.; Pohl, M.; Jaeger, K.E. Catalytically-active inclusion bodies-Carrier-free protein immobilizates for application in biotechnology and biomedicine. *J. Biotechnol.* **2017**, *258*, 136–147. [CrossRef]
19. Hrabárová, E.; Achbergerová, L.; Nahálka, J. Insoluble protein applications: The use of bacterial inclusion bodies as biocatalysts. In *Insoluble Proteins*; Springer: New York, NY, USA, 2015; pp. 411–422.
20. Carrio, M.; Gonzalez-Montalban, N.; Vera, A.; Villaverde, A.; Ventura, S. Amyloid-like properties of bacterial inclusion bodies. *J. Mol. Biol.* **2005**, *347*, 1025–1037. [CrossRef]
21. Morell, M.; Bravo, R.; Espargaro, A.; Sisquella, X.; Aviles, F.X.; Fernandez-Busquets, X.; Ventura, S. Inclusion bodies: Specificity in their aggregation process and amyloid-like structure. *Biochim. Biophys. Acta* **2008**, *1783*, 1815–1825. [CrossRef]
22. Carrio, M.M.; Villaverde, A. Protein aggregation as bacterial inclusion bodies is reversible. *FEBS Lett.* **2001**, *489*, 29–33. [CrossRef]
23. Groot, N.S.d.; Sabate, R.; Ventura, S. Amyloids in bacterial inclusion bodies. *Trends Biochem. Sci.* **2009**, *34*, 408–416. [CrossRef] [PubMed]
24. Wu, W.; Xing, L.; Zhou, B.; Lin, Z. Active protein aggregates induced by terminally attached self-assembling peptide ELK16 in Escherichia coli. *Microb. Cell Fact.* **2011**, *10*, 1–8. [CrossRef] [PubMed]
25. Zhou, B.; Xing, L.; Wu, W.; Zhang, X.-E.; Lin, Z. Small surfactant-like peptides can drive soluble proteins into active aggregates. *Microb. Cell Fact.* **2012**, *11*, 1–8. [CrossRef]
26. Talafová, K.; Hrabárová, E.; Chorvát, D.; Nahálka, J. Bacterial inclusion bodies as potential synthetic devices for pathogen recognition and a therapeutic substance release. *Microb. Cell Fact.* **2013**, *12*, 16. [CrossRef]
27. Vazquez, E.; Corchero, J.L.; Burgueno, J.F.; Seras-Franzoso, J.; Kosoy, A.; Bosser, R.; Mendoza, R.; Martinez-Lainez, J.M.; Rinas, U.; Fernandez, E.; et al. Functional inclusion bodies produced in bacteria as naturally occurring nanopills for advanced cell therapies. *Adv Mater.* **2012**, *24*, 1742–1747. [CrossRef]
28. Liovic, M.; Ozir, M.; Zavec, A.B.; Peternel, S.; Komel, R.; Zupancic, T. Inclusion bodies as potential vehicles for recombinant protein delivery into epithelial cells. *Microb. Cell Fact.* **2012**, *11*, 67. [CrossRef]
29. Rueda, F.; Cano-Garrido, O.; Mamat, U.; Wilke, K.; Seras-Franzoso, J.; García-Fruitós, E.; Villaverde, A. Production of functional inclusion bodies in endotoxin-free Escherichia coli. *Appl. Microbiol. Biotechnol.* **2014**, *98*, 9229–9238. [CrossRef]
30. Vázquez, E.; Villaverde, A. Microbial biofabrication for nanomedicine: Biomaterials, nanoparticles and beyond. *Nanomedicine (Lond.)* **2013**, *8*, 1895–1898. [CrossRef]
31. Seras-Franzoso, J.; Steurer, C.; Roldan, M.; Vendrell, M.; Vidaurre-Agut, C.; Tarruella, A.; Saldana, L.; Vilaboa, N.; Parera, M.; Elizondo, E.; et al. Functionalization of 3D scaffolds with protein-releasing biomaterials for intracellular delivery. *J. Control. Release* **2013**, *171*, 63–72. [CrossRef]
32. Céspedes, M.V.; Fernández, Y.; Unzueta, U.; Mendoza, R.; Seras-Franzoso, J.; Sánchez-Chardi, A.; Álamo, P.; Toledo-Rubio, V.; Ferrer-Miralles, N.; Vázquez, E.; et al. Bacterial mimetics of endocrine secretory granules as immobilized in vivo depots for functional protein drugs. *Sci. Rep.* **2016**, *6*, 35765. [CrossRef] [PubMed]
33. Unzueta, U.; Seras-Franzoso, J.; Cespedes, M.V.; Saccardo, P.; Cortes, F.; Rueda, F.; Garcia-Fruitos, E.; Ferrer-Miralles, N.; Mangues, R.; Vazquez, E.; et al. Engineering tumor cell targeting in nanoscale amyloidal materials. *Nanotechnology* **2017**, *28*, 015102. [CrossRef]
34. Sánchez, J.M.; López-Laguna, H.; Álamo, P.; Serna, N.; Sánchez-Chardi, A.; Nolan, V.; Cano-Garrido, O.; Casanova, I.; Unzueta, U.; Vazquez, E.; et al. Artificial Inclusion Bodies for Clinical Development. *Adv. Sci.* **2020**, *7*, 1902420. [CrossRef] [PubMed]
35. Slouka, C.; Kopp, J.; Spadiut, O.; Herwig, C. Perspectives of inclusion bodies for bio-based products: Curse or blessing? *Appl. Microbiol. Biotechnol.* **2019**, *103*, 1143–1153. [CrossRef] [PubMed]
36. Steele, D. Infrared Spectroscopy: Theory. In *Handbook of Vibrational Spectroscopy*; John Wiley & Sons, Ltd.: Hoboken, NJ, USA, 2006; pp. 44–70. [CrossRef]
37. Barth, A. Infrared spectroscopy of proteins. *Biochim. Et Biophys. Actabioenerg.* **2007**, *1767*, 1073–1101. [CrossRef] [PubMed]
38. Wiercigroch, E.; Szafraniec, E.; Czamara, K.; Pacia, M.Z.; Majzner, K.; Kochan, K.; Kaczor, A.; Baranska, M.; Malek, K. Raman and infrared spectroscopy of carbohydrates: A review. *Spectrochim. Acta Part A Mol. Biomol. Spectrosc.* **2017**, *185*, 317–335. [CrossRef] [PubMed]
39. Schindler, R.; Lendl, B.; Kellner, R. Determination of amyloglucosidase activity using flow injection analysis with Fourier transform infrared spectrometric detection. *Analyst* **1997**, *122*, 531–534. [CrossRef]

40. Schindler, R.; Lendl, B.; Kellner, R. Simultaneous determination of alpha-amylase and amyloglucosidase activities using flow injection analysis with Fourier transform infrared spectroscopic detection and partial least-squares data treatment. *Anal. Chim. Acta* **1998**, *366*, 35–43. [CrossRef]
41. Schindler, R.; Lendl, B. Simultaneous determination of enzyme activities by FTIR-spectroscopy in an one-step assay. *Anal. Chim. Acta* **1999**, *391*, 19–28. [CrossRef]
42. Wurm, D.J.; Quehenberger, J.; Mildner, J.; Eggenreich, B.; Slouka, C.; Schwaighofer, A.; Wieland, K.; Lendl, B.; Rajamanickam, V.; Herwig, C.; et al. Teaching an old pET new tricks: Tuning of inclusion body formation and properties by a mixed feed system in *E. coli*. *Appl. Microbiol. Biotechnol.* **2018**, *102*, 667–676. [CrossRef]
43. Doglia, S.M.; Ami, D.; Natalello, A.; Gatti-Lafranconi, P.; Lotti, M. Fourier transform infrared spectroscopy analysis of the conformational quality of recombinant proteins within inclusion bodies. *Biotechnol. J.* **2008**, *3*, 193–201. [CrossRef] [PubMed]
44. Slouka, C.; Kopp, J.; Hutwimmer, S.; Strahammer, M.; Strohmer, D.; Eitenberger, E.; Schwaighofer, A.; Herwig, C. Custom Made Inclusion Bodies: Impact of classical process parameters and physiological parameters on Inclusion Body quality attributes. *Microb. Cell Fact.* **2018**, *17*, 148. [CrossRef] [PubMed]
45. El-Safory, N.S.; Fazary, A.E.; Lee, C.-K.J.C.P. Hyaluronidases, a group of glycosidases: Current and future perspectives. *Carbohydr. Polym.* **2010**, *81*, 165–181. [CrossRef]
46. Menzel, E.J.; Farr, C. Hyaluronidase and its substrate hyaluronan: Biochemistry, biological activities and therapeutic uses. *Cancer Lett.* **1998**, *131*, 3–11. [CrossRef]
47. Guo, X.; Liu, F.; Zhu, X.; Su, Y.; Ling, P. Expression of a novel hyaluronidase from Streptococcus zooepidemicus in Escherichia coli and its application for the preparation of HA oligosaccharides. *Carbohydr. Polym.* **2009**, *77*, 254–260. [CrossRef]
48. Rahmanian, M.; Pertoft, H.; Kanda, S.; Christofferson, R.; Claesson-Welsh, L.; Heldin, P. Hyaluronan Oligosaccharides Induce Tube Formation of a Brain Endothelial Cell Linein Vitro. *Exp. Cell Res.* **1997**, *237*, 223–230. [CrossRef] [PubMed]
49. Reichelt, W.N.; Brillmann, M.; Thurrold, P.; Keil, P.; Fricke, J.; Herwig, C. Physiological capacities decline during induced bioprocesses leading to substrate accumulation. *Biotechnol. J.* **2017**, *12*, 1600547. [CrossRef] [PubMed]
50. Kopp, J.; Slouka, C.; Strohmer, D.; Kager, J.; Spadiut, O.; Herwig, C. Inclusion Body Bead Size in *E. coli* Controlled by Physiological Feeding. *Microorganisms* **2018**, *6*, 116.
51. Soldatova, L.N.; Crameri, R.; Gmachl, M.; Kemeny, D.M.; Schmidt, M.; Weber, M.; Mueller, U.R. Superior biologic activity of the recombinant bee venom allergen hyaluronidase expressed in baculovirus-infected insect cells as compared with Escherichia coli. *J. Allergy Clin. Immunol.* **1998**, *101*, 691–698. [CrossRef]
52. Astériou, T.; Vincent, J.-C.; Tranchepain, F.; Deschrevel, B. Inhibition of hyaluronan hydrolysis catalysed by hyaluronidase at high substrate concentration and low ionic strength. *Matrix Biol.* **2006**, *25*, 166–174. [CrossRef]
53. Haxaire, K.; Maréchal, Y.; Milas, M.; Rinaudo, M. Hydration of hyaluronan polysaccharide observed by IR spectrometry. II. Definition and quantitative analysis of elementary hydration spectra and water uptake. *Biopolymers* **2003**, *72*, 149–161. [CrossRef] [PubMed]
54. Gilli, R.; Kacurakova, M.; Mathlouthi, M.; Navarini, L.; Paoletti, S. Ftir Studies of Sodium Hyaluronate and Its Oligomers in the Amorphous Solid-Phase and in Aqueous-Solution. *Carbohyd. Res.* **1994**, *263*, 315–326. [CrossRef]
55. Nahálka, J.; Vikartovská, A.; Hrabárová, E. A crosslinked inclusion body process for sialic acid synthesis. *J. Biotechnol.* **2008**, *134*, 146–153. [CrossRef] [PubMed]
56. Gasteiger, E.; Hoogland, C.; Gattiker, A.; Wilkins, M.R.; Appel, R.D.; Bairoch, A. Protein identification and analysis tools on the ExPASy server. In *The Proteomics Protocols Handbook*; Springer: Berlin/Heidelberg, Germany, 2005; pp. 571–607.
57. Ceroni, A.; Passerini, A.; Vullo, A.; Frasconi, P. DISULFIND: A disulfide bonding state and cysteine connectivity prediction server. *Nucleic Acids Res.* **2006**, *34*, W177–W181. [CrossRef] [PubMed]
58. Dudler, T.; Chen, W.-Q.; Wang, S.; Schneider, T.; Annand, R.R.; Dempcy, R.O.; Crameri, R.; Gmachl, M.; Suter, M.; Gelb, M.H. High-level expression in Escherichia coli and rapid purification of enzymatically active honey bee venom phospholipase A2. *Biochim. Biophys. Acta* **1992**, *1165*, 201–210. [CrossRef]
59. Ceroni, F.; Algar, R.; Stan, G.B.; Ellis, T. Quantifying cellular capacity identifies gene expression designs with reduced burden. *Nat. Methods* **2015**, *12*, 415–418. [CrossRef]

60. Dvorak, P.; Chrast, L.; Nikel, P.I.; Fedr, R.; Soucek, K.; Sedlackova, M.; Chaloupkova, R.; de Lorenzo, V.; Prokop, Z.; Damborsky, J. Exacerbation of substrate toxicity by IPTG in Escherichia coli BL21(DE3) carrying a synthetic metabolic pathway. *Microb. Cell Fact.* **2015**, *14*, 201. [CrossRef]
61. Silva, F.; Queiroz, J.A.; Domingues, F.C. Evaluating metabolic stress and plasmid stability in plasmid DNA production by Escherichia coli. *Biotechnol. Adv.* **2012**, *30*, 691–708. [CrossRef]
62. Heyland, J.; Blank, L.M.; Schmid, A. Quantification of metabolic limitations during recombinant protein production in Escherichia coli. *J. Biotechnol.* **2011**, *155*, 178–184. [CrossRef]
63. Malakar, P.; Venkatesh, K.V. Effect of substrate and IPTG concentrations on the burden to growth of Escherichia coli on glycerol due to the expression of Lac proteins. *Appl. Microbiol. Biotechnol.* **2012**, *93*, 2543–2549. [CrossRef]
64. Haddadin, F.T.; Harcum, S.W. Transcriptome profiles for high-cell-density recombinant and wild-type Escherichia coli. *Biotechnol. Bioeng.* **2005**, *90*, 127–153. [CrossRef] [PubMed]
65. Shiloach, J.; Fass, R.J.B.a. Growing *E. coli* to high cell density—A historical perspective on method development. *Biotechnol. Adv.* **2005**, *23*, 345–357. [CrossRef] [PubMed]
66. Van de Walle, M.; Shiloach, J. Proposed mechanism of acetate accumulation in two recombinant Escherichia coli strains during high density fermentation. *Biotechnol. Bioeng.* **1998**, *57*, 71–78. [CrossRef]
67. Peternel, Š.; Jevševar, S.; Bele, M.; Gaberc-Porekar, V.; Menart, V. New properties of inclusion bodies with implications for biotechnology. *Biotechnol. Appl. Biochem.* **2008**, *49*, 239–246. [CrossRef]
68. Bisswanger, H. Enzyme assays. *Perspect. Sci.* **2014**, *1*, 41–55. [CrossRef]
69. Lenormand, H.; Amar-Bacoup, F.; Vincent, J.-C. Reaction–complexation coupling between an enzyme and its polyelectrolytic substrate: Determination of the dissociation constant of the hyaluronidase–hyaluronan complex from the hyaluronidase substrate-dependence. *Biophys. Chem.* **2013**, *175*, 63–70. [CrossRef]
70. Lenormand, H.; Amar-Bacoup, F.; Vincent, J.-C. pH effects on the hyaluronan hydrolysis catalysed by hyaluronidase in the presence of proteins. Part III. The electrostatic non-specific hyaluronan–hyaluronidase complex. *Carbohydr. Polym.* **2011**, *86*, 1491–1500. [CrossRef]
71. Koch, C.; Brandstetter, M.; Wechselberger, P.; Lorantfy, B.; Plata, M.R.; Radel, S.; Herwig, C.; Lendl, B. Ultrasound-Enhanced Attenuated Total Reflection Mid-infrared Spectroscopy In-Line Probe: Acquisition of Cell Spectra in a Bioreactor. *Anal. Chem.* **2015**, *87*, 2314–2320. [CrossRef]
72. Koch, C.; Posch, A.E.; Herwig, C.; Lendl, B. Comparison of Fiber Optic and Conduit Attenuated Total Reflection (ATR) Fourier Transform Infrared (FT-IR) Setup for In-Line Fermentation Monitoring. *Appl. Spectrosc.* **2016**, *70*, 1965–1973. [CrossRef]
73. DeLisa, M.P.; Li, J.; Rao, G.; Weigand, W.A.; Bentley, W.E. Monitoring GFP-operon fusion protein expression during high cell density cultivation of Escherichia coli using an on-line optical sensor. *Biotechnol. Bioeng.* **1999**, *65*, 54–64. [CrossRef]
74. Kopp, J.; Zauner, F.B.; Pell, A.; Hausjell, J.; Humer, D.; Ebner, J.; Herwig, C.; Spadiut, O.; Slouka, C.; Pell, R. Development of a widely applicable reversed-phase liquid chromatography method for protein quantification using analytical quality-by-design principles. **2020**, under review.

© 2020 by the authors. Licensee MDPI, Basel, Switzerland. This article is an open access article distributed under the terms and conditions of the Creative Commons Attribution (CC BY) license (http://creativecommons.org/licenses/by/4.0/).